Available online at www.sciencedirect.com

ScienceDirect

journal homepage: www.elsevier.com/locate/he

Green synthesis of molybdenum-based nanoparticles and their applications in energy conversion and storage: A review

Aneesa Awan [a,1], *Ayesha Baig* [a,1], *Muhammad Zubair* [a], *Abbas Rahdar* [b], *Muhammad Faizan Nazar* [c], *Ahmad Salam Farooqi* [d], *Ahmed Esmail Shalan* [e,f,**], *Senentxu Lanceros-Méndez* [e,g], *Muhammad Nadeem Zafar* [a,*]

[a] *Department of Chemistry, University of Gujrat, Gujrat, 50700, Pakistan*
[b] *Department of Physics, University of Zabol, Zabol, 98615-538, Iran*
[c] *Department of Chemistry, University of Education Lahore, Multan Campus, 60700, Pakistan*
[d] *Department of Chemical Engineering, Universiti Teknologi PETRONAS, Bandar Seri Iskandar, Perak, 32610, Malaysia*
[e] *BCMaterials-Basque Center for Materials, Applications and Nanostructures, Martina Casiano, UPV/EHU Science Park, Barrio Sarriena S/n, Leioa, 48940, Spain*
[f] *Central Metallurgical Research and Development Institute, P. O. Box 87, Helwan, Cairo, 11422, Egypt*
[g] *IKERBASQUE, Basque Foundation for Science, Bilbao, 48009, Spain*

HIGHLIGHTS

- An overview on research results and progress of Mo-NPs in energy applications.
- An overview of different greener routes for the synthesis of Mo-NPs.
- Important and interesting energy applications of Mo-NPs are highlighted.
- Major accomplishments are summarized in different tables for instant information.
- Existing challenges and possible explanations are summarized for future research.

GRAPHICAL ABSTRACT

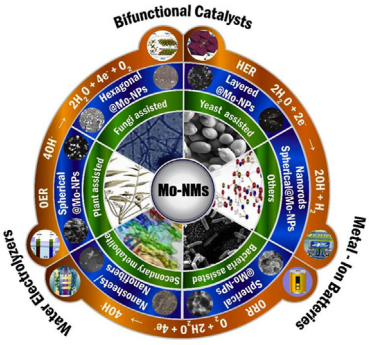

* *Corresponding author.*
** *Corresponding author.* BCMaterials-Basque Center for Materials, Applications and Nanostructures, Martina Casiano, UPV/EHU Science Park, Barrio Sarriena s/n, Leioa, 48940, Spain.
E-mail addresses: ahmed.shalan@bcmaterials.net, a.shalan133@gmail.com (A.E. Shalan), znadeempk@gmail.com, nadeem.zafar@uog.edu.pk (M.N. Zafar).
[1] Contributed equally.
https://doi.org/10.1016/j.ijhydene.2021.10.076

ARTICLE INFO

Article history:
Received 30 June 2021
Received in revised form
7 September 2021
Accepted 12 October 2021
Available online 12 November 2021

Keywords:
Green synthesis
Molybdenum nanoparticles
Energy
Water splitting
Batteries

ABSTRACT

In the scope of the rapid technological advancements, nanoparticles (NPs) have gained prominence due to their excellent and tunable biological, and physicochemical properties. Nowadays, different methods are used for their synthesis. In particular, the green synthesis of metal precursors for the synthesis of NPs, represents a cost-effective, environmentally friendly, and hazardous chemical-free method for developing a large variety of NPs. By exploiting plant extracts, the production rate of NPs is relatively faster. Due to fossil reserves and high fuel consumption, renewable and clean energy materials are urgently needed to improve environmental sustainability. With outstanding electrochemical and physicochemical characteristics, molybdenum-based NPs (Mo-NPs) are gaining increasing attention in the fields of energy conversion and storage. Considering the significance of Mo-NPs synthesized from greener routes and their energy applications, it is necessary to review recent trends and developments in this field. This review summarizes important research studies and future research guidelines for the preparation of Mo-NPs through green routes and their applications to meet global energy and environmental demands. Moreover, future research directions are also highlighted to achieve sustainable greener precursors and Mo-NPs based energy storage devices.

Introduction

From the past few decades, nanotechnology has become a promising approach to tackle relevant societal challenges in areas such as communication, energy, environment, and health. It is the field of science that deals with the synthesis, properties and applications of nanoparticles (NPs) [1,2], i.e. particles with size in the range of 1–100 nm [3]. NPs are categorized into two main classes i.e., inorganic, and organic NPs. Inorganic NPs include metallic NPs (Zn, Mo, Mn), semiconductor NPs (Mo_2S, CdS, ZnO) and magnetic NPs ($ZnFe_3O_4$, SnF_2O_4), while organic NPs include carbon nanotubes, carbon nano-horns and polymer-based NPs. Nanomaterials possess specific properties as compared to their bulk counterpart on the basis of their specific surface to volume ratio [4–6]. Based upon their physical, electrical and chemical properties, these NPs have been utilized in the different fields i.e., mechanics, catalysis, optics, biotechnology, pharmaceutical science, microbiology, material science and numerous engineering fields [7]. Small nanometer scale materials with varying distribution, size and morphology are used to fabricate various complex bulk materials with controlled physical and chemical properties. Excessive energy demand leads to energy shortages and various environmental challenges. Sustainable energy development is essential to access alternative energy sources. However, molybdenum-based NPs (Mo-NPs) synthesized from greener routes are efficient sources of energy conversion and storage.

Various methods have been employed for the production of metal NPs including precursors from three (solid, gas and liquid) states of matter exploiting different experimental strategies [8,9]. There are two main strategies available that are used to fabricate metal NPs i.e., "top-down" and "bottom-up" [10–12]. In top-down approach, there is breakdown of bulk materials into smaller ones. These approaches include etching, ball-milling [13], sputtering [14] or lithographic techniques. Nano-sphere lithography, photolithography and beam lithography are sub-types of lithography. Nano-scale lithography is a cost-effective treatment to produce NPs of particular size and effectively controlled spacing. Many metal NPs, especially silver and gold have been prepared by lithographic method [15,16]. In case of bottom-up approach, smaller materials are assembled to form bulk substances by biological and chemical methods. Bottom-up approaches comprises spray pyrolysis, vapor deposition, sol-gel processes, laser pyrolysis and molecular condensation [14]. In top-down strategies, evaporation condensation is the most commonly used procedure to synthesize particles [17]. Different combinations of silver, gold and lead NPs have been prepared by this technique. There are some limitations associated with this technology such as consumption of large amounts of energy, occupying more space, crystallographic damage to processed materials, intensive labour, more time and high temperature is required [16,18,19].

The most commonly used bottom-up technique is chemical reduction. In this technique, different inorganic, and organic reagents such as dimethylformamide (DMF), sodium citrate and sodium acetate are used for the reduction of metal ions (e.g., Ag). The main disadvantage of this technique is the use of toxic and carcinogenic reagents. In both approaches, the morphology and size of nanomaterials can be controlled by varying parameters including temperature, reaction time, pH, etc. However, there are some drawbacks associated with these approaches such as destructive reagents, harmful organic solvents, need of skilled operators and expensive instruments [18]. To overcome these limitations, researchers develop simple, cost effective and environment friendly "green synthesis" to synthesize metal NPs. Carcinogenic chemicals, high pressure, temperature and large amounts of energy are not required for green methods [20,21].

Recently, green chemistry is the preferred approach for the production of metal NPs based upon its advantages like biocompatible solvents, environmentally benign reagents, cost-effective treatment, higher production and easily available resources e.g., plants [22–28] and microorganisms [20,29–32]. Green methods also possess recyclability that can convert waste material into useful forms. Least by-products are formed by this method (Fig. 1). It is estimated that various living organisms like fungi, algae, bacteria and actinomycetes have been implicated in the production of stable metallic NPs by the reduction of various metabolites present in these organisms [33–35]. In this strategy, inorganic ions are converted into metal NPs by biological components. Metal NPs fabricated through green chemistry exhibit a wide range of applications in different fields [36–41].

However, microorganism assisted synthesis is vulnerable due to tedious procedures, culture defilement and least control over size and morphology of NPs. Another way of NPs production in "green synthesis" is using plant extract. Various plant extracts are used to synthesize different NPs of unique size and morphology. NPs are also made from polypeptides [42,43]. Among all the green methods available for the synthesis of metal NPs, plant extract mediated synthesis is facile and cost effective compared to microorganism mediated synthesis [44]. As previously mentioned, the two basic principles of synthesis, bottom-up and top-down methods particularly green synthesis were utilized to fabricate nanoparticles of desired size, shape and functionalities (Fig. 2).

Among the different NPs, Mo-sulfides and oxides related NPs have gained great interest attributed to their uncommon catalytic and electrochemical properties with specific surface to volume ratio, making it a suitable candidate for energy conversion and storage. Molybdenum trioxide (MoO_3), with a unique layered nanostructure and high theoretical potential, is currently under comprehensive research as a highly promising lithium ion anode material [46]. With the increasing risk of environmental pollution, the concept of environmental protection has become more and more popular, and the green synthesis has received much attention. Therefore, many research studies have used green pathways for the synthesis of Mo-NPs [47,48]. The production of hydrogen from electrochemical water splitting is considered to be the most economical and sustainable technique for the production of green fuels. It is highly challenging to develop a low cost and most efficient noble metal-free electrocatalyst [49,50]. Exploring multifunctional electrocatalysts is crucial for the development of energy storage and conversion equipment, such as water splitting devices, zinc-air batteries and fuel cells. Presently, Mo-based electrocatalysts were regarded as potential alternatives for the HER [51–55].

The evolution of nanomaterials has played a key role in changing the structure and shape of materials at the nanoscale to achieve the desired applications. Among them, Mo-disulfide (MoS_2) is considered a reliable multipurpose material as it exhibits the ability to show various characteristics as it changes from bulk to nanoscale. The promising features and characteristics of MoS_2 make it suitable for a variety of practical applications [56]. Many electrocatalysts with excellent electrochemical performances for hydrogen evolution have been reported recently. Mo is more abundant in nature than noble metals. However, molybdenum alloys exhibit less stability in acidic media. Therefore, Mo-based compounds such as selenides, carbides, sulfides, nitrides, etc. are being investigated as electrocatalysts because they are highly stable in acidic media. Of these compounds, molybdenum carbides have therefore been found to be a good alternative to platinum because of its high stability and excellent catalytic activity in acidic and basic mediums

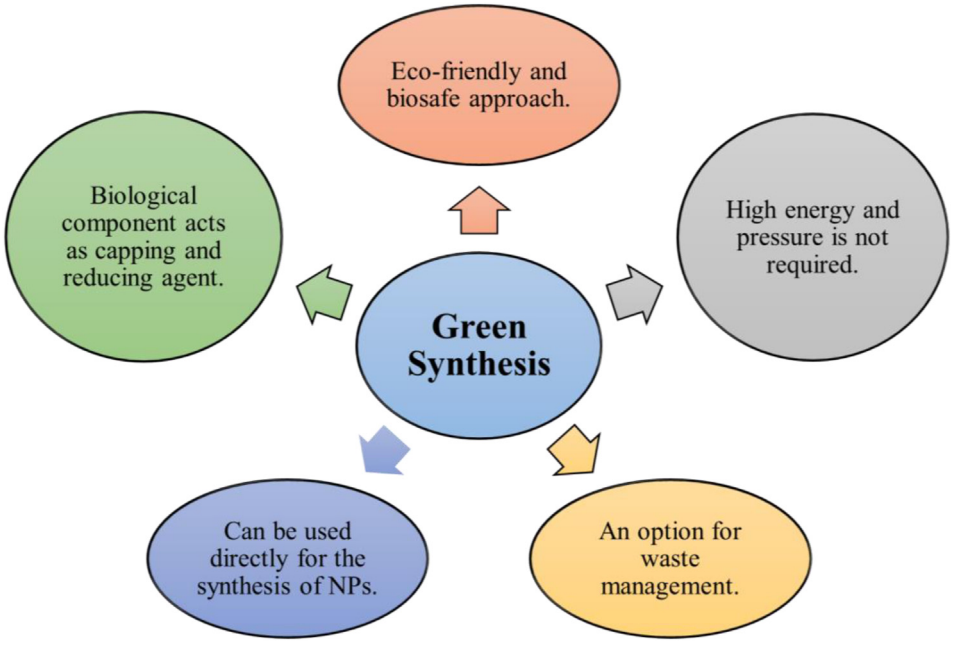

Fig. 1 – Some key merits of green synthesis methods. (For interpretation of the references to color in this figure legend, the reader is referred to the Web version of this article.)

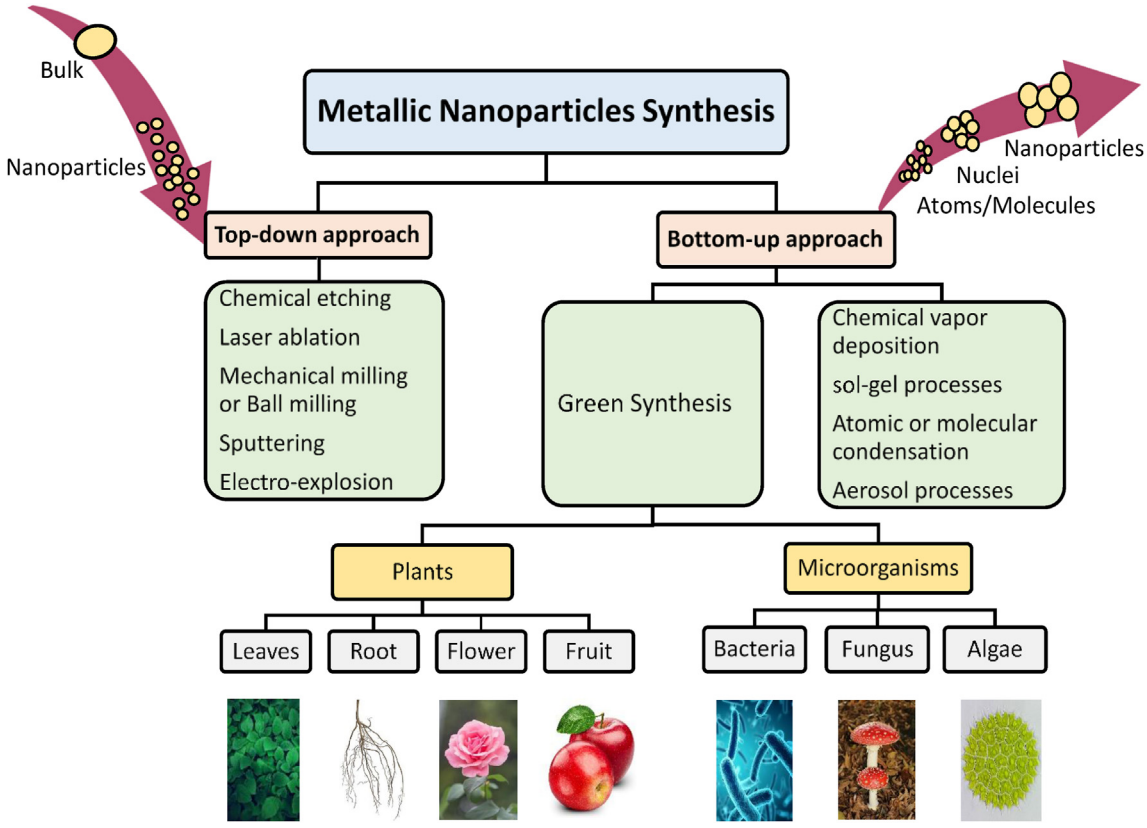

Fig. 2 – Green synthesis of metal NPs via different approaches, including green synthesis. Reprinted with permission from Singh et al. [45] ©2018, BMC. (For interpretation of the references to color in this figure legend, the reader is referred to the Web version of this article.)

[57]. Exploiting efficient and inexpensive electrocatalysts for HER of water electrolysis is a big challenge. Therefore, Gong et al. designed an efficient electrocatalyst of Ni-induced nitrogen-doped carbon @ molybdenum carbide @ molybdenum disulfide sphere (NC@Mo_2C@MoS_2-(Ni)). The catalyst NC@Mo_2C@MoS_2-(Ni) exhibited relatively good catalytic performance of overpotentials of 216 and 205 mV at 10 mA cm^{-2} and Tafel slopes of 42.7 and 61.4 mV dec^{-1} in basic and acidic media, respectively. This work provided a way to rationally fabricate more efficient catalyst than other functional electrocatalysts [58]. Similarly many other Mo-NPs based electrocatalysts are widely used for efficient hydrogen evolution in acidic and basic media [59–61].

Mo-NPs are fabricated by physical and chemical methods. However, these methods incorporate toxic and carcinogenic reagents that may cause detrimental effects to plants, animals and ultimately to human beings. To overcome all these effects, researchers move toward environmentally sustainable and economically viable "green method" for the synthesis of Mo nano-scale materials due to their potential applications in lithium-ion batteries, electrochemistry, petroleum industry, sensors, optical devices, energy storage devices, catalysis and plasmonics. In the present work, the synthetic approaches that are used to fabricate Mo-NPs and their use for energy related applications, is reviewed. In the first segment, synthetic methods especially "green synthesis" of nanomaterials are discussed. Then, applications in the fields of catalysis, batteries, storage devices and electrochemical studies are presented.

Green synthesis

The safest way of Mo-NPs synthesis is green synthesis, being of significant interest because Mo is an essential component required for all forms of life. There are three main branches of green synthesis for the synthesis of Mo-NPs i.e., (a) plant mediated green synthesis (b) microorganisms mediated green synthesis and (c) secondary metabolites mediated green synthesis.

Green synthesis using plant extracts

Among all the available green methods, plant mediated synthesis is a more useful approach as compared to microorganisms or metabolites mediated synthesis. Plants provide an efficient, environment friendly alternative method for the synthesis of metallic nanomaterials. In the presence of metal salts, extraction from different parts and species of plants results in the formation of NPs of different shapes and sizes, as indicated in Fig. 3.

Shaheen et al. investigated the use of *Nasturtium officinale* leaves for preparation of MoO_3 nanostructures and also elaborate its synthesis by using biologically active compounds of

leaves with ammonium molybdate terahydrate. Phytochemical extraction of leaves was performed at low temperature and the phytochemicals like octodrine, acetic acid, alanine, cyclohexamethylamine and decanoic acid were identified by certain techniques namely UV–vis, FTIR and GC-MS. Acetic acid, octodrine and alanine are reducing and stabilizing agents for synthesizing MoO_3 NPs and are confirmed by GC-MS. X-ray diffraction (XRD) certified that NPs were certainly crystallized with orthorhombic system with average diameter of 40.1 nm. Scanning Electron Microscope (SEM) analysis revealed that presence of phytocompounds averted the agglomeration of particles [62].

Leela and Vivekanadan, illustrated the simplest, feasible and evergreen strategy by incorporating certain plant parts (stem, seed, root and leaves) for the fabrication of metal NPs. In one pot synthesis, numerous plants are incorporated for reduction and stabilization of metal and metal oxide NPs [24]. Plants exhibit the ability to detoxify metal ions rapidly as compared to other mechanisms (catabolism). If metal ions are concentrated in the tissue region of plants, they activate reactive oxygen species that lead to severe cellular damage and irregularities in morphology. There are certain chelating agents present in plants that are able to surmount such problems. Plants produce stable metal NPs and have proven to be the best candidates for fast and large-scale synthesis. Biological mechanisms include capping and stabilization mediators (phytochemicals such as flavonoids, cofactors, terpenoids, and phenolics) that contribute to higher stability (Fig. 4) [63].

In a similar study, *Azadirachta indica* extract was used for cost-effective and biocompatible synthesis of silver and Mo-doped copper oxide NPs [64]. The *Azadirachta indica* species belongs to the Meliacea family and it is used as a therapeutic agent due to its antimicrobial, antidiabetic and antifungal properties. It behaves like a surfactant in fabrication of Ag–Mo/CuO NPs. X-ray diffractometers describe the crystal structure of NPs. According to Kanneganti, Mansa, and Doddapaneni, the synthesis of MoO_3 by utilizing *citrus limetta* extract was a highly sustainable and ecofriendly approach. In this approach, pitch was considered as waste material to prepare useful extract for the production of MoO_3 nano-based material. These manufactured NPs were capable of performing oxidative catalysis and used in electrochemical studies. Kanneganti et al. reported the uniform and spherical shape of Mo-NPs with the size in the set range of 24–50 nm. Transmission electron microscope (TEM) analysis revealed the unique size controlling ability of green synthesis (Fig. 5). The orthorhombic structure of the product MoO_3 was confirmed through X-ray analysis. The absorption spectrum confirmed the lambda maximum within the ultraviolet region at 257 nm [65].

MoO_3 vibrating (400-200 cm^{-1}) and stretching (1000–600 cm^{-1}) modes have been confirmed by Raman spectroscopy. TEM analysis clearly indicates formation of spherical shaped NPs with few nanometers in thickness. ED x-ray spectroscopy was used to confirm the elemental composition of the nanostructure and no impurities were found in the structure [66]. Abbbasifer, ValizadehKaji and Iravani reported fabrication of Mo-NPs by vermicompost extract that causes reduction of Mo-ions. The effect of elemental Mo and green synthesized Mo-NPs on activity of nitrate reductase in spinach was also observed. The product confirmation was carried out by various characterization techniques such as Dynamic light scattering (DLS), Energy dispersive x-ray (EDX) and SEM. It was revealed that Mo-NPs

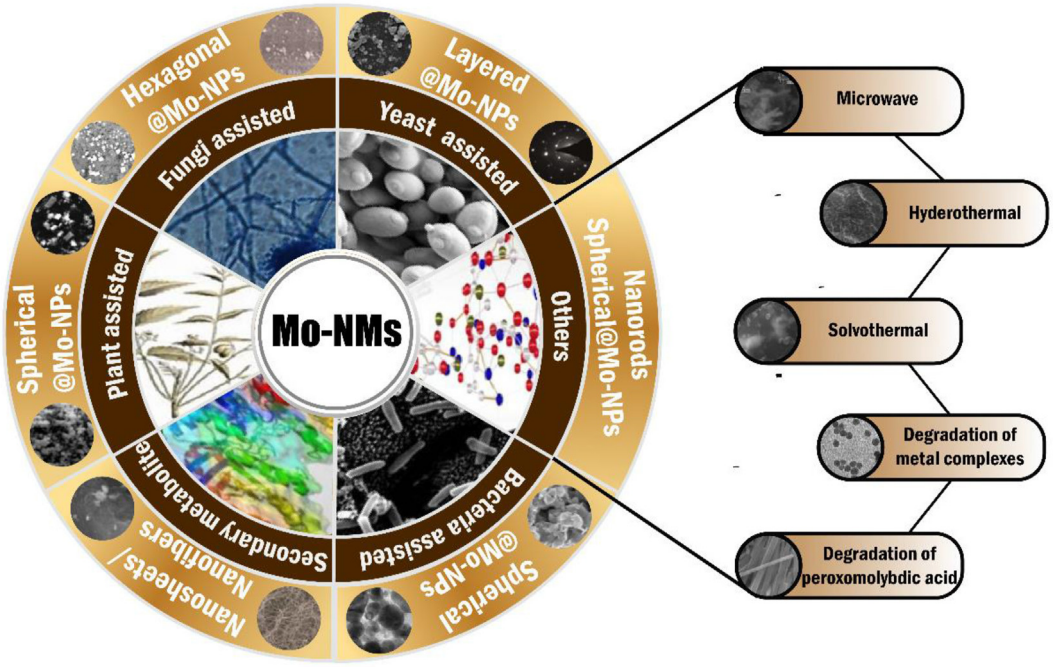

Fig. 3 – Green synthesis of Mo-NPs though various facile green approaches. (For interpretation of the references to color in this figure legend, the reader is referred to the Web version of this article.)

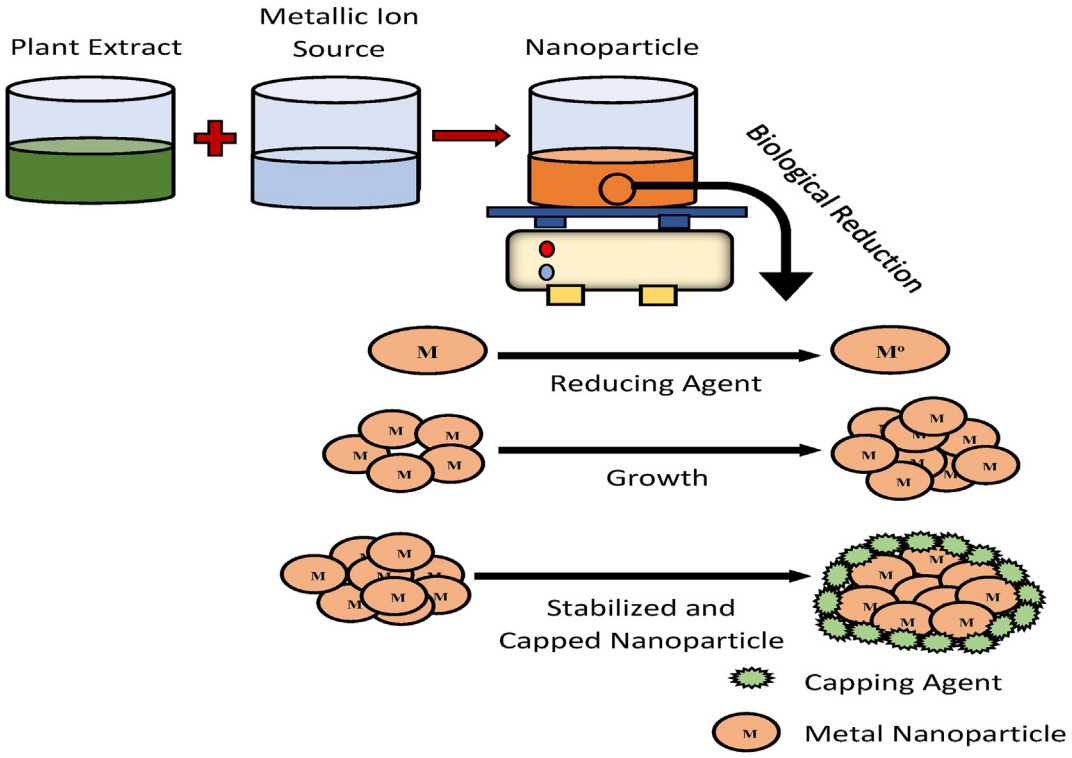

Fig. 4 – Plant mediated synthesis of metal NPs. Reprinted with permission from Qidwai et al. [63] ©2018, OMICS International.

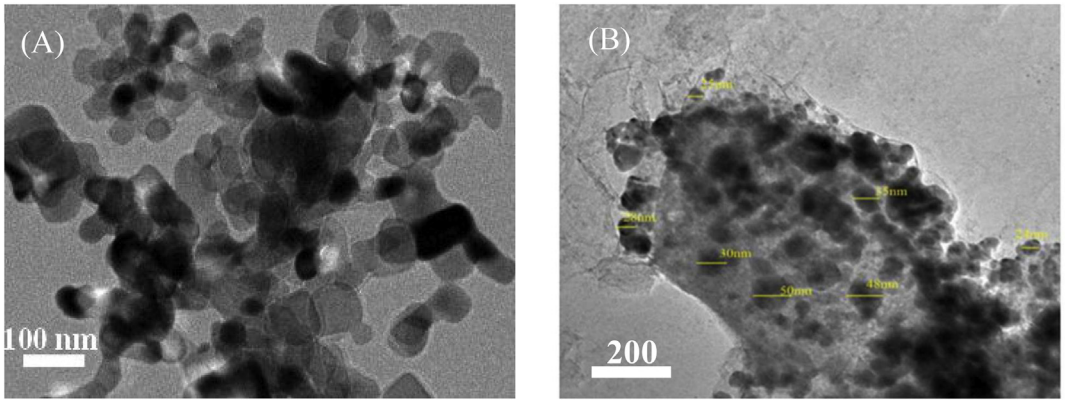

Fig. 5 – TEM micrograph of MoO_3 NPs (A) at 100 nm scale (B) at 200 nm scale. Reprinted with permission from Kanneganti et al. [65] ©2014, Blue Eyes Intelligence Engineering & Sciences Publication Pvt. Ltd. (For interpretation of the references to color in this figure legend, the reader is referred to the Web version of this article.)

are more effective in lowering the accumulation of NO_3 ions and enhancing the activity of nitrogen reductase enzyme in spinach relative to elemental Mo. These green synthesized NPs are available in the form of fertilizers [67]. Kannegnati et al. used extract of flower (*Syzygium Aromaticum*) buds for the production of MoO_3 NPs. This synthesis was reported to be simple, non-hazardous and cost effective. The origin of *Syzygium Aromaticum* is an island in Indonesia and the flower buds of the plant species are named as clove. This plant exhibits unique properties like antiviral and antimicrobial and is used for various pharmaceutical applications. XRD of as-synthesized MoO_3 NPs confirmed its orthorhombic crystal packing. The FTIR spectra of clove extract revealed the stretching of the N–H bond. The UV spectra represented maximum absorption at 252 nm. Based upon their characteristic TEM micrograph, the morphology of synthesized NPs was determined to be spherical with the average size of about 19.47 nm [68].

Sivan et al. revealed the use of gum arabic for production of MoO_3 NPs. Gums are naturally occurring hydrocolloids having great ability for fabrication of metallic NPs. Various gums with unique properties are easily available for assemblage of different nano-based materials for different applications. Many metallic NPs including Au, Pt, Pd, Ag, Se etc.,

and metallic oxide NPs including CuO_2, FeO_2, ZnO_2, TiO_2 were prepared from various hydrocolloid gums. These are isolated in various forms from trees and act as an economically active component for MoO_3 synthesis due to its specific properties like recyclability, reproducibility, harmless and facile degradability. Green synthesized MoO_3 has been successfully used for detoxification of *p*-nitrophenol, a water pollutant released from paper, plastic, leather and textile industries, which is highly toxic and carcinogenic. The prepared MoO_3 NPs were analyzed showing the stretching and bending of C–O and N–H bonds corresponds to the existence of gum arabic. XRD results showed an orthorhombic crystal system of MoO_3 along with sharp distinctive peaks in specified regions [66].

Fungi assisted synthesis

Green synthesis of metallic NPs by fungi involves reduction of hazardous metal ions into sustainable and eco-friendly nanomaterial. Based upon their biological properties, fungi have been exploited as a viable candidate for NPs production. Numerous NPs like palladium, silver, zinc, gold, platinum and many others were grown up and synthesized by a wide variety of fungi. These fabricated particles have shown great potential against toxic fungi (*Magnaporthe grisea* and *Bipolarissoro kiniana*) and they are responsible for reduction in fungal diseases.

Mo-NPs with significant beneficial effects on chickpea or crop productivity are synthesized by utilizing fungal species *Aspergillus tubingensis*. This fungus is isolated by microbial plate method from CAZRI (central arid zone research institute) in Rajasthan. This method involves a medium, which is very useful in cultivating fungi. Biological oxygen demand (BOD) incubator was used for incubation of plates and dextrose agar medium was used for purification of selected colonies [69]. The Mo-NPs synthesized by action of protein released from the fungal specie *Aspergillus tubingensis* with the average size of 20 nm that is demonstrated in TEM micrograph (Fig. 6).

The fungal derived Mo-NPs, where protein released from *Aspergillus tubigenesis* TFR29 breaks down the precursor salt of $(NH_4)_6Mo_7O_{24}$. Electrophoresis concluded that the protein group (32 KDa) resulted in the breakdown of ammonium molybdate which was responsible for the encapsulation of individual NPs (Fig. 7) [69].

Mo is essential for plant growth as much as nitrogen. Mo is most frequently required by nitrogen fixation bacteria to fix nitrogen and required for synthesis of amino acids from plants by converting nitrate to ammonia. Molybdenum deficiency is closely related to nitrogen deficiency. When the pH of growing media moves towards the acidic region, the availability of Mo gets lower. The fungi assisted green synthesis is more efficient as they release enzymes that catalyze the conversion of carcinogenic metallic ions into metal and metal oxide based nanostructures. It is the negative potential of fungi, that attracts positive ions towards it and therefore assists fabrication of metallic NPs. The DLS analysis was used to measure size of NP by observing fluctuations in light intensity. The hexagonal geometry of the Mo particle was confirmed by viewing the TEM image. The smoothness of surface and crystal nature of synthesized NP was revealed by Atomic force microscopy. Mo-NPs synthesis with Aspergillus Niger utilizing EG as reducing agent while PVP as capping agent was investigated. In the chemical route, catalytic activity of Mo enzyme was described. It catalyzes oxidative conversion of sulphite into sulphate. In the case of biological methods, fungi play a key role in oxidation of SO_3^{2-} into SO_4^{2-} in presence of enzyme sulphatase. TEM and SEM allowed to determine particle sizes within the 10–20 nm range [70].

Bacteria assisted synthesis

Synthesis of metal and metal oxide NP by bacteria is the most sustainable approach among all microorganisms due to their efficient growth rate and facile handling. They simply involve certain organic compounds that are responsible for heavy metal ion removal and convert them into biocompatible nanomaterial [43,71,72]. As compared to the other microbial agents, easy manipulation, and mineralization of hazardous metal ions by bacteria is reported. Catalytic applications of various NPs fabricated by this method have also been investigated [73,74]. The extent of catalysis depends upon size to volume ratio of NP, which in turn depends upon reaction conditions. Yue et al. revealed biosynthesis of lead

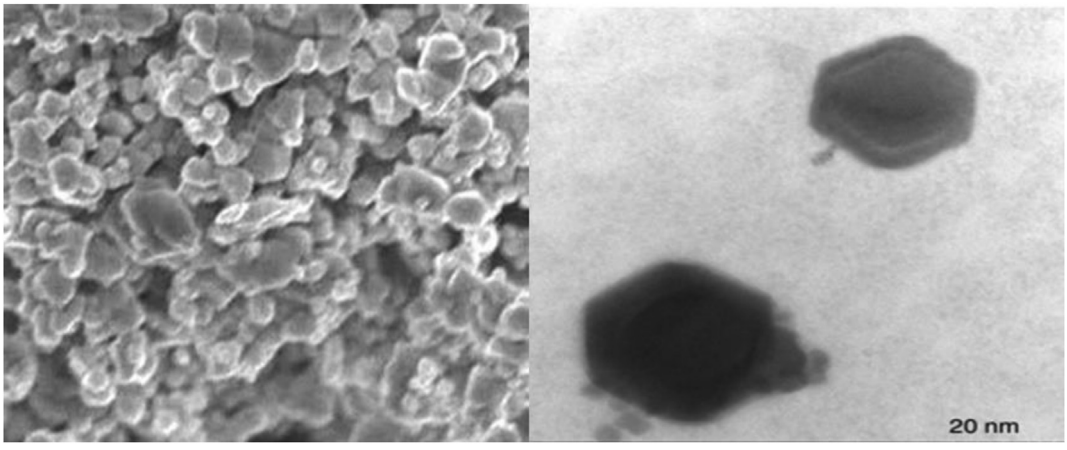

Fig. 6 – SEM and TEM Images of Mo-NPs produced from protein released from *Aspergillus tubingenesis*. Reprinted with permission from Thomas et al. [69] ©2017, American Scientific Publishers.

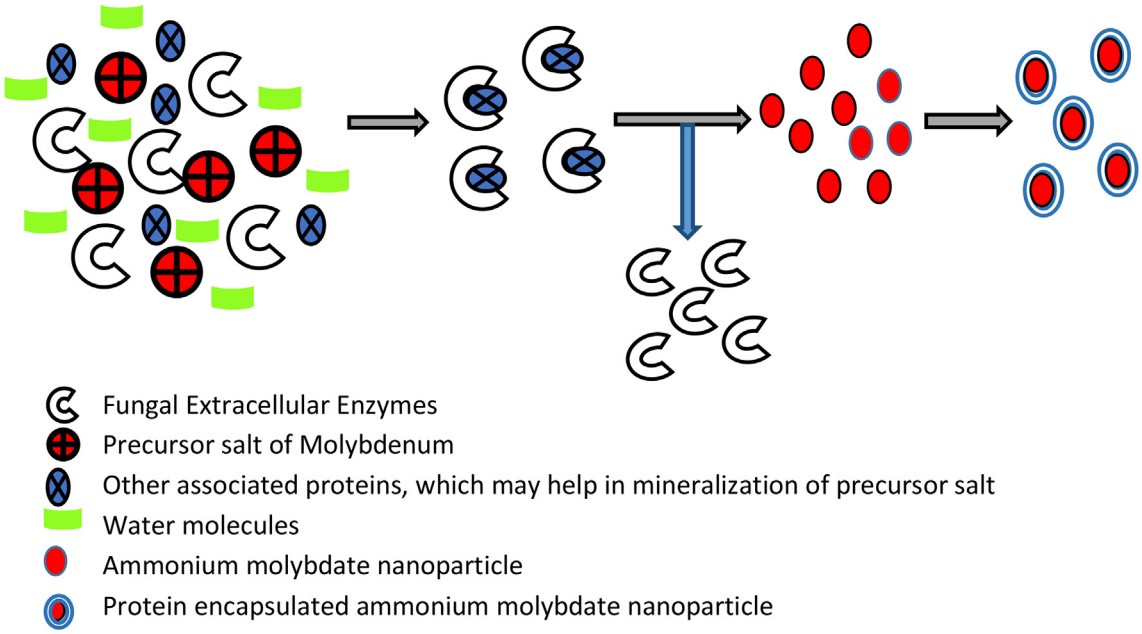

Fig. 7 – Fungi assisted synthesis of Mo-NPs. Reprinted with permission from Thomas et al. [69] ©2017, American Scientific Publishers.

sulfide NP for methylene blue degradation [75]. Srivastava et al. reported a microorganism-mediated synthesis of tin oxide NPs for dye degradation. Rhodamine B is efficiently reduced by hydrated Se NPs compared to Selenium NPs. Hydrated Se NPs utilize visible light for degradation of Rh dye [76]. Zhang et al. reported synthesis of Pd/Au NPs for the reduction of *p*-nitrophenol utilizing bacterial species (Bacillus gram stain). Metal NPs are fabricated by bacteria either in an intracellular or extracellular way utilizing their defense mechanisms like segregation and outflow pumps [76]. Biosynthesized NPs are more attractive and useful than chemically or physically prepared NPs because they come out in an environment with large area and more catalytic efficiency. Mo-NPs fabrication by biological protocol have been reported in the literature [77]. Rahman et al. Halmi et al. and many other researchers revealed utilization of numerous bacteria for the synthesis of Mo blue dye [78,79]. The synthesis of Mo-NPs involves reduction of hexavalent Mo-ions into metal molybdenumutilizing *Clostridium pasteurianum* species for efficient degradation of methyl orange (Fig. 8). Transmission electron micrographs provided information that nanometer scale particulates of Mo, ranging from 5 to 20 nm were obtained with highly smooth surface and uniform distribution of nanoparticles. The crystal nature was confirmed by XAS, XRD and XPS. The average size of Mo nanostructure is round about 20 nm with uniform distribution and smooth surface. The characteristic pattern of bacterial assisted synthesized Mo-NPs is similar to the pattern of JCPDS no. 00-042-1120 [80].

Rees et al. revealed synthesis of NPs of Mo-disulfide by using bacterial specie *Shewanella oneidensis* in presence of sodium thiosulfate and Mo-trioxide. This bacterial specie exhibit reducing capacity that reduces sulfur and various other metal compounds and transform into NP form. Various characterization tools such as EDS, TEM and XRD were performed to analyze fabricated NPs of MoS_2. SEM analysis described the rhombohedral and hexagonal morphology of aggregated MoS_2 nanobased particles within the set range between 50 and 300 nm. According to XRD experiment, prepared MoS_2 NPs showed orthorhombic crystalline pattern [81]. The characteristic pattern of bacterial assisted synthesized Mo-NPs is similar to the pattern of JCPDS no. 12 [81].

Green synthesis from secondary metabolites

Like *in-vivo* green synthesis, *in-vitro* nanotrapping of NPs using plant materials can be extended further to design high-throughput apparatus for extracting specific classes of different compounds from the crude extracts (Fig. 9) [82]. In another approach of green synthesis, secondary metabolites are also employed for the preparation of metal and metal oxide NPs [83].

The graphite carbon sheets labelled with Mo_2C NPs are fabricated by sodium alginate and ammonium molybdate. The potential of 120 mV, current density of 12.5×10^{-3} mA cm^{-2} with excellent conductivity are the optimum conditions for Mo_2C/GCSs composite to catalyze hydrogen generation reaction in acidic media. The extent of catalysis is based upon the ratio of ALG and ammonium molybdate. This reaction was carried out at 900°C in an inert atmosphere. Characterization of Mo_2C/GCSs NP showed the Raman spectrum peaks at 1590 and 1350 cm^{-1} belong to the G and D band of carbon. The intense peak with maximum percentage corresponded to carbon as compared to other elements in EDS spectra. TEM micrograph represented the size of NPs in the range of 5–23 nm [84]. Wu et al. reported an other facile, cost effective and green route for the preparation of Mo-carbide (Mo_2C) based catalyst (Fig. 10) for hydrogen generation [85].

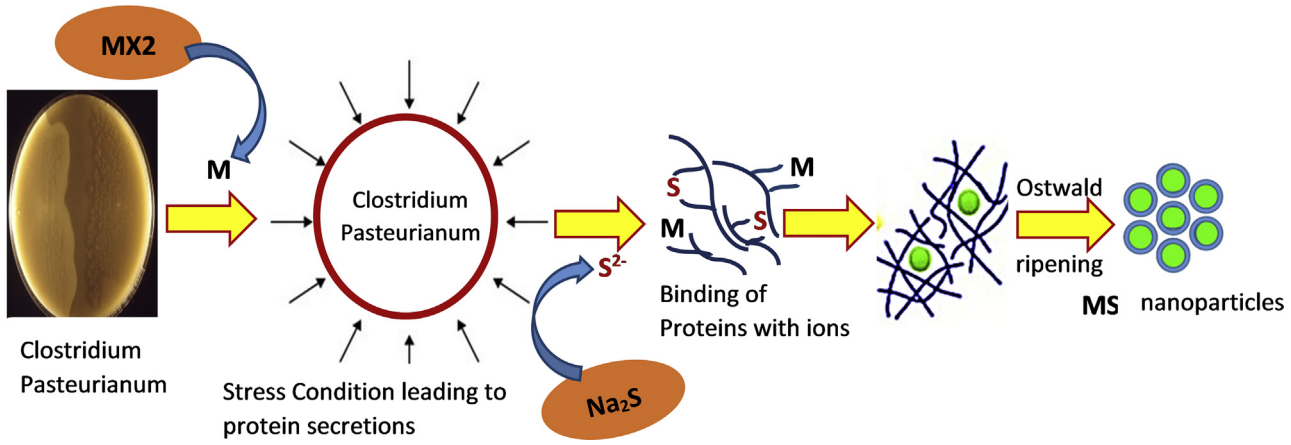

Fig. 8 – Synthesis of metal sulfide NPs from *Clostridium Pasteurianum* species. Reprinted with permission from Nordmeier et al. [80] ©2018, Elsevier.

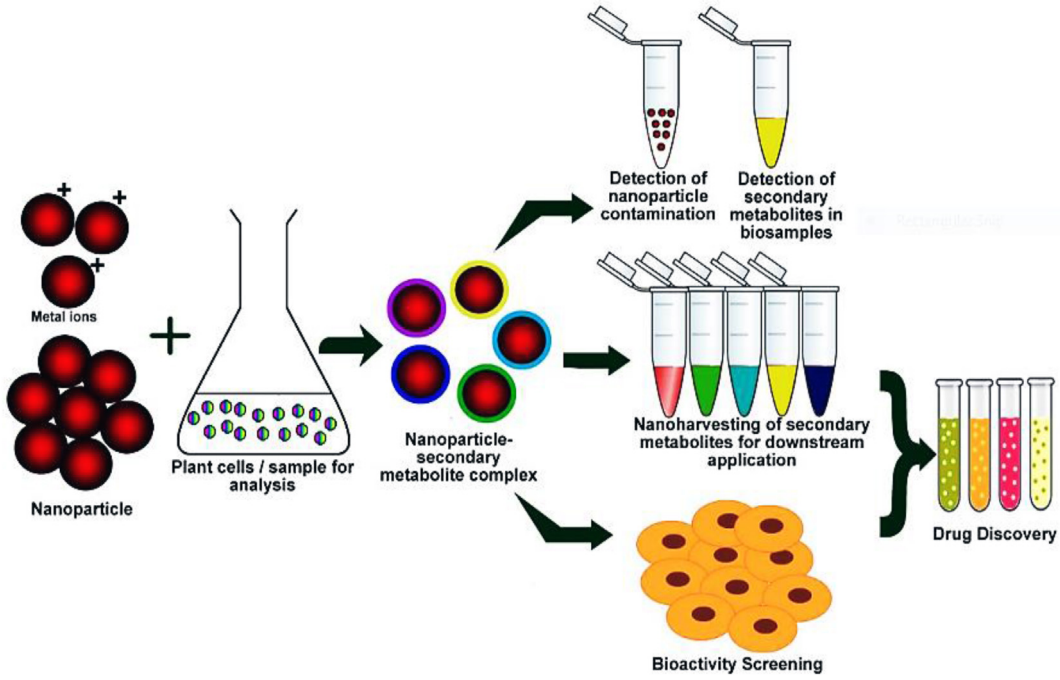

Fig. 9 – Secondary metabolite assisted green synthesis of metal NPs. Reprinted with permission from Marslin et al. [82] ©2018, MDPI. (For interpretation of the references to color in this figure legend, the reader is referred to the Web version of this article.)

The main constituents of this electro-catalyst are carbon nano-fiber labelled with three-dimensional Mo_2C nano-structure material implanted within bacterial cells and the nanofiber was doped with nitrogen. This innovative composite is highly stable and sustainable even in acidic and basic mediums. Solid-state reaction was carried out between ammonium molybdate and bacterial cellulose. The precursor of carbon nanofiber was bacterial cellulose (BC) and for Mo_2C was ammonium molybdate. Industrially, BC is produced in the fermentation process and it is a non-toxic and cost effective biofuel. There is significant interaction between nitrogen doped-CNF and 3-D Mo_2C NP that is responsible for its remarkable efficiency in generation of hydrogen. The crystalline domain of Mo_2C@N-CNFs was demonstrated by the diffraction pattern in SEAD. The homogenous distribution of all elements (N, Mo, O and C) within the composite was shown by SEM-EDX photograph. The two most prominent peaks in the Raman spectrum belongs to G and D bands of C at 1593 and 1347 cm^{-1}. TEM showed the size range of hybrid material within 10–20 nm. All the results obtained from different techniques revealed that this electro-catalyst with striking hydrogen production activity possesses an overpotential (167 mV) and current density of 4.73×10^{-2} mA cm^{-2}.

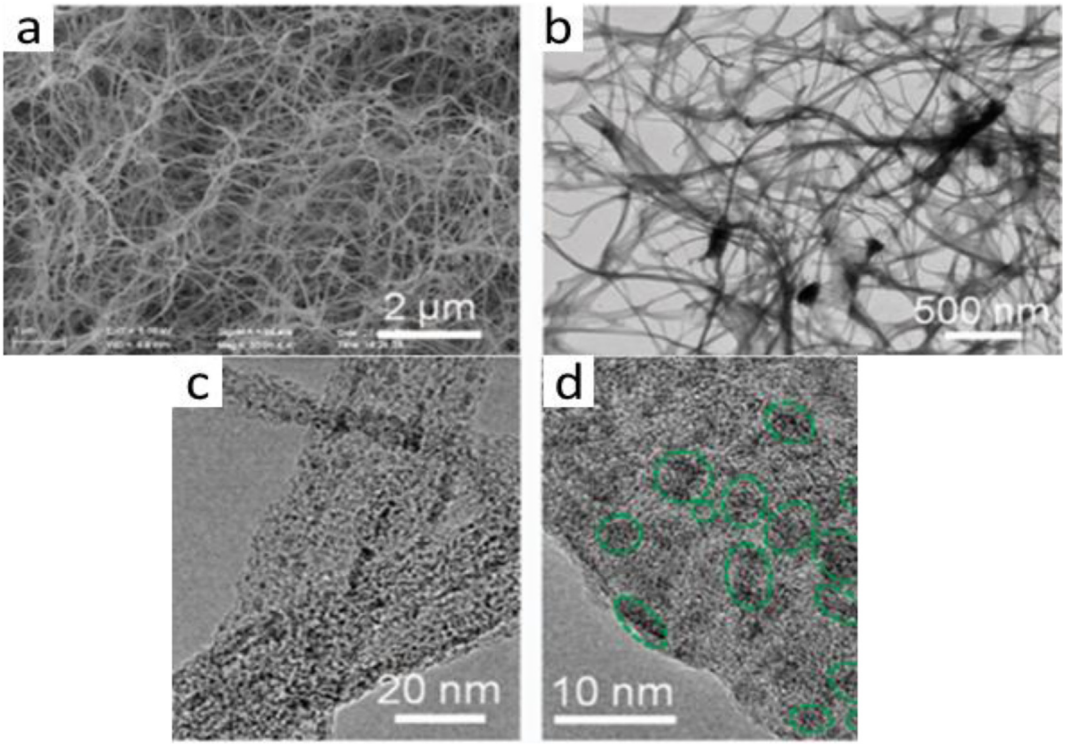

Fig. 10 – Characterization of Mo_2C@N-CNFs electrocatalysts. (a) SEM, (b–d) TEM images. Reprinted with permission from Wu et al. [85] ©2016, Nature Portfolio.

Green synthesis by other methodologies

The Mo-NPs are also synthesized by adopting various other methodologies like chemical reduction, hydrothermal and solvo-thermal methods. In this respect, Ho et al. reported an efficient, scalable, safe cost-effective fabrication of G/MoO_3 composite and its application in supercapacitors as an electrode material. MoO_3 with significant charge density pose to be the best candidate for catalysis as well as for electrode material. In this work, the R.A is ethylene glycol, and it was previously used for synthesis of many other nanostructured materials like Pt, Au and Ag. The structural studies revealed the spherical shape of MoO_3 NPs. According to cyclic voltammetry curves, the more significant current more will be the capacitance (148 F g^{-1}) of the hybrid material in Na_2SO_3 electrolyte [86]. Fang et al. reported a green and simple approach to fabricate NPs of alpha MoO_3 via hydrothermal degradation and condensation of peroxomolybdic acid. This green route towards NPs synthesis was facile due to avoidance of precipitation of catalysts/reagents and use of easily available precursors. The controlled morphology and crystallinity of nanostructured alpha MoO_3 was analyzed with different techniques (SEM, TEM, FTIR and HT-TEM) and NPs with 300 nm width, 10 μm length have been synthesized [87]. The solution based strategy, in which breakdown of metal complexes with protective agents (amines and carboxylic acids) takes place, can be utilized to prepare iron-Mo-NPs within 3–14 nm range under different experimental conditions and further employed as an efficient catalyst for the growth of carbon nanotubes [88].

Microwave irradiation as a simple, fast and power saving methodology was developed for production of MoO_3 in ionic liquids from metal carbonyls under an inert atmosphere provided by argon [89]. Results indicated preparation of small uniform Mo-NPs of 5 nm without any kind of protective or stabilizing agent. In addition, the Mo-NPs in ionic liquids acted as a reproducible hydrogenation catalyst, which was responsible for the conversion of cyclohexene into cyclohexane. Graphene MoO_3 composites had been also prepared using a hydrothermal process and this material was characterized as a supercapacitor electrode [90]. In this process, precursors were graphene oxide and ammonium molybdate while reducing agent was acetic acid. All these reagents were non-toxic to living organisms including human and aquatic life. According to the SEM image, the combination ratio of 1:12 existed between ammonium molybdate and GO. In the Raman spectrum, there were different peaks obtained at various values corresponding to stretching and bending of terminal Mo to oxygen bond. The synthesis of composite was confirmed by visibility of peaks of both the components (GO and $(NH_4)_2$ MoO_4) at same time.

Guo et al. proposed a convenient approach to synthesize ultrafine Mo_2C NPs in average sizes of 3–4 nm embedded in porous N-doped carbon material calcined from bimetallic ZnMo-MI (MI = 2-methylimidazole). The crystalline hybrid metal-organic framework of ZnMo-MI was fabricated from zeolitic imidazolate framework of Zn-MI precursors via solvothermal reaction [91]. In another research study, the technology has been developed to form NPs of Mo and tungsten disulfide solid solution through chemical deposition with the help of

aerosol from the gas phase. Unlike traditional methods of forming such solid solutions with oxide sulfurization methods, this technology allows the acquisition of NPs in gas flow with the ability to control the particle size and composition. Single source precursor thiotungstate and ammonium thiomolybdate are used, their ratio defines the ratio of metals in NPs. Particle size control is available through the initial solution concentration variation [92]. In a similar study, WMo nanopowders were prepared by sol-gel synthesis method. The phase distribution of the powders with reduction and calcination at different temperatures was analyzed to determine the effect of temperature on the reaction process. Then, the calcined powders were further analyzed by differential thermal analysis (DSC) and thermogravimetric analysis (TGA). The grain size, powder morphology and phase composition of the resulted WMo NPs have been characterized by SEM, TEM, XRD and EDS [93].

Chen et al. reported one-pot fabrication of MoS_2@n-C@$CoFe_2O_4$ hybrid and explored the performance of electromagnetic (EM) absorption by this composite. The hybrid constituted a MoS_2 NPs along with carbon hybrid, which was doped with nitrogen and then grafted over NPs of cobalt ferrite. The one-pot process was environmentally benign and absence of heavy metal ions in reaction system. Various characterization tools were employed to investigate elemental composition, crystalline form, structure, functional moieties, and stability and absorbance wave of EM. The optimized absorbance performance was attained at high annealing temperature 600°C. The reflection curve disclosed remarkable absorbance of EM wave with minimum loss of −46.7 dB with thickness value of 2.4 mm. This response is attributed to interfacial polarization, relaxation and electromagnetic matching. The morphological aspects revealed out plump appearance and cladding of MoS_2 nanosheets by N-doped $CoFe_2O_4$ and carbon [47]. The Mo-oxide nanostructures had also been successfully prepared though simple sol-gel approach and its impacts on germination of seeds (*Vigna unguiculata*) are also evaluated. The shape, morphology, size of as-synthesized MoO_3 nanostructure was characterized via certain tools such as XRD, FTIR and SEM at different 5, 3 and 1 μm scales as shown in Fig. 11. The uniform even distribution, smooth surface and hexagonal shape of MoO_3 NPs was revealed via SEM analysis. The crystal structure was determined via XRD technique and confirmed its orthorhombic structure which was in complete agreement with the JCPDS 35–0609. Results showed that MoO_3 NPs restricted the germination and growth of *Vigna unguiculata* [94].

Energy applications of Mo-NPs

With the increasing demand of energy, the production of clean and sustainable energy has attained much importance to overcome impacts of fossil fuels overuse on the environment. Fuel cells are regarded as a promising source of power generation based upon their operating reliability and environmental sustainability. Hydrogen is one of the green sources of energy that has positive impacts on the environment and ultimately to human health. Mo-oxides have a wide range of applications (as shown in Fig. 12.), in various fields especially in catalysis based upon its unique electrical, electrochemical, and optical properties.

Hydrogen catalytic generation

Hydrogen energy is the basic need of industrial, aquatic and human life [95,96]. As compared to other energy sources (solar energy, hydrothermal energy, wind energy etc.), hydrogen energy is more useful due to its significant energy on the basis of mass, facile transportation in the form of natural gas, non-toxic nature and applications in various fields like electricity generation, synthesis of ammonia, electronic industry, automobiles etc. [2,97–99]. Various methodologies including auto-thermal decomposition of methane, reforming of hydrocarbons, decomposition of water, solar based electrolysis and many others were applied for the generation of hydrogen [97,99–102].

Numerous research works have been carried out on transition metal alloys [103,104], complexes and their hybrids like metal sulfides, carbides, nitrides and phosphides as an electro-catalysts for generation of hydrogen [105,106]. In catalysis history, the most promising catalyst for hydrogen evolution reaction (HER) is platinum-based compound with its fast kinetics at minimum potential [107–109]. But the use of noble metals as electro-catalyst is very costly, therefore

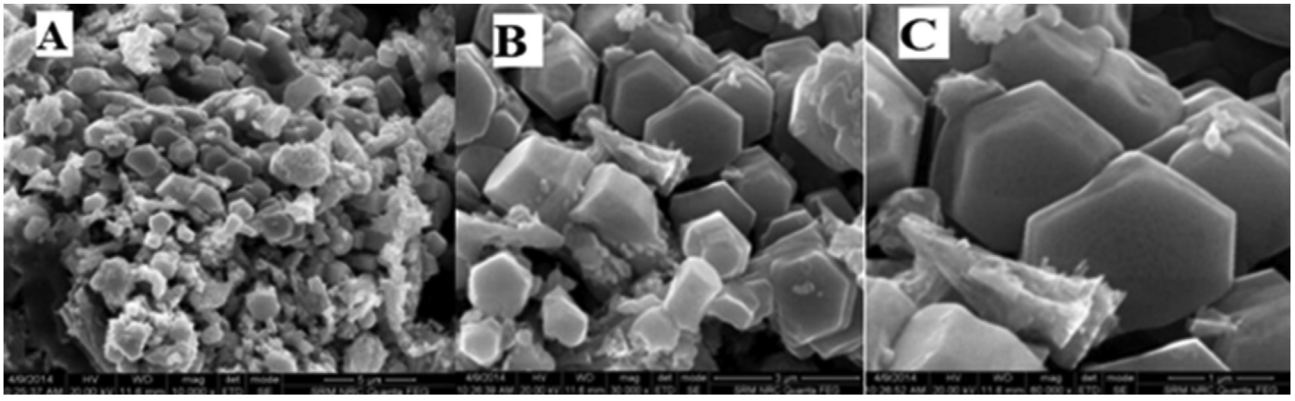

Fig. 11 – SEM micrograph of MoO3 at (A) 5 μm scale (B) 3 μm scale (C) 1 μm scale. Reprinted with permission from Kanneganti et al. [94] ©2014.

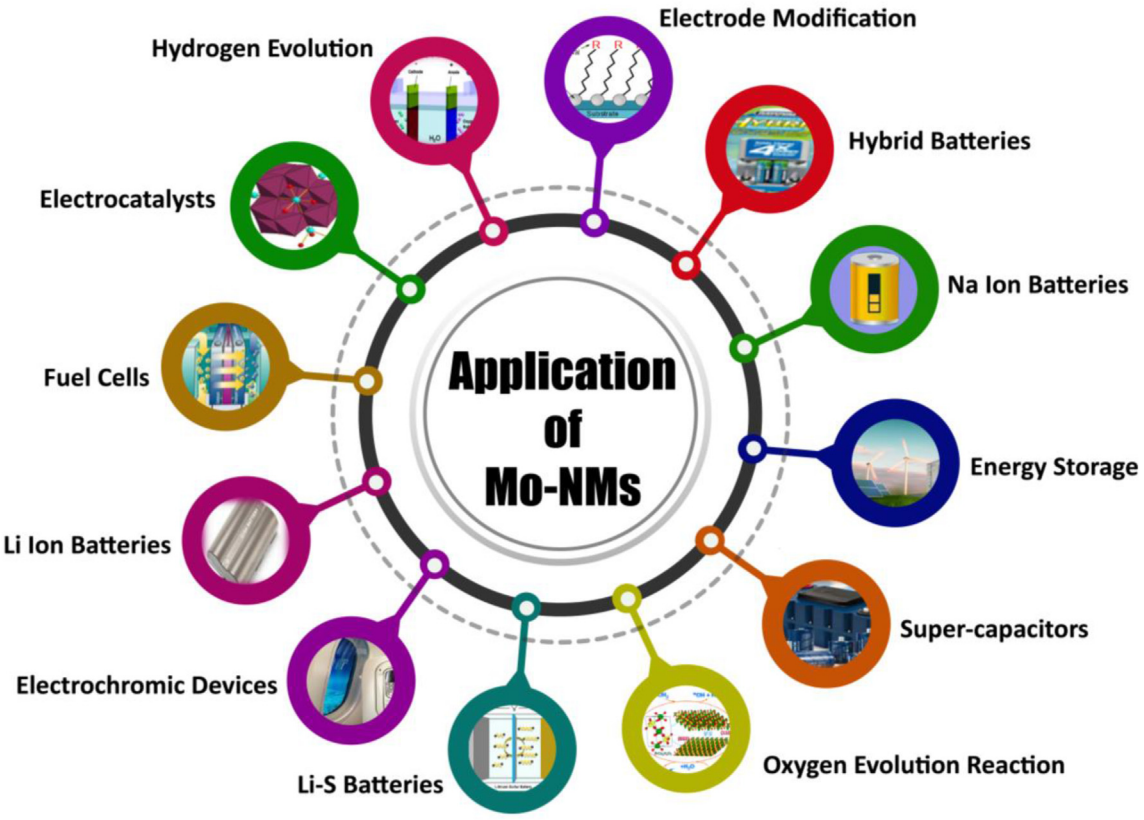

Fig. 12 – Applications of Mo-NPs in energy conversion and energy storage devices.

researchers continue their work on the development of non-noble metal catalysts for HER [109]. For example, Fig. 13 shows the synthesis of CoP/$MoSe_2$ composites, suitable as catalyst for hydrogen generation. In this method, the nano-sheets of $MoSe_2$ were synthesized by the method of chemical exfoliation, and then sonicated with the CoP NPs to form the composite. This successful exfoliation of $MoSe_2$ nanosheets was investigated by XRD and the Raman spectroscopic analysis, which was very consistent with earlier reports.

Mo_2C is the most commonly used catalyst for HER in four following ways: (1) steam decomposition of methanol (2) reforming of methane (3) WGS reaction (4) evolution of hydrogen from different reactions. The effective strategy for synthesis of hydrogen is "DRM" in which reaction is carried out in presence of cost effective Mo_2C to give carbon mono-oxide and hydrogen [71,97,111]. According to Darujati and Thomson the catalytic activity of Mo_2C towards DRM is diminished rapidly due to oxidative effect of CO_2 [112]. Therefore, it is essential to enhance Mo_2C stability via doping of metal over it. It has been shown that doping of Ni over Mo_2C catalyst causes increment in decomposition of methane molecules which ultimately leads to the maximum stability and significant activity towards conversion of CH_4 and CO_2 into H_2 and CO [97]. J. Cheng and Huang reported synthesis of cobalt modified Mo_2C catalyst via the temperature-program reaction process and further studied its application in DRM. Results indicated that stability and activity was increased up to such a level that 90% of CH_4 conversion was completed without any sort of deactivation within a few hours [113].

At present, the safest and cost effective way to generate commercial hydrogen is SRM (steam reforming of methanol) [114,115]. This process has some advantages like (a) under normal conditions, methanol exist in liquid state (b) 200–400°C is activation temperature of methanol (c) high C:H ratio (d) deposition of carbon content on catalyst surface is reduced due to absence of C–C bond (e) no sulfur content. Szizybalski et al. synthesized Mo_2C through carburization of molybdenum tri-oxide and further investigated its application in hydrogen evolution [116]. MoC_2 modified with metals of 4th period (Co, Ni and Fe) have been synthesized by TPRe process along with methane-hydrogen mixture at a temperature of 200–400°C for SRM reaction [117]. The enhancement in catalytic performance of Mo_2C towards HER, by converting methane into hydrogen and carbon mono-oxide, is due to the loading of nickel over it [118]. This loading is responsible for creation of an active site, which in turn inhibits deactivation. According to Ma et al. there is a positive impact of copper loading on stability and activity of Cu-Mo_xC_y catalyst towards SRM reaction and ultimately towards generation of hydrogen. It has been further explored the synthesis of Mo_2C modified with noble metals especially platinum and also explained its significant activity in terms of 100% methanol conversion with utmost durability at lowest temperature of 200°C [119].

An efficient method of hydrogen generation is the "Water-gas shift" method which uses gasification of biomass and reforming of hydrocarbons as a source of CO. Thompson reported fabrication of platinum modified Mo_xC_y via wet impregnation process to explore its catalytic activity towards

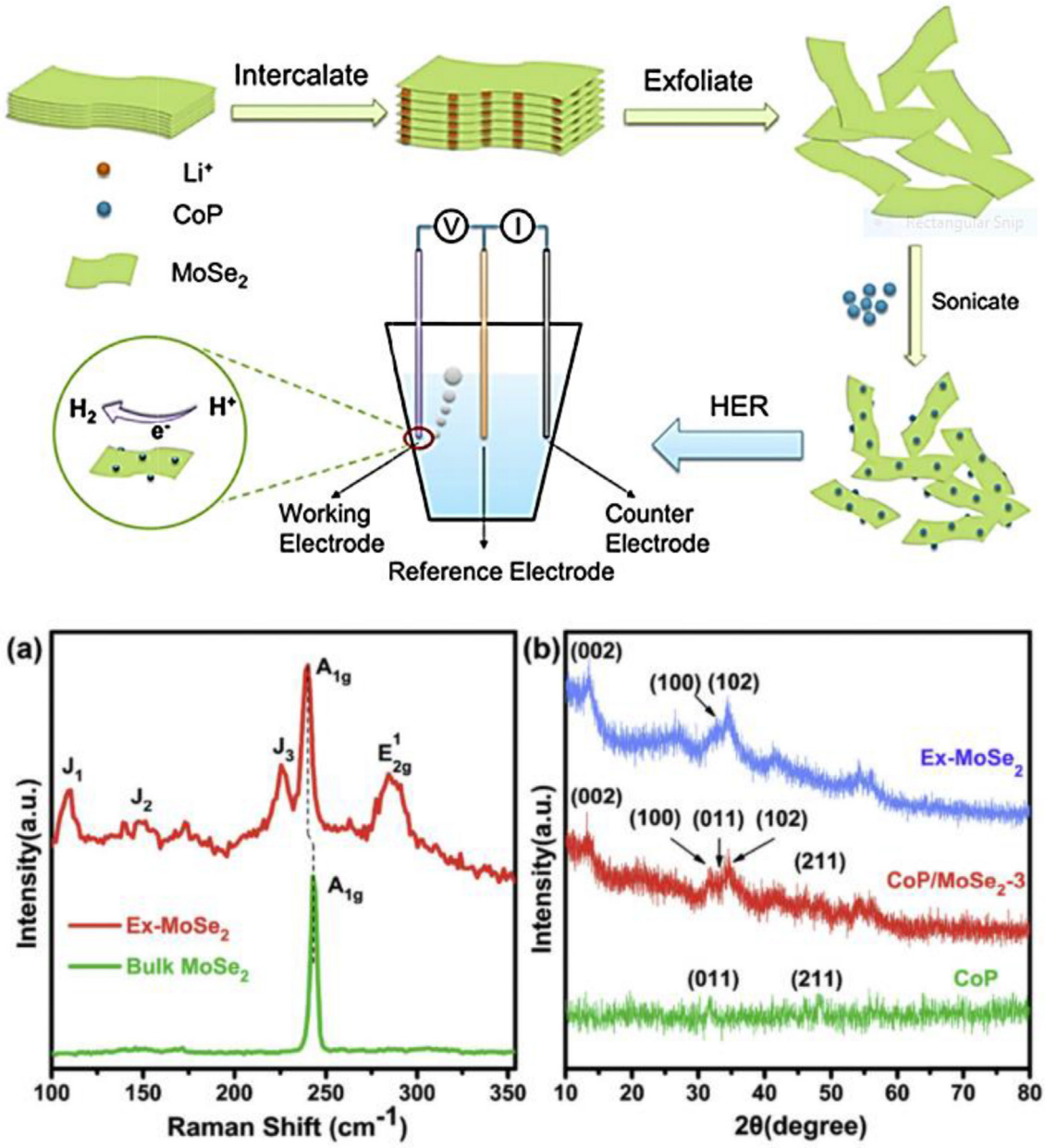

Fig. 13 – (A) Illustration of the synthesis of $CoP/MoSe_2$ composite and it's HER. (a) The Raman spectrum of exfoliated $MoSe_2$ and bulk $MoSe_2$, (b) the XRD patterns of exfoliated $MoSe_2$, $CoP/MoSe_2$-3 composite and CoP NPs. Reprinted with permission from Ding et al. [110] ©2018, Elsevier.

evolution of hydrogen by WGS reaction [120]. Hydrogen has been also produced via WGS reaction by employing cobalt modified Mo_2C as a catalyst in TPRe method [121].

According to Vrubel and Hu the most promising catalyst for evolution of hydrogen in the whole pH range (0–14) is Mo_2C, without any significant change in its working ability [122]. The significant increment in catalytic performance of Mo_2C is to support it on CNT [123]. Nano-porous MoC_2 is fabricated by the decomposition of hybrid precursors of amine and molybdenum oxide. The decomposition or breakdown of ammonia is an efficient way to produce hydrogen utilizing a Mo-carbide catalyst. Kaewpanha et al. showed synthesis of biomass supported MoC_2 from MoO_3 utilizing solid state reaction for hydrogen generation [124]. According to Koós and Solymosi carbon-supported Mo_2C is another catalyst required for HER which in turn is produced by the catalytic breakdown of formic acid [125]. In another research study, cobalt disulfide-molybdenum disulfide nanocomposite supported by nitrogendoped reduced graphene oxide and multiwalled carbon nanotubes (CoS_2/MoS_2@NrGO-MWCNT) was reported as an excellent electrocatalyst for HER. Ternary hybrids and CoS_2/MoS_2@N-rGO-MWCNT composed of CoS_2, N-rGO/MWCNT and MoS_2 were investigated. The electrocatalysts were synthesized by a facile hydrothermal method. It was found that the

co-existence of MoS_2, CoS_2 brings incorporation of MWCNT offered stability and abundant active sites. The results suggested catalyst as a viable alternate for HER [126].

In another research study, Laszczyńska examined the catalytic activity for the HER of the electrodeposited Ni–Mo/WC composites in 1 M KOH solution. The surface morphology, surface composition and structure were investigated using SEM, XRD and X-ray photoelectron spectroscopy. The electrocatalytic activities for the HER were evaluated based on cyclic voltammetry, electrochemical impedance, chronopotentiometry methods and cathodic polarization. The results showed that Ni–Mo/WC composites have an effective catalytic activity for HER [127]. In order to significantly achieve long-time working stability and increase the number of active sites, the design of hybrid-type electrodes is essential. Therefore, Ramanavičius et al. reported the synthesis of a new hybrid material composed of molybdenum oxides and molybdenum disulfides that are heterostructured with strontium molybdate. Considerable higher catalytic activity at the surface of this hybrid film, a Tafel slope of 66 mV dec^{-1} attaining ~80 mA cm^{-2}, with the onset potential of 190 mV *vs* RHE at 0.35 V overvoltage was ascertained. An exciting HER stability in comparison with the pure synthetic MoS_2 was evaluated and verified by prolonged potential cycling from 0.05 to −0.35 V *vs* RHE potential at a constant current density [128]. In a similar study, the well-dispersed and ultra-small Mo_2C NPs anchored on 2D carbon nanosheets were prepared by following pyrolysis and designing chelate precursor, which was proved to be an efficient approach for fabricating carbon-loaded Mo_2C NPs. The as-obtained Mo_2C/C material exhibited outstanding stability and activity in HER. It needs an overpotential of 147 mV to drive 10 mA cm^{-2} implying that Mo_2C/C nanomaterial will be a potential noble metal-free electrocatalyst for the HER [49].

Huang et al. synthesized Mo_2C nanosheets that were coated with 2- dimensional Mo-sulfide by carbonaceous material and applied in the generation of hydrogen by water catalysis. In this methodology, the source of Mo (MoS_2) was exfoliated followed by carburization towards preparation of Mo_2C. The catalytic activity of CNT encapsulated MoC_2 nanosheets was described by electrochemical measurements that were performed in H_2SO_4. Tafel slope of 58.7 mV dec^{-1} represented best HER performance as compared to commercial and downside MoC_2. This effect was attributed to the simultaneous adsorption and desorption of protons. EIS of 208.1 mV, EGSA of 2.63 mF cm^{-2} and long-term stability in acidic solution made U–Mo, the best candidate for catalytic behavior as compared to C–Mo and D-Mo [129]. Another study reported on the use of carbon microflower dispersed 3 nm Mo_2C as an effective catalyst for HER [130]. The increment in catalytic activity of Mo_2C for HER was observed due to the incorporation of iron into its crystal lattice [131]. Lin et al. studied template assisted synthesis of MoC–Mo_2C nanowires and their role as an efficient catalyst in generation of hydrogen [85].

Another source of evolution of hydrogen is transition metal NPs, but this is not as effective because its high temperature annealing strategy results in sintering of particles. To overcome this, the starting materials of all metals (PMo_{12} for Mo, melamine for C and phytic acid for P) should exhibits strong interaction that results in large surface area, significant porosity and excellent robustness and ultimately leads to dispersion of particles on carbonaceous support at high temperature without sintering of particles [132]. Electrochemical studies represent the efficient catalytic activity of final products (MoPS and MoP) with the current density of 10 mA/cm^2 at potential of 158 mV in alkaline media and 92 mV in acidic media. The decrease in overpotential from 120 to 92 mV and 170 to 158 mV is because of sulfur doping in controlled amounts.

According to Ren et al. Mo based nanomaterials are an efficient catalyst for hydrogen production as compared to many other catalysts (IrO_2, Pt, and RuO_2) or many other methodologies including chemical water splitting [133]. Because of the structure, excellent performance in pH 1–14, conductivity and structural stability, Mo based NPs are significantly enhanced by their coupling with carbon sheets. The Mo-NPs, which are used for this purpose namely: Mo_2C, Mo-phosphide and Mo-sulfide. These NPs and N & P doped CNS act like the best electrode for enhancement in HER performance. There is remarkable interaction developed between carbon nano sheets and Mo-NPs on the behalf of carbonization (Mo_2C) sulphonization (Mo_2S) and phosphorization (MoP). The resulting Mo-hybrids (MoP@NPCS) exhibit better catalytic activity for HER as compared to the simple Mo based nanostructured material due to certain reasons (1) carbon texture avoid accumulation of Mo based NPs (2) porosity of CNS (3) space for charge transfer (4) operating stability of catalyst (5) contact between Mo based NPs and heteroatom doped CNS [134–136]. Another method developed for the fabrication of two dimensional (2D) Mo_2C NS and their application in the production of hydrogen [137], compares the catalytic activities of both single-layered as well as multilayered Mo_2C nano-sheets. Different methods have already been reported for the synthesis of 2D Mo_2C but these are not useful on a large scale due to their complexity. Thus, there is a method, in which a layered oxide precursor (MoO_3) is exfoliated and centrifuged. Single layered Mo_2C nanosheets pretend to be a more efficient catalyst for hydrogen evolution reaction as compared to multilayered Mo_2C. This is because of surface area values (293 m^2/g for single layered and 2.6 m^2/g for multilayered) confirmed by physiosorption isotherm. Electrochemical studies also reveal the mass activity of single layered (59.3 ± 6 mA/mg) is higher than multilayered (5.3 ± 2 mA/mg) which shows its more active surface (increased number of active sites and significant binding energy) towards hydrogen production/generation reaction [138,139].

In another method, MoC/Mo_2C nanowires with an overpotential of 38 mV and long-term durability were synthesized by carbonization of Mo-species under controlled conditions. By template engaged strategy, beta Mo_2C NT were synthesized and showed reproducible results (82 mV overpotential at 0 pH) due to unique morphology of catalyst, rapid transfer of charge and specific surface area. Recently, carbon nanotubes especially single walled are used to modify Mo_2C NPs which lead to an increment in their catalytic activity towards generation of hydrogen on large scale [140]. The rigidity of carbon nanotubes (CNTs) can cause physical and abrasive damage, even under controlled conditions, to the NPs and upon exposure to air, Mo_2C is oxidized. Therefore, it is better to disperse Mo-NPs into the inner surface of single walled CNTs. Compared to

the exterior located MoC NPs in SWCNTs, interior ones show small Tafel slope and lower potential. This response is attributed towards confinement of interior dispersion of MoC NPS in SWCNTs that avoid agglomeration of Mo-NPs, smaller particle size of 2.9 nm and large surface area of 467 m^2/g. The fabricated hybrid catalyst is useful for HER even in acidic medium. Additionally, there is another factor responsible for excellent catalytic performance: the minimum adsorption of hydrogen on a confined surface.

Recently, Chai et al. reported a cost effective and facile synthesis of Mo_2C NPs that are deposited onto the nitrogen doped carbon polyhedron via metal organic framework (MOF) assisted synthesis and illustrate their potential application in HER. In this work, an excellent increment in catalytic activity of Mo_2C (Fig. 14) is observed while utilizing porous MOF and N-doped C matrix due to adsorption of proton. The Mo_2C@HCNPs within particle size range of 800–900 nm are prepared through (a) calcination of starting materials to get polyhedron (b) implantation of MOF on polyhedron surface (c) breakdown of AM/ZnO@MOF (d) wrapping of polyhedron with Mo-NPs. The fabricated Mo_2C@HCNPs with onset over-potential possess remarkable activity over all pH ranges in basic as well as in acidic medium. Additionally, in order to achieve stability, reproducibility and specified current up to 10 mA cm^{-2}, this composite requires overpotential of 87 and 89 mV in basic (0.1 M KOH) and acidic (0.1 M H_2SO_4) medium respectively. Such striking response is attributed due to porosity of Mo-NPs and interaction between nitrogen, carbon of hetero structure and that of Mo_2C NPs [141].

Carbon based materials (graphene and CNTs) are also known as efficient catalysts in hydrogen production reaction for energy storage due to their stability, specific surface area and sustainability [142–144]. Carbon nano-horns with great conductivity, efficient pore size and intimate stability have attained great attention in various fields especially as a catalyst in energy storage application [145,146]. The combination of MoS_2 and carbon compounds have showed enhanced catalytic activity towards HER as compared to MoS_2 due to synergistic effect between Mo-NPs and the carbon compound [147]. Noble metal NPs are also known for their electro-activity and their activity is increased by carbon based compounds [148]. Devadas et al. fabricated Mo-sulfide, carbon nanohorns supported Mo-sulfide, hybrid of carbon nanohorns and palladium NPs stabilized with poly-dopamine via hydrothermal and chemical methods. The functionality of MoS_2 towards HER was compared with CNH/MoS_2 and results revealed better performance of CNH/MoS_2 over the other ones (−185 mV at 10 mA cm^2) due to least starting potential of −165 mV at increased current of 10 mA cm^2 as well as least Tafel slope value of 86 mV dec^{-1}. However, this MoS_2 composite was not so better electro-catalyst than the other composite of noble metal. The encapsulated palladium NPs in polydopamine were anchored on CNH to give PDA-Pd/CNH. PDA acted as a size controlling and protecting agent of Pd NPs from accumulation. PDA-Pd/CNH with Tafel slope of 61 mV dec^{-1} produced hydrogen more efficiently than PDA-Pd with Tafel slope of 111 mV dec^{-1}. The defective carbon was responsible for hydrogen generation and this active site for HER was blocked by Mo sheets and lead to agglomeration of particles. More active sites blocked least synergistic effect least hydrogen generation. Results revealed onset and over potential of CNH/MoS_2 (−165 and −246 mV) and PDA-Pd/CNH (−6 and −124 mV). That is why CNH/MoS_2 could not be the better electro-catalyst for HER than PDA-Pd/CNH. Moreover, PDA-Pd/CNH exhibited remarkable durability and long-term stability [149].

Xing et al. synthesized cost effective and non-noble metal catalyst "Carbon doped Mo_2C@N-doped CNT" for electrocatalysis of water by using ammonium molybdate and C_3N_4 as Mo and carbon source respectively. This nano-composite was grafted on 3D nickel foam by hydrothermal method followed by carburization at high temperature Mo_xCo_y@N-CNSs/CNTs with extra-ordinary structure, 3D conductivity and effective electron transfer rate display excellent performance towards OER and HER in basic medium. This optimized Mo_xCo_y@N-CNSs/CNTs catalyst represented power output of 10 mA cm^{-2} and least voltage of 1.63 V at over-potential of 300 mV and 99 mV for OER and HER respectively [150].

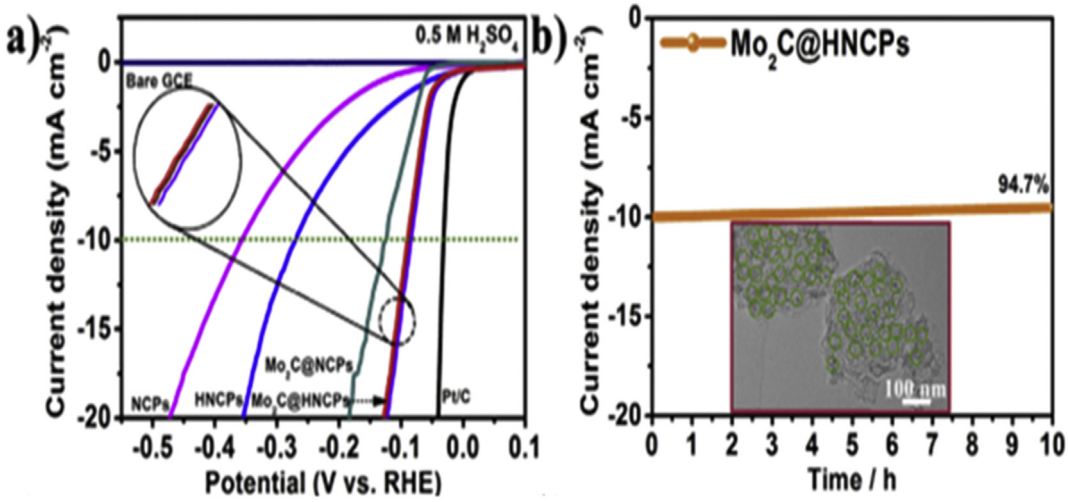

Fig. 14 – (a) LSV curves, (b) Chronoamperometry curves of Mo_2C@HNCPs. Reprinted with permission from Chai et al. [141] ©2019, Elsevier.

Tao et al. reported an effective and environmentally benign method for fabrication of Mo_2C and further applied it for production of hydrogen utilizing N-doped carbon as a substrate. Characterization studies displayed the beneficial impact of nitrogen in terms of best electro-catalytic response towards HER. By viewing results obtained from TEM, it was inferred that Mo_2C NPs were uniformly distributed over N-doped carbon substrates. By varying the ratio of glucosamine hydrochloride and glucose, the content of nitrogen was being adjusted. The optimized ratio of G/GH was 0.6 at which Mo_2C/NC-0.6 displays current density of 10 mA cm^{-2} at an overpotential of 168 mV and the value of Tafel slope, at starting potential of 95 mV was, 79.2mVdec^{-1}. The prepared composite exhibited significant electro-catalytic activity towards HER due to the presence of numerous active sites, conductive carbonaceous substrate, interactions between nitrogen and Mo_2C species and the large surface area. Rozenfeld et al. investigated synthesis and application of MoS_2 electrode in microbial electrochemical cells for production of hydrogen. Exfoliated method was used to fabricate Mo-disulfide electrode via intercalation of lithium ions. Different physical, chemical and electrochemical techniques were used to analyze exfoliated MoS_2 anode material. The kinetics of hydrogen production depended upon the anode material used. The resultant particle size was in the range of 200 ± 50 nm. LSV showed the power density of MoS_2-EF higher than platinum in phosphate buffer solution and opposite response was observed in 0.5 M acidic solution. The rate of hydrogen production for MoS_2-EF and Pt were 0.083 and 0.133 $m^3d^{-1}m^{-3}$ respectively [151]. Information on the morphology, surface area, onset potential, Tafel slope and current densities of Mo-NPs based various electrocatalysts is summarized in Table 1. Overall, an excellent increment in catalytic activity of Mo-NPs (Mo_2C) is observed, while utilizing porous MOF and N-doped C matrix due to adsorption of proton. The Mo_2C@HCNPs within particle size range of 800–900 nm are prepared [141].

Oxygen evolution reaction

The rapid increase in environmental pollution problems associated with the energy consumption from fossil fuels have led to extensive research to find renewable alternatives. The electrically powered water splitting is considered an associated path to environmentally friendly and sustainable process for hydrogen generation as this process is usually combined with energy from sustainable energy sources such as solar and wind. However, this perception is still to be achieved, as the response of two half-cells splitting into two parts, including the hydrogen evolution reaction (HER) at the cathode and the oxygen evolution reaction (OER) at the anode suffer from dynamic overpotentials and thus improving efficient energy conversion efficiency requires effective electrocatalysts. Therefore, Mo_2C based electrocatalysts, namely Mo_2C NPs (CoxMoy@NC) possess a long-term stability and high activity for electrocatalyzing both the OER and HER

Table 1 – Mo-NPs as a catalyst for hydrogen evolution reaction.

Morphology	Electro-catalyst	S_{BET} (m^2/g)/surface area	Onset potential of H_2-generation (mV)	Tafel slopes (mV/dec)	Current density (mA cm^{-2})	Ref.
Hexagonal and uniformly dispersed	Mo_2C@NCS	101	−92	78	10	[133]
Size: ~5 nm	MoS_2@NSCS	123	−79	82	10	
	MoP@NPCS	2.6	10.7	183	10	
Layered nano-sheets	Single-layered Mo_2C	2.6	10.7	~70	–	[137]
~1.5 nm (single)	Multi-layered Mo_2C	293	24.1	~70		
Hexagonal and unique hollow	Mo_2C@HNCPs	512	–	49	10	[141]
Size: 800–900 nm	Mo_2C@NCPs	68.20		84	10	
Uniform, Spherical	Mo_2C@NC	79.4	330 pH: 7.0	99	10	[152]
Size: 80–100 nm	Mo_2C/MoP@NPC	104.5	228 pH: 7.0	75	10	
Hierarchical nano-tubes	MoCx/SWNTs	406	82	162	10	[140]
Size: 1.0–4.0 nm	MoCx@SWNTs	467	345	115	10	
Flake/sheet-like	MoS_2	–	185	92	10	[149]
Size: 100 nm	MoS_2/CNH		165	86	10	
Nanosheets	UeMo	–	0.332 to 0.168 V	58.7	10	[129]
Size: 10–200 nm	DeMo			67.3	10	
	CeMo			84.5	10	
Hexagonal	Mo_2C@N-CNFs	81.98	−0.7 V	70.0	10	[85]
Size: <5 nm						
Size: 200 ± 50 nm	(MoS_2-EF)	–	0.3–0.9 V pH: 8	–	12.67	[151]
Size: 12, 15 and 29 nm respectively.	10% wt Mo_2C/C	389	pH: 2.3 to 7	110	56–58	[153]
	20% wt Mo_2C/C	348	30–70 °C	92	56–58	
	50% wt Mo_2C/C	264		82	56–58	
Well-defined hexagonal nanowire	nw-W_2MoC	44	0.26–0.61	53	80	[154]
Size: 15–20 nm	nw-W_4MoC	44		52	80	
Bulk micro-structures	Mo_2C/GCSs	–	120 mV	62.6	12.5×10^{-3}	[84]
Size: 5–23 nm						
Bulk micro-structures	Mo_2C NTs	82 mV	–	62	1.7×10^{-2}	[155]
Size: 50–500 nm						

process. In addition, CoxMoy@NC offers good performance towards the overall splitting of water in basic solutions. The observed catalytic characteristic will be attributed to the high conductivity of each element in the CoxMoy@NC [156]. Kim et al. reported a new strategy to promote electrochemical OER on the surface of cobalt (Co) by adding Co to Mo_2C. Chemically coupled Mo_2C NPs and Co were synthesized through heat treatment of the mixture of graphitic carbon nitride and Mo and Co precursors. This study provides a novel way to create a new class of promising substances for OER in alkaline electrolysis through basic research [157]. Tariq et al. used a facile hydrothermal method and reported a mixed oxide composite of iridium and Mo-oxides beneficial for OER phenomenon. Tafel slope was obtained as 57 mV dec^{-1} as compared to 77 mV dec^{-1} for IrO_2 composites, respectively synthesized under the same conditions. This research opened a new venue for the applications of Mo-oxides in the field of electrochemistry. This will be very helpful in overall processes of water splitting in future [158]. Dymerska et al. fabricated $MoSe_2$ functionalized with Co/Ni particles which offer good electrochemical performance in HER and OER due to their unique physicochemical properties. These electrolytic reactions are usually essential for electrochemical energy storage [159]. Ji et al. reported transition metal-based electrocatalysts with their comparable durability, electrocatalytic properties and low cost for OER. 79% of current density retention and Tafel slope as 64 mV dec^{-1} was obtained during oxidation in the alkaline electrolyte [160]. Anjum et al. synthesized a hybrid (B,N:Mo_2C@BCN) noble metal-free electrocatalyst via an environment friendly organometallic complex of boric acid and Mo-imidazole. The B,N:Mo_2C@BCN showed long-term stability and high activity in basic electrolytes, when used for OER and HER reactions in an alkaline solution [161]. In another study, Wang et al. used a feasible, green and electroless deposition method and fabricated a series of ternary Fe–Mo–B substances with nanochain structure which (Fig. 15) showed a remarkable performance for the OER process [162].

In a similar research study, $NiCo_2O_xS_y$@$NiMoO_4$ was also an efficient electrode for many electrochemical reactions involving the process of OER [163]. Similarly, many other research studies have also revealed that Mo-NPs are very efficient for OER processes [164–169]. Chai et al. described cost-effective Mo_2C NPs with an excellent increment in catalytic activity to generate hydrogen. Ternary Fe–Mo–B substances with nanochain structure showed a remarkable performance for OER process. MoC–Mo_2C/NCNT nano-rod, with overpotential of 0.5 V, and high reversibility, posed to be the stable and highly efficient catalyst for LIBs. Flowers like MoS_2/CNTs composites were responsible for high performance and high sulfur utilization on cathodes of Li–S batteries. The hierarchical MoNPs/NF synthesized via hydrothermal sulfurization, with capacitance of 1.06C cm^{-2} at specific current of 1.0 mA cm^{-2} displayed excellent performance in SCs. Ai reported fabrication of bamboo structured nanotube (Co–Mo_2C@NCNT). This structure was comprised of a carbon nanotube doped with nitrogen and encapsulated with Mo-carbide NPs and cobalt metal. The pyrolysis process was employed to develop and synthesize the material that proved as a stable and well-organized catalyst for OER and by splitting of water. This reaction was carried out in a basic medium. Based upon its significant synergistic interaction in structure and composition, the material (Co–Mo_2C@NCNT) depicted better performance towards OER, HER and water splitting. The material required ~186 and ~377 mV of overpotential with minimum voltage of ~1.628 V in order to obtain current density of magnitude 10 mA cm^{-2} for electrolysis of water to generate oxygen [170].

The Co_3O_4 NPs doped with Mo and grafted over carbon nanotubes (Mo–Co_3O_4/CNTs) is developed for improving OER. The Mo–Co_3O_4/CNTs is prepared through phosphomolybdic acid assisted pyrolysis of CNTs. The as-synthesized material possesses significant OER capacity and maximum durability with a maintained small over potential of 280 mV and onset potential value of 1.42 V at 10 mA cm^{-2}. The wonderful

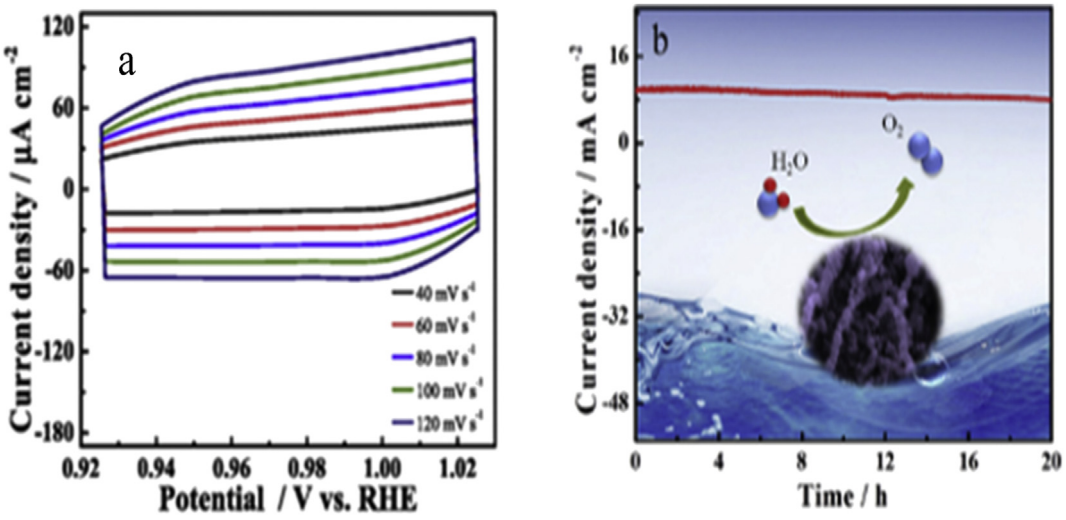

Fig. 15 – (a) CV curves of Fe–Mo–B (FMB) (b) Chronoamperometry test of FMB electrocatalysts. Reprinted with permission from Wang et al. [162] ©2020, Elsevier.

performance is particularly assigned to the doping of Mo regulates the structure and electronic characteristics of Co_3O_4 and established great surface area, large proportion of Co^{2+} binding sites, electrophilic centers and favorable transfer of charge [171]. Rani et al. investigated the role of lanthanum molybdates electrode, the binary oxide, towards the generation of oxygen through electrochemical oxidation of water in a half-cell. The $La_2Mo_2O_7$ electrode showed excellent current of 241 ± 1 mA/g as well as a small 197 mV overpotential at neutral pH 7. The accelerated migration of ions bring out low 59 mV/dec^{-1} Tafel slope value with rapid generation of oxygen [172].

Battery applications

Lithium ion batteries (LIBs)

Due to the increase in energy demand and energy harvesting processes, together with the increase mobility in modern society, the development of energy storage devices has gained much interest. LIBs are an efficient energy storage device due to their significant charge densities. Transition metal oxides and carbides are suitable anode materials for Li^{+1} batteries as compared to the graphite anode material [173,174]. The capability of mixed Mo and V NPs as active anode material for LIB is higher as compared to MoO_2 and VO_2 due to the availability of reduction-oxidation couples [175,176]. $LiVMoO_6$ at current of 0.1 A g^{-1} displays specific capacity of 900 mAh g^{-1} and at specified current of 5 A g^{-1} shows capacity of 285 mAh g^{-1}. Similarly, excellent results were obtained with the composite of vanadium oxide, carbon, and Mo-oxide due to their hybridization and amorphous nature. The hybrid of graphene with Mo-dioxide demonstrates a reversible capacity of 600 mAh g^{-1} at the current of 0.8 A g^{-1}. Bauer et al. synthesized vanadium and Mo-hybrid via hydrothermal flow method and demonstrated their energy applications regarding LIBs. XRD confirms the monoclinic packing of those synthesized hybrid NPs. In Li-ion batteries, the efficient anode performance was shown by the composition ($Mo_{0.5}V_{0.5}O_2$ and $Mo_{0.33}$ $V_{0.67}O_2$) with specific reversible capacities of 200 mAh g^{-1} and 160 mAh g^{-1} at a constant current of 10 A g^{-1} due to their charge storage mechanism. The contribution of a pseudo-capacitive charge was more than 90% of the total charge. The increment in pseudo-capacitive charge leads to the peak broadening in cyclic voltammogram [177].

Ren et al. demonstrated the preparation of 3D flexible foam GF@CNT/MoS_2 and it was employed as effective electrode material in Li^+ ion batteries. This composite was made up of graphene foam and CNTs, GF@CNT and further loaded or modified with Mo-sulfide NPs. This composite was based on three layers: 1) inner graphene layer 2) middle CNTs layer 3) outer MoS_2 layer. There was no need for additional conductive or binding agents with this GF@CNT/MoS_2 foam, in the presence of graphene support material. There were some other merits associated with graphene foam including (a) providing 3D skeleton (b) porosity providing remarkable interaction between the electrode material and the electrolytic solution (c) larger diffusion of Li^+ ions (d) enough space to accommodate MoS_2 NPs changes. The coating of CNTs over graphene foam resulted in facilitated transport of electron/ions. This may be attributed to the conductivity, flexibility, and the mechanical support of CNTs. The loading of MoS_2 NPs GF@CNT over hybrid caused increment in its working capacity/ability. Henceforth, this GF@CNT@MoS_2 anode material showed outstanding performance with a high capacity of 935 mAh g^{-1}, power density of 0.1 A g^{-1} and reversibility at 0.2 A g^{-1} is 606 mAh g^{-1} [178].

It is challenging to develop such a catalyst that would be able to enhance the performance of Li–O_2 batteries with a long duration. An effective catalyst consisting of Mo_2C nanorods and CNTs doped with nitrogen, is made to improve the activity of lithium oxide batteries. This nano-hybrid is fabricated by treating ZIF coated MoO_X NPs with a wet chemical strategy followed by a hydrothermal process. The resultant MoC–Mo_2C/NCNT catalyst exhibits distinguished structure with Mo-carbide crystals and extending NCNT legs. This catalyst possesses high conductivity based upon faster electron transport, which in turn due to the existence of numerous active sites and enough storage space for Li_2O_2, the discharge product. Results showed that this MoC–Mo_2C/NCNT nano-rod pose to be the stable and highly efficient catalyst (Fig. 16) with overpotential of 0.5 V, high specific capacity 34,862 mAh g^{-1} and high reversibility [179].

The effective electro-catalyst with high capacities and great cycling life and minimum over-potential for rechargeable LIB was prepared for the first time by scalable method. This electrode catalyst was composed of MoC_2/carbon hybrid, Ni NPs and nitrogen doped CNTs. The prepared composite (mNi-NCNT-Mo_2C–C) showed excellent performance in terms of reduction and generation of oxygen [180]. Bulusheva et al. investigated the effect of deposition of Mo-sulfide over graphene matrix for enhancing anode performance in Li^+ ion batteries. Different sized MoS_2 NPs were prepared by annealing of MoS_3 at high temperature (up to 1000 °C) and then grafted on multilayered graphene to get MoS_2/graphene composite. HTEM and Raman spectroscopy confirmed that the rise of temperature results in growth of MoS_2 NPs. XPS revealed the successful conversion of Mo-tri-sulfide into di-sulfide under optimized conditions [181].

A novel high performance anode material was fabricated by coupling of tungsten oxide with carbon loaded Mo-trioxide (MoO_3) nanorods [182]. Hydrothermal method is used to synthesize MoO_3/WO_2@C hybrid via encapsulation of MoO_3 with carbon layer, then further decorated with WO_2 NPs, and employed as successful anode material for LIB. This anode material delivers high capacity with cyclic stability due to the combined effect of WO_2 NPs and the amorphous carbon layer.

Palladium doped metallic Mo-disulfide has been reported as a freestanding efficient cathode for high-performance Li–O batteries [183]. Metallic MoS_2 coated with palladium and then anchored on the surface of carbon textiles to fabricate Pd-TMS/CT electrocatalyst. Palladium assistance caused a transformation of hexagonal MoS_2 to stabilize MoS_2 utilizing the redox strategy. 1T-MoS_2 with its unique structure leads to the strikingly improved catalytic behaviour for lithium oxide batteries. This effect is ascribed with fast electron transport, exposed active sites and rapid reaction rates. The synergistic effect of carbon matrix and MoS_2 NPs favor reversible reactions to occur and inhibit side product formation. This electro-catalyst is highly stable with great charge density and cyclic stability up to 2488 h, which make it rendered against unfavorable environmental changes. Huo et al. demonstrated

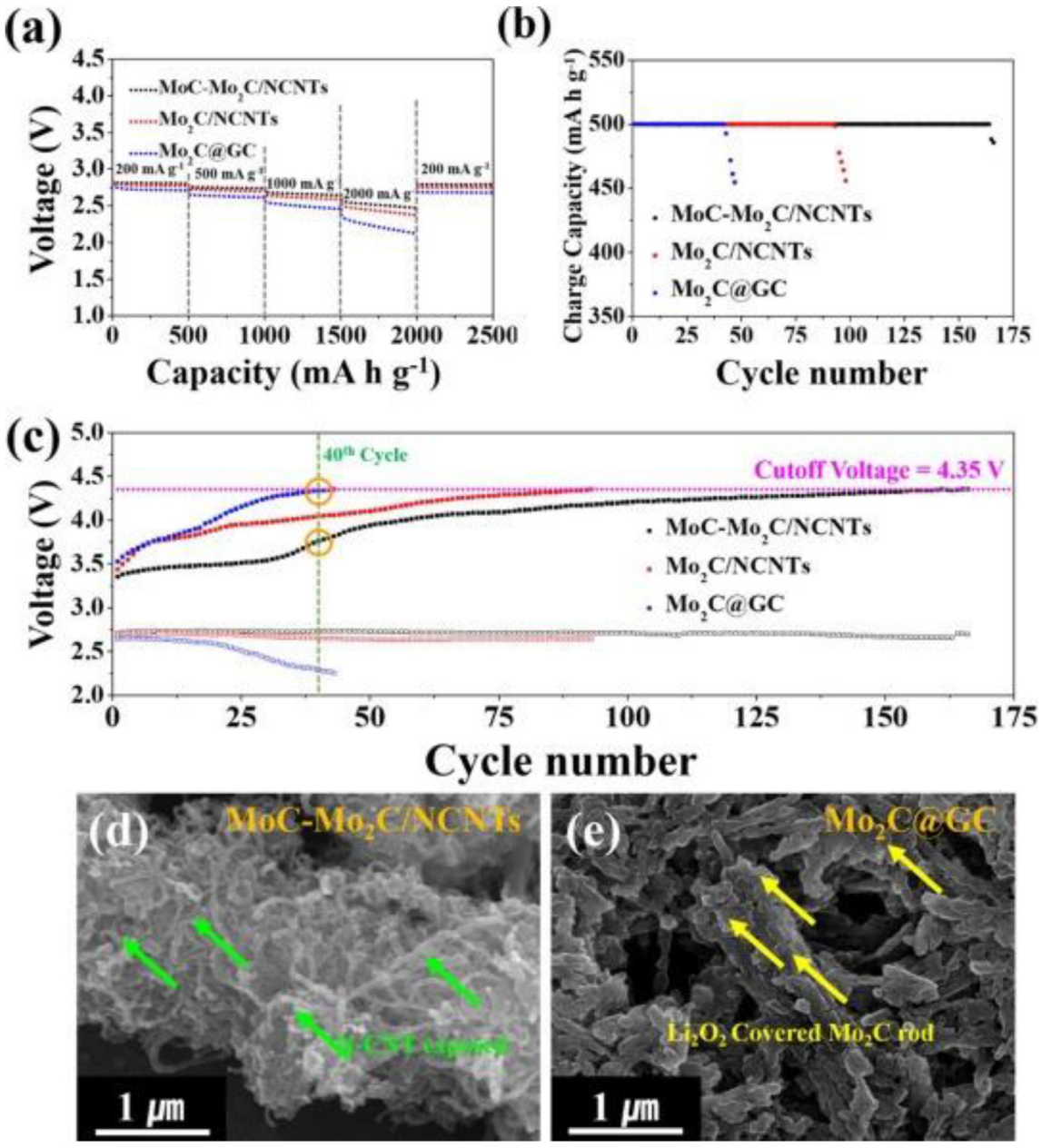

Fig. 16 – Galvanostatic performances of Li–O_2 cells: a) rate performance at different current density, b) cycling performance of the electrodes and c) terminal voltage profiles of the electrodes Corresponding FE-SEM images of d) MoC–Mo_2C/NCNTs and e) Mo_2C@GC. Reprinted with permission from Oh et al. [179] ©2020, Elsevier.

Poly vinyl alcohol induced synthesis of carbon encapsulated Mo dioxide via sol-gel method and its application as anode material in LIB. The prepared micro-composite (MoO_2/C) was highly stable so that it inhibits any sort of changes in its structure during insertion/extraction of MoO_2. In addition, PVA as a source of carbon further enhanced the stability and conductivity due to rapid diffusion of metal ions. The resultant MoO_2/C anode possessed a specific capacity of 610 mAh g^{-1} with the current density of 0.05 A g^{-1} [184].

The effect of the dimensions of carbonaceous support material (0D carbon, 1D CNTs and 2D graphite) on the activity of $MoSe_2$-carbon based nanohybrids were investigated as alternative candidates for anode material in Li- ion batteries [185]. These nanocomposites were fabricated by facile and scalable HEBM (high-energy ball milling) method. The synergistic effect of graphite and $MoSe_2$ causes enhancement in cycling stability and reaction kinetics and ultimately evolves as a high-performance anode. The prepared composite was analyzed by various characterization techniques and results revealed excellent performance for $MoSe_2$-graphite in terms of high reversible capability of 909 $mAhg^{-1}$. This response was attributed to large areas and significant interactions between graphite matrices and $MoSe_2$ NPs. Mo-oxide NPs (1.5–3.5 nm) were dispersed over a carbon matrix which was doped with nitrogen to produce (3D-MoOx@CN composite via chelation followed by hard templating treatment and employed as

anode in LIB [186]. This 3D composite showed high performance in terms of current density of 100 mAg^{-1} along with high capacity of 742 $mAhg^{-1}$ due to porous carbon, binding of MoS_2 onto C-matrix, which in turn avoid aggregation of MoO_x NPs during lithiation/delithiation. An effective anode-material for lithium storage was designed on the basis of modification of $Li_4Ti_5O_{12}$ with Mo dioxide NPs via solution based strategy [187]. Results obtained from characterization of MoO_2– $Li_4Ti_5O_{12}$ revealed uniform distribution of Mo-oxide over $Li_4Ti_5O_{12}$, reduction in polarization of LTO and high storage capacity of Li ions compared with untreated $Li_4Ti_5O_{12}$ complex. Mo-oxide modified LTO complex showed superior performance in terms of high cyclic stability, efficient reversible capacity, and great storage capability. Lou et al. investigated the effect of anchoring of cobalt oxide NPs onto the MoS_2 nanosheets for generating outstanding anode in Li-ion batteries. This nanocomposite MoS_2/Co_3O_4 with smooth distribution of Co_3O_4 NPs was successfully prepared by exfoliation followed by a solution-phase process. The resultant composite was quite flexible in that it facilitates transportation of ions at higher rate and also accommodates contraction/expansion of ions during the cycling process [188].

The anode material for LIB consisting of graphene oxide and Mo-oxide was simultaneously fabricated by ball milling and ultra-sonication strategies. The morphology and structural features of synthesized MoO_3/rGO were investigated by TEM, SEM, XRD and electrochemical techniques. Results revealed excellent performance of composite with great cyclic stability, high columbic efficiency, significant charge density and large storage capacity, based upon ultrafine particles (150–200 nm), diffusion of metal ions, phase purity and surface area [189].

Lee et al. prepared uniform and non-accumulated nanofilm of MoS_2, which was being deposited over carbon cloth (MoS_2@PCC) having pores and this was applied as anode electrode in LIBs. This anode electrode was prepared utilizing set of three processes including dip coating, wire explosion and thermal sulfidation. The variety of carbon content containing explosion media was employed to control phase, texture and morphology of as prepared electrode. The explosion of metallic Mo wire resulted in preparation of solution in which coating of carbon content was performed and uniform particles with zero aggregation were attained with the help of thermal sulfidation treatment. This assisted the transfer of charge and adjustment of volume expansion of activated MoS_2 on cycling. Accordingly, MoS_2@PCC electrode possessed maximum rate capability, durability, recyclability, high reactivity of lithium compared with the MoS_2 NP electrode material [190].

Duan et al. narrated the remarkable stability and high-performance MoO_2/Mo_4O_{11} nanocomposite towards LIBs. The working capability of MoO_2 nanostructures was enhanced with the assistance of lithiated Mo_4O_{11} phase. Annealing treatment had been performed in order to obtain this composite MoO_2/Mo_4O_{11} while reduction of Mo_4O_{11} was carried out to produce MoO_2 NPs by employing urea as reducing agent. In LIB, two-step reaction happened in which first step was intercalation reaction at charging/discharging phase, which was generally followed by conversion reaction. Although, the presence of Mo_4O_{11} phase was responsible for rapid transformation of intercalation reaction to conversion reaction over a complete cycle. The composite MoO_2/Mo_4O_{11} represented maximum specific capability of 400 mAh g−1 and discharge capability of 1113 mAh g^{-1} at 100 mA g^{-1} after 100 cycles. In comparison to this composite, MoO_2 provided 300 mAh g^{-1} in similar condition. The astonishing cyclic stability was corresponded to the rapid transformation of reactions and therefore preventing collapse of anode material [191].

Ke et al. synthesized 3D hierarchical quantum dots comprised of MoS_2 nanosheets grafted on carbon nanosheets MoS_2@SnS-QDs/CNN and described its application in LIBs, as an efficient anode electrode. The electrode material with remarkable performance was prepared via controllable strategy on a large scale. The 3D carbon nanosheets were utilized to retain the textural stability and durability of the anode but also to prevent the exposure of SnS to electrolyte mixture. Additionally, the active lithium ions were being carried by exposed bind sites of MoS_2 nanosheets. The enhancement in charge transfer and Li-storage capabilities was due to the formation of junction at interface as long as contact between SnS and Mo-disulfide. Owning to their unique distinct structure, morphology and wonderful synergies, MoS_2@SnS-QDs/CNN anode depicted astonishing durable cycling and electrochemical performance. The half-cell electrode material showed 713 mAh g^{-1} reversible capacity to acquire current density value of 2 A g^{-1} after 1000 cycles. However, in case of full-cell electrode, it provided the capacity of 713 mAh g^{-1} at current of 1 A g^{-1} after 100 cycles [192]. Information on the morphology, synthesis method, surface area, specific capacity, and current densities of Mo-NPs based modified electrodes used in LIBs is summarized in Table 2.

Lithium-sulfur (Li–S) batteries

The most popular way to improve the rate performance and cycling stability of the sulfur electrode in Li–S batteries is by the feasibility of using lithium sulfide, which is obtained by the electrochemical conversion of Mo-sulfide into lithium sulfide and metallic Mo at lower voltages, as a highly active component in Li–S batteries. Metallic Mo enhances the conductivity of electrodes and prevents the dissolution of lithium polysulfides into the solution of an electrolyte. Thus, the in situ prepared Li_2S/Mo nanocomposite exhibit both high sulfur consumption and high cycling stability [208]. Zhuang et al. obtained Mo-dioxide–carbon nanofibers (MoO_2–CNFs) after heat treatment and used them as matrix for the preparation of sulfur/MoO_2–CNF cathodes for Li–S batteries. The electrochemical performance and polysulfide adsorption tests showed that MoO_2–CNFs cathodes did not only improve the electrochemical reactions but also alleviate the shuttle effect [209]. In many other studies, it was also indicated that the Mo_2C–C nano-octahedrons alleviate the shuttle effect and improve the reaction kinetics of the electrochemical processes taking place in a cell [194,210,211]. Han et al. synthesized MoS_2 NPs by using the one-pot method and as an efficient lithium polysulfide mediator in Li–S batteries [212]. Mosavati et al. also employed nanostructured Mo_2N as effective cathode materials in the Li–S batteries [213].

He et al. investigated stabilizing effect of KB/Mo_2C separator for constructing durable Li–S batteries. The cycling

Table 2 – Applications of Mo in LIBs.

Morphology	Modified electrode	Method	Conditions	S_{BET} (m^2/g)/surface area	Specific capacity (mAh g^{-1})	Current Density (A g^{-1})	Ref.
Interconnected 3D macro-porous Diameter: 5 nm	GF@CNT@MoS_2	Hydro-thermal	0.1–3 V	–	935	0.1 to 5	[178]
Well-defined 1D nano-structure Diameter: 2–80 nm	MoC–Mo_2C/NCNTs	wet-chemical process	25–700 °C 2.0–4.35 V	79.9	34,862	200	[179]
Uniformly lamellar nano-flowers	MoS_2/C	–	0.001 and 3.0 V	326	338.3 F g^{-1}	0.1	[193]
2D Nano-crystals Size: 0.5–2 nm	MoS_2/C	–	1.8–1.2 V	59	1031	50	[181]
Nano-rods Size: 5–10 nm	MoO_3/WO_2@C	Hydro-thermal	0.01–3.5 V	–	–	0.1–2C	[182]
Octahedral Size: 800 nm	Mo_2C–C NOs@S		25 °C 1.7–2.8 V	196.46	1396 & 1050	0.1–1C	[194]
Spatially dispersed Size: 300–350 nm	HMS/CT Pd-TMS/CT	Hydro-thermal	2.0–4.5 V	3.21, 16.81	7441	500–2000 m A g^{-1}	[195]
Monoclinic, micro-rod with wrinkled surface Size: 500 nm	MoO_2/C (Ar/H_2)	–	0.01–3 V	1.34	610	0.05 to 2	[184]
0D/2D hetero/spot-like Size:100–500 nm Diameter:~4 nm	TiO_2/MoS_2 hybrids	Facile, scalable method	0.01–3 V	–	410	1.0	[196]
Crystalline structure Size: 150 nm to a few μm	MoSe2-carbon nanocomposite anodes ((2D)$MoSe_2$@(2D)Gr) electrode	–	0.01–3.00 V 0.01–3.00 V	70.68 48.34	611 611	3 3	[185]
Uniform nano-colloids/orthorhombic Size: ~5 nm	multiple Mo–MoO3- graphene nanocomposites	Wire-explosion process	25 °C 0.01–3.00 V	–	611	0.1	[197]
3D hierarchically porous carbon Size: 1.5–3.5 nm	(3D-MoO_x@CN)-600 (3D-MoO_x@CN)-700 (3D-MoO_x@CN)-800 MoO_x@CN-700	–	25 °C 0.01–3.00 V 25 °C 0.01–3.00 V 25 °C 0.01–3.00 V 25 °C 0.01–3.00 V	96.1 108.7 259.3 48.9	742 – – –	0.1 0.1 0.1 0.1	[186]
Smooth crystalline/monoclinic Size: 20–40 nm	$Li_4Ti_5O_{12}$ modified with 3% MoO_2	Hydro-thermal method	1.0–2.5 V	–	450	–	[187]
Hexagonal/Uniformly distributed Size & average diameter: 12.4 ± 2.6 nm	MoS_2/Co_3O_4 nanocomposite Co_3O_4 NPs	–	0.01–3.00 V 0.01–3.00 V	104.28 88.61	1474.9 –	0.1 0.1	[188]

Well dispersed/Hexagonal Size: 5 nm	HCS-Ru-Mo_4P_3 HCS-MoP HCS-RuP_2	–	0.32–0.37 V	964 1053 691.7	660	0.5C	[198]
Non uniform/Pure orthorhombic Size: 100–200 nm	MoO_3/rGO	High-energy ball-milling	1.8–2.8 V 25 °C	11.46	853	500 mA g^1	[189]
Hierarchical multi-room-structured Diameter: 25–50 nm	mNi-NCNT-MoC-C mNiMo-C fNi-NCNT-MoC fNiMo	Pilot-scale spray drying	2.0–4.35 V Overpotential: 0.20 and 0.21 V	36.8 16.4 33.7 25.9	500 – – –	– – – –	[180]
Spherical Diameter: 5–10 μm	Sn@SnO_x@MoS_2@C	CVD	3.00 to 0.005 V	–	500	2.0 A g^{-1}	[199]
Distinct particle nano-sheets	MoS_2@SnO_2–SnS/C	CVD	0.01–3.0 V, 25 °C	–	824	1.0 A g^{-1}	[200]
Hierarchical nano-fibrous composite Diameter: 6 nm	carbon@TiO_2@MoS_2	CVD	0.01–3.0 V	–	1314.4	100 mA g^{-1}	[201]
Well-dispersed spherical Diameter: 2.8 nm	MoO_2-CDs	Hydro-thermal route	0.01–3.0 V	94.83	236	0.10–1.50 A g^{-1}	[202]
Wrinkle 3D fibrous Size: 200 nm	MoS_2	Solvo-thermal process	0.1–2.0 V Overpotential: 194 mV	645	~700	1.2 A g^{-1}	[203]
Hexagonal nano-flowers Size: 100–500 nm	RGO/MoS_2	–	0.01–3.0 V	–	680	–	[204]
Bar-like Diameter: ~500 nm	MoOC	Facile, scalable strategy	0.01–3.0 V	3.06	361	2 A g^{-1}	[205]
Monoclinic/novel core-shell Diameter: ~80 nm	MoO_2@C MoO_3 MoO_3@ZIFs	Facile solvo-thermal method	0.01–3.0 V	29.6	787.7	1 A g^{-1}	[206]
Unique layered Size: 1–3 nm	MoO_3/CCNFs	–	0.01–3.0 V	–	801.1	–	[46]
Loosely aggregated		Hydro-thermal route	0.01–2.6 V	–	1117	–	[207]

capacity of Li–S batteries is mainly restricted dye the shuttle influence of intermediate comprises of lithium polysulfide. The acceleration of reaction rate of conversion of lithium polysulfide is responsible for restraining its migration. MoC_2 exhibit significant affinity with lithium polysulfide and hence it depicted remarkable activity of catalysis and grafting capacity for conversion. The rate of reduction of lithium polysulfide is accelerated when it is anchored on MoC_2 surface and additionally the reduction in potential of lithium sulfide happens. The Li–S battery employing separator KB/Mo_2C showed maximum utilization of activated material, durability, and stability of cycling with minimum decaying rate of 0.076% at 1C up to 600 cycles. The feasibility of Li–S batteries is demonstrated by maintained value of areal capacity 5.2 mAh cm^{-2} even after 60 cycles with the stability of 87% [214].

Jiang elaborated an approach to anchored MoC_2 nanostructures over the surface of ketjen black substrate to make polypropylene separators functional to facilitate kinetics of conversion of lithium polysulfides and thus efficiently enhanced the employment of Li–S batteries. Significantly, the MoC_2 nanostructures exhibit numerous sites for adsorption of polysulfides and KB with conductive networks of carbon exhibit porous cross-linked structures that facilitate charge transfer, provide space by expansion of volume and physical barrier to polysulfides. The modified composite KB/US-Mo_2C@PP comprises of combined impact of KB, MoS_2 utilizing KB/US-Mo_2C nanocomposite modified with PP separator explore specific capacity value of 1212.8 mAh g^{-1} at 0.2C with constant capacity value of 1053.3 mAh g^{-1} even after a series of 100 cycles. Moreover, these cells having areal capability of 2.3 mAh cm^{-2} with greater loading of sulfur about 4.9 mg cm^{-2} [215]. The MoC_2–C octahedrons along with MoC_2 nanostructures deposited in carbon matrix were fabricated via MOF approach where the sulfur atom is used as a host in Li–S batteries. In these batteries, lithium polysulfides are responsible for shuttle effect that remarkably lessens utilization of sulfur and also reduce cyclability. The Mo_2C–C NOs@S electrode material depicted a maximum specific capability of 1050 and 1396 mAh g^{-1} at 1C and 0.1C respectively, with minimum decay rate value of 0.0457% at 1C per cycle. Furthermore, this cathode with significant loading of sulfur 4.2 mgS cm^{-2} can give discharge capacity of 4.2 mgS cm^{-2} and 4.2 mgS cm^{-2} at 0.5C after 100 cycles. The presence of MoS_2 NPs make Mo–S bond that inactivate lithium polysulfide but also facilitate conversion reaction while the carbon with interconnected pores accelerate transportation of Li^+ ions [194]. Walle et al. used flowers like MoS_2/CNTs composites for high performance (Fig. 17) and high sulfur utilization on cathodes of Li–S batteries [216].

Information on the morphology, synthesis method/conditions, surface area, specific capacity, and reversible capacity of Mo-NPs based electrodes used in sulfur batteries is summarized in Table 3.

Sodium ion batteries

As an alternative or complement to LIBs, development of sodium ion batteries (SIBs) with long-term life cycle is needed. Due to the significant high performance and cost advantage, SIBs are candidates to replace LIBs in large scale and automotive energy storage applications. However, in comparison to the LIBs, the energy density and cyclic stability of SIB has not met with the basic requirements of applications in practical fields. Therefore, the progress and energy density of SIBs has been enhanced by the development or synthesis of new electrode materials with high specific capacity. For instance, transition metal oxides, including MoO_2 have gained attention as useful cathode materials for applications of SIBs because of their layered-stacking structure and high reversible capacity [231–233]. Wang et al. reported a cost effective and facile method for the fabrication of MoS_2 NPs through using precursor (MoS_2 sheets) by sodium modification. A voltage range of 0.01–2.6 V was used for the measurements of galvanostatic charge-discharge. The sodium Mo-sulfide NPs exhibit high reversible discharge capacity (190 mA g^{-1}) with a high capacity [234]. Vadahanambi Sridhar and Hyun Park reported synthesis of carbon encapsulated Mo_2N anchored on the reduced graphene oxide (rGO) (Mo_2N@C-rGO) by a facile and fast microwave technique. The applicability of Mo_2N@C-rGO in SIBs was also studied [235]. Pan et al. demonstrated that MoS_2 is usually considered a promising electrode material for SIBs due to its graphene-like structure and high capacity [236]. Similarly, many other research studies have revealed that the Mo-oxides or sulfides have a wide range of applications in SIBs [237–240].

Lim et al. described the attractive features of MoS_2 nanostructures such as its 2-layered texture and significant theoretical capability and investigated it as an efficient anode for Na^+ batteries. However, there are some limitations like poor conductivity, large change in volume, minimum rate capability, low cyclability associated with the use of MoS_2 based anode. In order to overcome the limitations some modifications were made by doping MoS_2 with nitrogen anchored on carbon skeleton. The composite N–MoS_2/C is eagerly fabricated through a simple and facile acid catalyzed approach. Additionally, the assistance of polymerization property of furfural as a source of carbon and self-doping impact of thioacetamide as a source of nitrogen and sulfur is taken. The interlayer composite N–MoS_2/C offer numerous active sites for diffusion of sodium ions and electrons, and it is a buffer texture that can adjust change in volume during sodiation. Based on distinct structure of N–MoS_2/C nanocomposite, it explored superior electrochemical properties and enhanced performance than MoS_2 in terms of charge capability of 387.9 mAh g^{-1} at 10 C-rate, remarkable cyclability i.e., 78% retention capacity at 0.2 C-rate after 200 cycles and maximum rate of cycling i.e., 96% retention capacity at 1 C-rate after 100 cycles [241].

Zhao et al. reported dual interface nanocomposite MoO_2@$MoSe_2$/rGO comprises of $MoSe_2$ layered structure grafted over graphene oxide and decorated with MoO_2 nanostructure as anode material. The great diffusion of sodium ions and rapid transfer of charge could be credited to graphene, MoO_2 NPs and interface coupling of $MoSe_2$ and MoS_2, which is being analyzed and confirmed with DFT technique. MoO_2@$MoSe_2$/rGO electrode displays remarkable storage capability of Na^+ ions 394 mAh g^{-1} at 3.2 Ag^{-1} with no degradation at 5 A g^{-1} even after 5000 cycles. The pairing of carbon cathode with Na^+ ion capacitor take advantage of great density of energy 51 W h kg^{-1} at 7920 W kg^{-1} with durable cyclability 97% retention capacity after 4500 cycles at 10 A g^{-1} [242]. Information on the morphology, synthesis method/conditions, surface area, specific capacity, discharge capacity,

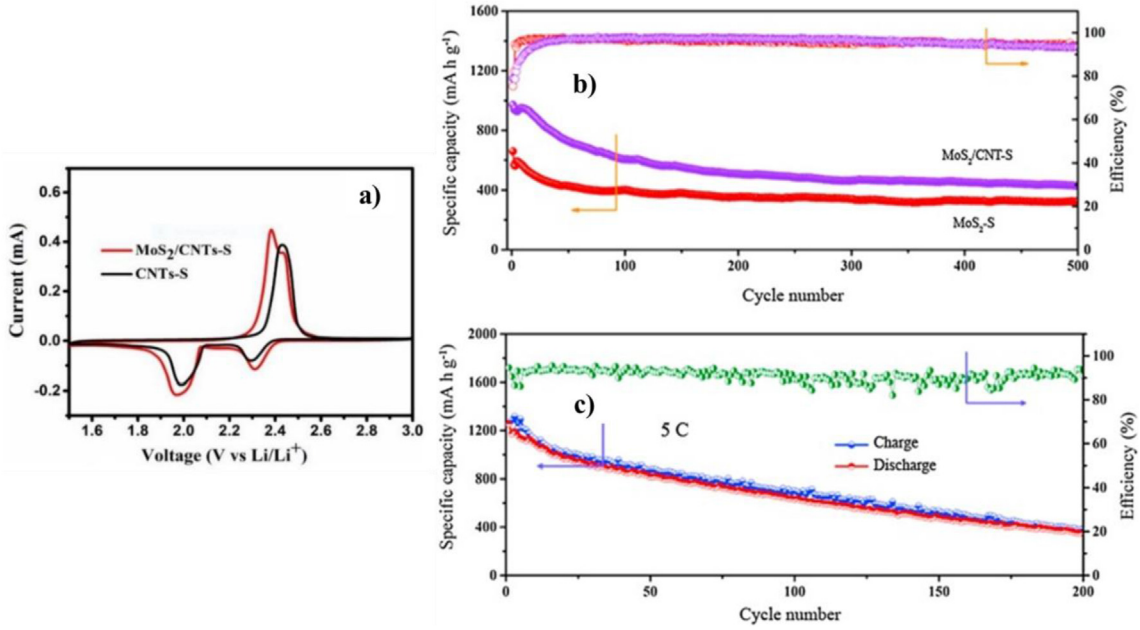

Fig. 17 – (a) Cyclic voltammogram, EIS curve, cycling performance of MoS_2/CNTs-S cathode at the current rate of (a) 0.5 and (b) 5C. Reprinted with permission from Walle et al. [216] ©2019, Elsevier.

and current density of Mo-NPs based electrocatalysts used in sodium batteries is summarized in Table 4.

Microbial fuel cells (MFCs)

Electrocatalysts in electrode modification

Electricigens are the active micro-organisms that were utilized by MFC, a renewable energy source that converts chemical energy into electrical power [248]. MFCs are an alternative to hydrogen based fuel cells by converting organic matter into energy with the help of microbes [249,250]. The minimum power density of MFC due to their large anodic potential is proved to be the crucial obstacle in their energy applications [251]. Therefore, the choice of the anode is of great importance, based upon its significant compatibility, flexibility, robustness and availability of a large interface for electron exchange in bacteria [252,253]. Transition metal carbides especially tungsten and Mo are potential bio-electrocatalyst with excellent catalytic activities for many biomolecules [254]. Both of these have the ability to oxidize certain metabolites including H_2, CH_3OH & $HCOO^-$. Zou et al. reported the production of bioelectricity from oxidation-reduction of riboflavin catalyzed by carbon-supported Mo-carbide [255].

The promising electrode material with excellent flexibility and conductivity, a large area with good strength for MFC, was proved to be graphene. This also enhances the growth of different microbes [256,257]. Graphene supported Mo-carbide hybrid with improved catalytic activity was synthesized by layer electrostatic procedure followed by carburization with PDDA at high temperature. The support material (graphene) is responsible for the growth of the biofilm of microbes and ultimately leads to the production of biomolecules. Nano-porous Mo_2C with good biocompatibility is uniformly distributed on porous surface of graphene, which causes great adhesion/sticking of electricigen cells to make microbial biofilm, which in turn generate bioactive molecules around interfacial surface being utilized by the Mo-carbide catalyst, and ultimately promotes transfer of electron between electrode and bacterial cells for electrocatalysis. Results (Fig. 18) indicated that nano-composite Mo_2C@G anode shows excellent response towards electro-catalysis in terms of significant power density of 1697 mWm^{-2} with long-term durability as compared to un-decorated graphene [258].

Another highly efficient electro-catalyst Co–MoO_2/NCND was developed by dispersion of cobalt modified MoO_2 NPs on the nitrogen-doped CND matrix in order to enhance the performance of MFC. Electrochemical studies show that the prepared composite gives output of 2.06 ± 0.05 W m^{-2} compared to bare carbon 0.49 ± 0.04 W m^{-2} and also possess excellent electro-catalytic performance in terms of high conductivity due to loading of N on CND, high charge transfer rate, enhanced stability and improved sensitivity towards redox reactions. In electro-active micro-organisms, the catalytic activity of MoO_2 was increased by modifying it with cobalt for oxidation and reduction reactions and it also exhibits excellent compatibility with bacteria [259]. The most promising and effective MoO_2/Polyaniline hybrid electro-catalyst was developed for the improvement in the performance of MFC The modified anode material was prepared by grafting Mo-dioxide and a polymer (polyaniline) onto the carbonaceous matrix. Cyclic voltammetry and charge-discharge technique showed the high conductance and capacitance of the prepared catalyst. The reason behind enhancement in the catalytic activity of MFC was the transfer of electrons from anode to bacteria and the modified anode facilitated this transfer. This MoO_2/PANI anodic electrocatalyst represented 7–8 folds' higher power output of 1101 mW/m^2 than non-modified carbon electrode (141 mW/m^2). EIS results showed that the synthesized hybrid reduced the resistance in charge

Table 3 – Applications of Mo-NPs in Li–S batteries.

Morphology	Electrode	Method/Conditions	S_{BET} (m^2/g)/surface area	Specific Capacity (mA h g^{-1})	Reversible Capacity (mA h g^{-1})	Ref.
Flower-like Size: 1–5 μm	MoS_2/CNTs MoS_2/CNTs-S	Hydrother-mal method	180.2 52.72	1473 1254	676.1 855.5	[216]
1D nanofibres Average Size: 42.93 nm Diameter: 425–575 nm Lattice spacing: 0.344 nm	MoO_2–CNFs	1.7–3.0 V	312.65	1095	860	[209]
Uniformly distributed	MoS_2 nanosheets	Electrophoretic deposity 1–0.001 V.	–	485	–	[217]
2D weave structure Uniformly dispersed Size: 300 μm	G/MoO_3 composite	–	–	1022	816	[75]
Nanoflower Size: 5–10 nm Interlayer spacing: 0.22 nm	MoS_2/graphene hybrid	Hydrothermal method 0.01–1.4 V	–	–	234.7	[218]
2-D sheets of MoS_2 in micron sized aggregate particles Size: 10–100 μm	MolyS50 cathode MolyS10-DIB10 based cathode	Scalable, one-pot process 2.6 to 1.7 V	–	–	500	[219]
Well-crystallized hexagonal MoS2 Size: 200 nm	Li_xMoS_2	0.01–3.00			350	[208]
Nano-octahedrons Size: about 600 nm lattice spacing of 0.23 and 0.18 nm	Mo_2C–C NOs@S cathode	–	Decreases from 686.26 to 97.30	–	1396	[194]
2D layered sheet-like structure MoS_2-NPs Interlayer spacing: 0.55 nm Size: 150–200 nm	MoS_2-NP-coated separator	1.0–1.0 V	–	–	983	[212]
Layered structure	MoO_3 nano-belts	−0.7 to 0.7 V	–	1675	1138.9	[210]
Nano-plate structure, face-centered cubic Average Size: 290 nm Thickness: 23 nm	Mo_2N WN	3.0 to 1.5 V	10.2 16.7	1675	–	[213]
3D interconnected nano-fibres Size: 2–10 nm d-spacing: 0.227 nm.	Mo_2C-NCNFs	1.8–2.8 V	14	1086	1675	[211]
Hierarchical MoS_2/SnO_2 nanocomposites Interlayer distances: 0.62 and 0.227 nm	MoS_2/SnO_2 nanocomposites	Two-step hydrothermal method. 1–0.001 V.	–	1673	905.8	[220]
Well dispersed Interlayer spacing: 0.63 nm	MoS_2/GO	Vacuum filtration	–	–	–	[221]
Size: <500 nm Thickness: 180 nm Lattice distance: 0.35 nm	GO/Mo-MOFs	Using Mo-MOFs precursor 0–0.8 V	–	404	–	[222]
Unique hierarchical structure Spicules-like	MoNPs/NF@Ni_3S_2	Hydrothermal method 0–0.6 V	–	361	–	[223]
3D-flower-like	Bi_2S_3/MoS_2	One-pot hydrothermal method −1 to −0.6 V	–	3040	–	[224]
Sponge-like 3D	MoO_2	Hydrothermal method −1.5 V–1.5 V	300	381	–	[225]

Nanoflower Average size: 60 nm	MoS_2/carbon aerogel	Facile hydrothermal route −0.8 to 0.2 V	918	260.0	–	[226]
Nano-architectured sheets	MoS_2/Mo	Hydrothermal method	–	192.7	–	[227]
Uniform Size: 50 nm	MoO_3	Temperature-program reaction −0.6 to 0.5 V).	–	172	–	[228]
Average diameter: 16 nm Hierarchical uniformly distributed Size: 1–180 nm	MoO_3 nanocomposites	Hydrothermal method			907	[229]
Spherical shaped 3D nanorods *Diameter:* 50–150 nm *Lattice spacing:* 2.69 Å	Ni_3S_8/O–MoS_2	*One-step hydrothermal synthesis* 0.3 to 0.6 V	——	907	——	[230]

transfer, which ultimately lead to increased transfer of electrons between bacteria and the modified electrode [260]. Information on the morphology, synthesis method, conditions, surface area, specific capacity, and current density of Mo-NPs based electrocatalysts used in electrode modification is summarized in Table 5.

Electrocatalysts in MFC

MFC is an emerging technology that assists the conversion of chemical energy to electricity and also remediate environment by eradicating polloutants utilizing catalytic mechanism of microorganisms. Mohamed et al. constructured ion molybdatre ($FeMoO_4$) based anode electrocatalyst for generation of electricity utilizing sugar as a substrate material. XRD analysis was carried out to determine crystalline nature of nanocatalyst while the morphological characteristics of nanocatalyst was analyzed by SEM. The obtained diffraction peaks are accordant to the JCPDS 22–0628 and determine the monoclinic crystal system of $FeMoO_4$. It is clearly depicted from SEM micrographs that $FeMoO_4$ nanostructures exhibit rod-like morphology. In MFC, the $FeMoO_4$ coated anode material attained large density value of 106 ± 3 mW/m^2, efficiency of COD removal 79.8 ± 1.5% and columbic capacity of 21.3 ± 0.5% [269].

In another study, an efficient cathode comprises of polypyrrole/MoO_2 nanocomposite is developed for generation of bioelectricity. The structure, crystalline phase, purity and elemental composition of as-preapred catalyst are determined by various analyzing techniques such as FTIR, XRD, SEM and EDS. The Tafel analysis, cyclic voltammetry are used to demonstrate the high capacity of charge transfer. The binding property of as-prepared composite is revealed by FTIR spectrum consisting of peaks 529, 995 cm^{-1} and 1207, 1561 cm^{-1} associated with MoO_2 and polypyrrole, respectively. The phase purity of material is obviously depicted from XRD analysis with orthorhombic crystalline phase and no other peaks observed. SEM images showed scaffold-like texture of Ppy/MoO_2 cathode material with great surface area due to polypyrrole coating over rood like surface of Mo-oxide. Results revealed that potential of MFC employing Ppy/MoO_2 cathode material (0.668) is comparitively 1.8 times higher than carbon cloth with potential value of 0.380 V. This catalyst is proved to be potential candidate alternative to Pt for electricity generation in MFC [270]. Zhang et al. triumphantly synthesized Mo_xC@C nanosphere by introducing Mo-species into MOFs as co-precursor. As expected, benefiting from the robust, porous structure and ultrafine nanocrystallites, Mo_xC@C displays a very high sensivity electrochemical response with low detection limit and wide linear range. Mo_xC@C electrode exhibits (Fig. 19) outstanding reproducibility, stability, selectivity, and anti-interference [271].

Information on the morphology, synthesis method, conditions, surface area, specific capacity, and current density of Mo-NPs based electrocatalysts used in MFC is summarized in Table 6.

Supercapacitors

A supercapacitor is an energy storing device with great list of merits like stability, large power density, long life, remarkable safety, cost effective, specified capacitance are used in electronic devices and in aerospace applications [283–286].

Table 4 – Applications of Mo-NPs SIBs.

Morphology	Electro-catalyst	Method/Conditions	S_{BET} (m^2/g)/surface area	Specific Capacity (mAh g^{-1})	Discharge Capacity (mA h g^{-1})	*Current density* (*A* g^{-1})	Ref.
2D nanosheets Size: 100–200 nm Thickness: 1–9 nm Lateral Dimensions: 50 nm to 1 μm	MoS_2-rGO composite	Liquid-Phase Exfoliation	–	164	376	20	[233]
Uniform, Hierarchical hollow structure	Mo-MOFs	Hydrothermal sulfuration	51.04	–	972	100	[232]
Three-dimensional porous-structured	$MoSe_2$	spray pyrolysis and process of	4.9	–	634	0.2	[243]
Size: 50 nm	N–$MoSe_2$/CNT	subsequent selenization	14.2		547	0.2	
	F–$MoSe_2$/CNT	0.001–2.5 V	22.4		626	0.2	
Uniform Thickness: 200 μm Lattice Spacing: 0.27 nm	MoS_2/SnS_2-GS	One-pot hydrothermal route 0.01–3.0 V	–	655	1244	0.15	[244]
amorphous-like structure d-spacing: 0.595 ± 0.3 nm	$Na_{0.375}MoS_2$	Liquid phase exfoliation of MoS_2			387.9	–	[245]
2D-layered structure Size: 500–600 nm Interlayer Spacing: 6.52 Å	N–MoS_2/C	acid-catalyzedmethod 3.0–0.001 V	10.22	–	745	0.1	[241]
cubic crystal	por–Mo_2N-NBs	facile hydrothermal treatment	176.4	214	437.04	100	[240]
Size: 200 nm	com–Mo_2N-NPs	method		134	317.54		
Pore size: 2.2–7.0 nm Interplanar spacing: 2.081 Å		1.9–1.0 V					
Well-crystallized MoC and ultrafine NPs Size: 2~3 nm Diameter: < 5 nm	(MoC)/graphitic carbon nanocomposites	Facile and green method 0.01–3 V	–	742	254	50	[246]
sandwich-like nanotube arrays (SNTAs) Diameter: 400–800 nm	C@MoS2@PPy	One-pot template-based hydrothermal process 1.0~3.8 V	–	723.3	615	201	[247]
Ultrafine Interplanar spacing: 0.236 nm	Mo_2C nano-plates	hydrolysis method 0.01–2.5 V	–	90.8	386.6	100	[239]
uniform nanocrystals d-spacing: 0.63 nm	$Fe_3O_4/Fe_{1-x}S$@C@MoS_2	facile hydrothermal process 0.01–3.00 V	–	420	1142	1.0	[238]
Hierarchical tubular hetero-structures	MoS_2/C MTs	simple hydrothermal method	–	563.5	791.8	0.2	[236]
Interlayer distance: 1.1 nm	MoS_2 MFs	0.01–3.0 V		326.4	607.8	0.2	
Hexagonal	graphene@MoS_2@C	acid-assisted hydrothermal route 0.01–3.0 V	–	520	962	0.1	[237]
Face centered cubic	Mo_2N@C-rGO	facile microwave technique 0.001–3.0 V	249	487	1049.6	500	[235]
Well-stacked layered structure Average size: 2–4 μm Interlayer distance: 6.2 Å	MoS_2	electrolysis of MoS_2 0.01–2.6 V	–	190	475	20	[234]
Nonuniform micro spheres	*MoO_2 electrode*	*Hydrothermal reaction* 0.01-3.0 V	——	——	151.1	107.9	[231]

Supercapacitors are divided into two main categories (a) Electrochemical Double layer capacitor (EDLC) based upon desorption and adsorption of ions (b) Pseudo-capacitor based on reduction and oxidation reactions [287–289]. Different studies were also carried out on symmetric SCs (battery and capacitor type electrodes) and asymmetric SCs (both electrodes are of the same type) [290–292]. The performance of electrode is highly based on characteristics (size, shape, structure and conductivity) of material (transition metal compounds, hydrocarbons, oxides, polymers, hydroxides, nitrides, sulfides, carbides, selenides and phosphides) that were going to employ in it [293–297]. Various studies have been reported on the excessive use of metal sulfides as electrode material in supercapacitors due to specific capacitance and higher conductivity [298]. Ni_3S_2 exhibits certain merits (high kinetic performance, efficient reversibility) and demerits (poor conductivity, actual capacity lower than theoretical ones, minimum stability) [299,300]. In order to conquer these constraints, researchers are now focusing on designing the hybrid of Ni_3S_2 with some sort of active and stable material [301]. Ni_3S_2 and Co hybrid was prepared through solvothermal ion-exchange method. This hybrid displayed capacitance of 142 F cm^{-3} at a specified current of 0.5 A cm^{-3}. Ag NPs deposited nickel sulfide shown significant capacitance of 5920 mF cm^{-2} at the specific current density of 5 mA cm^{-2} [200]. Recently, a simple, cost effective and non-hazardous modification strategy, which is the ion implantation process, is developed to fabricate such materials that can be used as an electrode in supercapacitors. Cheng et al. synthesized MoNPs/NF@Ni_3S_2 via a two-step process: (a) deposition of Mo-NPs onto Ni foam (b) Ni_3S_2 shell grown on MoNPs/NF via hydrothermal sulfurization and further illustrate their application in SCs. The resulting hierarchical structure with capacitance of 1.06C cm^{-2} at specific current of 1.0 mA cm^{-2} displays excellent performance (Fig. 20) like sufficient cycling ability for 7000 cycles and intimate kinetic capability. In addition to this, there is comparison carried out between Ni_3S_2/NF and MoNPs/NF@Ni_3S_2 and the results were in favor of Mo-composite due to doping of Mo-NPs, shape of Ni_3S_2 and interaction between Mo-NPs and Ni_3S_2. Symmetric supercapacitor with good capacity and efficient cycling ability can be formed by combining two MoNPs/NF@Ni_3S_2. Based upon the results obtained from various characterization technique it is concluded that the fabricated composite can also be used to construct high performance SCs [223].

Mo-disulfide and polypyrrole nanotubes were used to modify reduced graphene oxide to make supercapacitor electrode material. MoS_2-rGO nanosheets was prepared from self-assembly of graphene oxide and Mo-disulfide. The MoS_2-rGO/PPyNTs composite was fabricated by grafting PPyNTs onto the pre-synthesized MoS_2-rGO hybrid followed by hydrothermal treatment. The resultant electrode was further modified by irradiating it with swift heavy ions of 100 MeV. SEM results showed that incision and folding appear at the fluency of 3.3×10^{12} ions cm^2. According to XRD, the crystallinity of polymer first increases and then decreases due to the cross-linking of the polymer chain. Upon irradiation with SHI ions, the crystallinity of MoS_2 also increases due to periodic track formation and hammering effect. Different FTIR bands have specific sensitivities for SHI irradiation. According to RAMAN spectra, the structural defects of nano-composite first decreases due to calcination and then increases to the maximum fluency. CV curves indicate significant raise in capacitive response at 3.3×10^{12} and then decreased because of PPyNTs degradation. The stability and durability of fabricated electrode increases after SHI irradiation. This effect is attributed to the significant interactions in the polymer chain. MoS2-rGO/PPyNTs exhibits high reproducibility, good reversibility, excellent capability and recyclability [277].

The supercapacitor comprises carbon nanotube interface which is anchored with tungsten and Mo-carbide nanosheets, is constructed through one-pot synthesis along with carbonization. The MoC_2 based nanostructure Mo_2C@CNT possess great energy density value of 50.9 Wh·kg^{-1} at power of 500 W kg^{-1}, symmetry capacitance value of 367 F g^{-1} at current density value of 1 A g^{-1} as well as the 97% remarkable retention stability after 5000 cycles. Moreover, both tungsten and Mo based composites showed efficient HER performance in a basic and acidic environment with durability and stability for 24 h. The hierarchical nanostructured hybrids exhibit numerous pores, large number of binding sites and great contact area available and maximum conductivity and facilitated transport of electrons leads to excellent performance. In acidic media, Mo_2C@CNT and W_2C@CNT demonstrated a low overpotential of 121 and 155 mV with Tafel slope values of 77 and 85 mV·dec^{-1} respectively. However, in the basic medium, the values of small overpotential are 118 and 125 mV along with Tafel slope of 92 and 104 mV·dec^{-1} [302]. Mao et al. reported simple hydrothermal approach to fabricate Co–Mo–O–S microsphere electrode for supercapacitors of high performance. The as-prepared electrode material is investigated by certain characterization tools like XRD, TEM, EDS, SEM and XPS. SEM images revealed out its petal-like porous structure with large number of holes present. Co–Mo–O–S microsphere is made of porous outer core and solid inner structure depicted by TEM images. This supercapacitor electrode showed significant capacitance of 1134 F g^{-1} at 1 A g^{-1} along with high capability rate. The combined supercapacitor constituted graphene oxide and Co–Mo–O–S demonstrated extensive energy density value of 67.6 Wh kg^{-1} higher than Co–Mo–O–S electrode [303].

Miscellaneous applications

MoS_2-rGO composite was prepared by single-step hydrothermal treatment and further utilized as an effective electrode for dye-sensitized solar cells. Results obtained from XRD and SEM analysis revealed petal-like shape of Mo-sulfide NPs on the surface of rGO sheets. There are weak forces of interaction between rGO and MoS_2 depicted by RAMAN spectroscopy. Solar cells that are made up of modified (MoS_2-rGO) electrodes represent power efficiency of 7.83% higher than solar cells with Pt (7.57%) and with pristine MoS_2 (5.97%). CV and EIS revealed that the electro-catalytic performance is enhanced and resistance to electron transfer is decreased due to anchoring of rGO into the MoS_2 NPs that leads to the creation of numerous active sites and facile charge transfer. Lin Zhu described solar steam production utilizing Mo-nitride nanorambutans by a simple and cost-effective method. The development of photothermal conversion substance (PCM) is

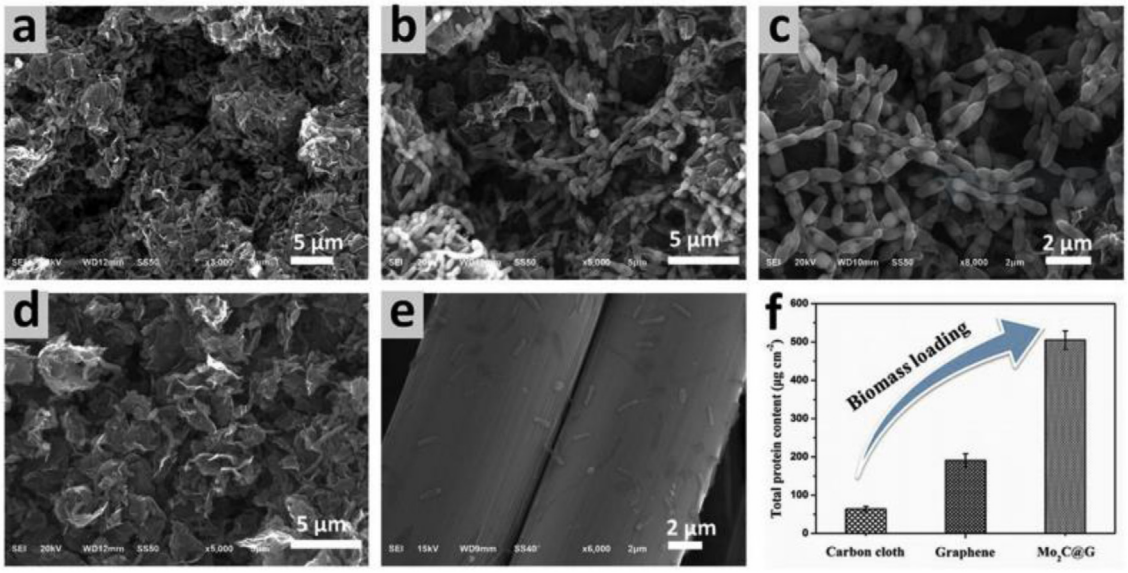

Fig. 18 – Bacterial biofilms grown on the electrodes. SEM images for the observation of *S. putrefaciens* CN32 cells adhered on the (a–c) Mo_2C@G nanocomposites, (d) graphene (e) carbon fibers. (f) Protein contents attached on various electrodes. Reprinted with permission from Zou et al. [258] ©2019, Elsevier.

considerably essential because of its applications in catalysis, energy production and splitting of water. Previously reported materials have been limited due to their complex procedure, costly experiments, bulkiness, and minimum absorbance. To overcome these limitations, the Mo based nanorambutans was developed for steam production considering their strong absorbance, maximum efficiency, high performance of steam production. In addition to this, the mesoporous surface of nanorambutans is responsible for further enhancement in transportation of water vapors and light harvesting capability. The efficiency of energy conversion is ~97% is demonstrated under the influence of cycling stability and sunlight. The rate of evaporation is ~1.70 kg m^{-2} h^{-1} is maximum which is produced by nanorambutans film with ~98% efficiency. Owning to its small size and texture, the outstanding performance of water evaporation has surpassed the already developed inorganic PCMs [304].

Matthew S developed cost effective earth abundant catalysts and their nanostructures for the conversion of energy that exhibit comparable activity to the highly expensive noble metals that are being utilized in certain energy production process including HER, OER and water splitting [305]. According to D. Jackson, many earth abundant metals (transition metals) such as Co, Mo, Cu, Fe, Ni have established use in industrial processes particularly the energy conversion application [306]. These materials are developed with low cost, least environmental impact, large surface area and better performance with high yield. Recently efforts have been made to develop catalyst containing transition metals that are able to produce hydrogen fuel by combining with light absorbing materials [307,308]. Jaramillo reported molecular catalyst comprises of Mo-sulfide $[Mo_3S_4]^{4+}$ when grafted on silicon cathodes (light absorbing) resulted in solar energy generation [309]. The alloys of transition metals show high activity as compared to the metals toward energy conversion applications. Ni–Mo alloy exhibit significant activity with minimum overpotential of 83 mV/v to derive the large current density of 1 A cm^{-2} than other alloys (Ni–V, Ni–Fe, Ni–W, Co–Mo, and Fe–Mo) towards energy conversion via evolution of hydrogen in basic and acidic conditions [310,311]. Mo-sulfide is proved to be the most active catalyst for energy conversion by catalyzing the production of hydrogen, particularly when it is deposited over carbon or gold [312,313]. Amorphous MoS_2 is found to have more activity and stability than fabricated MoS_2 nanostructure with the Tafel slope of 40 mV $decade^{-1}$ towards fuel cell and water splitting procedures [314]. Chen et al. narrated that transition metal nitrides particularly the Mo-nitrides were shown to exhibit enhanced electrocatalytic activity comparable to expensive noble metals towards energy transformations [315]. The minimum Tafel slope value of 35 mV $decade^{-1}$ contained by NiMoNx nanostructures depicted their improved performance over Ni–Mo alloy nanostructure in acidic environment towards hydrogen generation and energy transportation [316]. Based on great surface area and maximum diffusion through porous structure of Mo-carbide it exhibit high HER activity. Moreover the MoC_2 NPs grafted in supported carbon material attained better conversion efficiencies utilizing iodide electrode connected with counter platinum electrode in solar cells [317].

Jin Wei narrated development of catalyst comprises transition metal nanostructures of porous nature for electrochemical devices. These nanostructured materials especially the Mo based nanomaterials are highly advantageous for use in distinct energy conversion areas and storage devices including HER, water splitting, solar cells, fuel cells and batteries. This response is attributed to the attractive features like great surface area, numerous pores, large volume of pores, cost-effectiveness, feasibility, synergistic effect of

Table 5 – Applications of Mo in electrode modification.

Morphology of NPs	Electro-catalyst	Method	Conditions	S_{BET} (m^2/g)/surface area	*Specific capacity* ($mAh\ g^{-1}$)	*Current density* ($mA.cm^{-2}$)	Ref.
Uniformly dispersed Size: 5–20 nm	(Ni_2P@Ni_{10}Mo/Ni–Mo–O/NF	Hydro-thermal	0.3 V 25 °C	20.5 to 135.7	–	800	[261]
Cubic clusters Size: 2–5 nm	POM@ZIF-8 MoC NCs/N–C MoC NPs/N–C	–	0.65 V 1.64 V 1.65 V	672.7	750	6	[262]
Hexagonal shaped crystals Size: 50–60 nm	Mo/DAN/ZnO	–	Band gap: 3.11 eV, pH 7.4–7.9	21 to 13	–	–	[263]
Orthorhombic Size: 5–100 nm	CoP/$MoSe_2$e3	–	0.2–0.3 V	–	–	155.14	[110]
Scaffold-like arrangement Size:100–200 nm	MoO_2/PANI (3:1) MoO_2/PANI (2:1) MoO_2/PANI (1:1) MoO_2/PANI (1:2) MoO_2/PANI (1:3)	–	0.1–0.7 V, pH:7.2–8.0 0.1–0.7 V, pH:7.2–8.0 0.1–0.7 V, pH:7.2–8.0 0.1–0.7 V, pH:7.2–8.0 0.1–0.7 V, pH:7.2–8.0	636.8 mW/m^2 824.5 mW/m^2 970.9 mW/m^2 1101.2 mW/m^2 787.1 mW/m^2	40.36 F cm^2 87.43 F cm^2 374.63 F cm^2 109.27 F cm^2 621.25 F cm^2	–	[260]
Corrugated and curled Size: 5–500 nm	Ni–MoS_2/rGO		0.45–0.55 V				[264]
Uniformly dispersed/flower-like Size: 5–15 nm	MoP/NC	–	0.06–0.21 V	–	–	10	[132]
Uniform/isolated nano-deposits Size: <100 nm	Sparked Mo-SPEs	Green synthesis	0.100–1.150 V pH: 5	–	–	–	[265]
Highly dispersed Size: 500 nm Diameter: 5 nm	(Co–MoO_2/NCND)	–	−0.6 to 0.3 V, pH: 6.3	58.5	–	2.06 ± 0.05	[259]
Highly dispersed Size:~500 nm Diameter: 5 nm	Co–MoO_2/CND/CF		−0.6 to 0.3 V, pH: 6.3 Amplitude: 5 mV	–	–	1.61 ± 0.10	[259]
Highly dispersed Size: 500 nm Diameter: 5 nm	MoO_2/NCND/CF		−0.6 to 0.3 V, pH: 6.3 Amplitude: 5 mV	–	–	1.49 ± 0.05	[259]
Highly dispersed nano-rods Size: 500 nm Diameter: 5 nm	MoO_2/CND/CF		−0.6 to 0.3 V, pH: 6.3 Amplitude: 5 mV	–	–	1.21 ± 0.09	[259]
	MCTNMCPE	DPV	0.75–0.84 V, pH: 5.0	0.09 cm^2	–	–	[266]
Uniformly dispersed Size: 8–15 nm	Mo_2C/C composite	one-step solid reaction	0.1–0.3 V Overpotential: 50–170 mV	259 $m^2\ g^{-1}$	5.7 mF cm^{-2}	10	[267]
Uniformly dispersed Size: 8–15 nm	Mo_2C/C-850	one-step solid reaction	0.1–0.3 V Overpotential: 50–170 mV	259 $m^2\ g^{-1}$	21.8 mF cm^{-2}	10	[267]
Uniformly dispersed Size: 8–15 nm	Mo_2C/C-900	one-step solid reaction	0.1–0.3 V Overpotential: 50–170 mV	259 $m^2\ g^{-1}$	38.6 mF cm^{-2}	10	[267]
Uniformly dispersed Size: 8–15 nm	Mo_2C/C-950	one-step solid reaction	0.1–0.3 V Overpotential: 50–170 mV	259 $m^2\ g^{-1}$	20.0 mF cm^{-2}	10	[267]
Widely distributed Size: 5–50 nm Diameter: 16.5 nm	MoC_x@C-1	From PECP	~0.05–0.45 V Overpotential: 79 mV Amplitude: 10 mV	–	–	10s	[268]

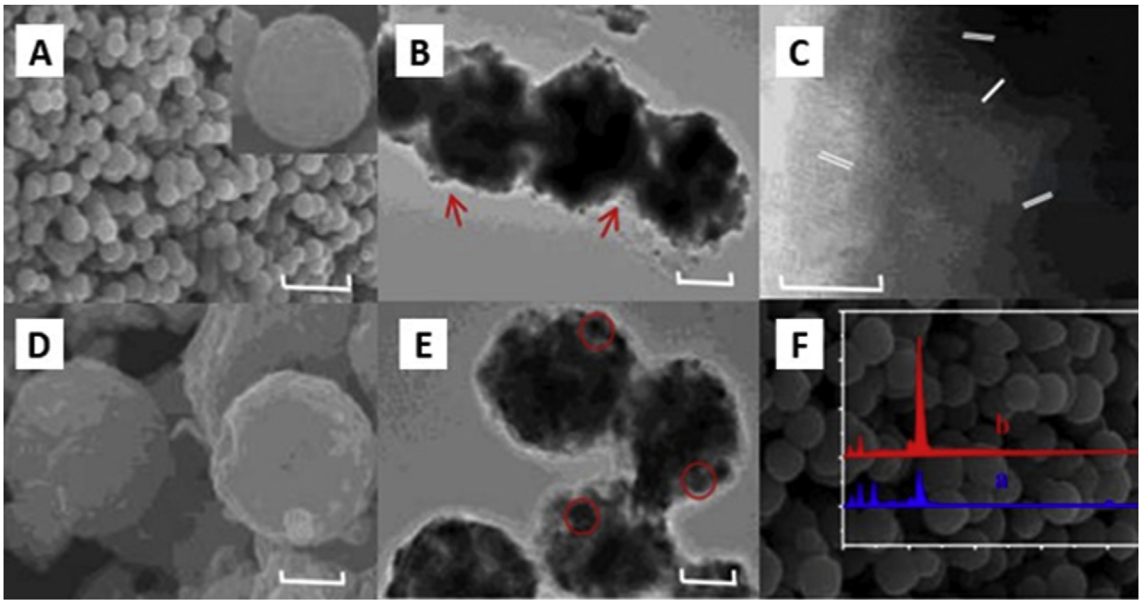

Fig. 19 – Characterization of the electrode materials: (A) and (B) SEM images of Mo–Cu-MOF and MoxC@C; (C) and (D) TEM images of Cu-MoxC@C and MoxC@C; (E) HRTEM of MoxC@C; (F) EDS patterns of Cu-MoxC@C (a) and MoxC@C (b). Reprinted with permission from Zhang et al. [271] ©2018, Elsevier.

atoms and stability associated with earth-abundant transition metals [318]. Lu et al. constructed amorphous MoS_2 nano film by a facile hydrothermal method where thiourea is being deposited over Mo substrate and as e result of this low value of Tafel slope 41 mV dec^{-1} with minimum overpotential of 120 mV are attained [319]. Hou et al. reported synthesis and application of Mo-disulfide nanostructured materials and its applications in energy transformation and storage. MoS_2, the dichalcogenide material have gained attention towards energy applications because of its electronic, physiochemical characteristics and distinct layered texture [320]. Some surface functionalization and modifications such as monolayered sheets, lattice defect, inter-layered expanded nanomaterial and doping of heteroatom have been performed to improve working ability of MoS_2 nano-based materials in discrete energy areas. The resultant MoS_2 nanostructure with these modifications and significant conductivity, high density of binding sites, surface area, and electronic structure is explored as highly efficient electrode material [321–323].

Ma et al. constructed hierarchical Co–Mo selenide nanospheres for high-performance hybrid batteries. Benefiting from the maximized utilization ratio and rationally hierarchical hollow structures of active materials, the novel transition metal selenides acquire high electrochemical performance with remarkable cycling stability (94.2% capacity) and high specific capacity (211.97 mA h g^{-1}). The assembled $CoSe_2/MoSe_2$-3-1//AC (activated carbon) battery-supercapacitor hybrid device renders preeminent cycling stability and a high energy density approximately up to 51.84 W h kg^{-1}. This provides a rational and effective design route to engineer advanced transition metal selenides with hierarchical hollow structures for electrochemical energy storage and conversion [324]. Ruan et al. synthesized a novel 3D hierarchical Ni NPs decorated $Ni_{0.2}Mo_{0.8}N$ structure for the high capacitance hybrid supercapacitors. Because of the excellent cycling stability, high power density, safety and fast charge/discharge time, these hybrid devices have attracted an intensive attention for the large-scale applications. The high performance of the Ni–Mo–N can be ascribed to the fast surface redox reactions for electrode materials and electrolyte ions and the low-contacted resistance between current collectors and active materials [325].

The electrochromic devices have received intensive attention for application including low-emission displays, and optoelectronic smart windows. However, it has been recognized that the electrochromic devices with transition-metal electrodes possess high charge transport barriers because of poor electrical conductivity, which reduces their electrochromic performance [326]. Yoonessi et al. fabricated a flexible transparent all-solid-state electrochromic patterned micro-supercapacitors based on 2D nanostructured MoO_{3-x}/poly (3,4-ethylenedioxythiophene)-polystyrenesulfonate nanocomposite electrodes. The electrochemical performance of this transparent micro-supercapacitor includes coulombic efficiencies of 99.7%, high specific capacitances (up to 79.2C g^{-1}, 99 F g^{-1}, 2.99 mF cm^{-2}). This exceptionally high-performance electrode also provides high charge storage capacity and high electrical conductivity [327].

Gao et al. constructed MoS_2 nanostructures with expanded-interlayer and terminated from edges by a temperature dependent facile microwave assisted approach. The end termination and interlayer spacing causes generation of highly electro-conductive MoS_2 with improved electronic texture is a potent candidate for energy conversion with Tafel slope value of 49 mV dec^{-1} and minimum onset potential of 103 mV under acidic conditions. The expansion of interlayer of MoS_2 was done by introduction of metal ions in particular ammonium ions [328,329]. Zheng et al. developed a strategy

Table 6 – Applications of Mo as electro-catalyst in MFC.

Analyte/morphology of NPs	Modified electrode	Method	Conditions	Specific capacity (mAh g^{-1})	Specific current range	Detection limit	Ref.
Oxygen dissolved in buffer solution	Pt/MoO3/GCE/GOx Pt/MoO3/GCE/GOx (FIA)	EDX, CV	1.05 to −0.25 V, pH: 5	–	–	0.025 Mm 0.053 mM	[272]
Monoclinic Size: below 50 nm	$Mo_{0.5}V_{0.5}$ O_2 $Mo_{0.33}V_{0.67}$ O_2 $Mo_{0.05}$ $V_{0.95}$ O_2 $Mo_{0.1}$ $V_{0.9}$ O_2	CHFS, CV, Hydro-thermal	0.05–3.00 V	560 450 300 75	0.1 to 10 Ag^{-1}	–	[177]
Width: 200 nm lattice spacing: 0.240 nm	MoNPs/NF@Ni_3S_2	CV, GCD, EDX, Hydro-thermal	0–0.6 V	361C cm^{-2}	1–40 mA cm^{-2}	–	[223]
Sheets like structure Size: 12.7–18.4 nm	Au@MoS2/Ch-GCE	EIS, CV and DPV exfoliation method.	20-25 °C, −0.3 to 0.7 V, pH: 6.2–7.4	–	–	0.03 μM	[273]
3D network structure	(MoCuSe rGO/GCE)	CV, DPV, EDX, EIS, Chronocoulometry	0.3 V–0.8 V, pH: 5.5 to 8.0	–	50s–180s	9.0×10^{-10} mol L^{-1}	[274]
3D web Size: 100–200 nm	Pt–MoO,/CNTs/graphite	CV, DPV, EDS,	0.7 V to −0.10 V	–	–	–	[275]
Uniform Size: 20–100 nm	GCE/MnO_x -MoO_x/Pt	Refractometric method	4 °C −0.25 to 1.05 V, pH: 6.0 to 7.5	–	–	–	[276]
Nano-sheets	MoS_2-rGO/PPyNTs	CV, EIS, GCD 100 MeV O^{7+} SHI irradiation	−0.3 to 1.3 V	Initial: 1561 Fg^{-1} Final: 1875 Fg^{-1}	1–11 A g^{-1}	–	[277]
marigold flower-like Size: 200 nm	MoS2-rGO	EDS, EIS	0.7 V	–	13.75 mA/cm^2	–	[278]
Homogenous/spherical & uniformly distributed Size: 70 nm	rMoS_2-PAA/GCE	CV, EIS, ECL	−0.1–0.6 V, pH 7.4	–	–	1.2×10^{-14} M.	[279]
Layered structure	MoS_2/NF/GCE	CV	25 °C 0.6 V to −0.2 V	–	Average peak current:5.95 μA	–	[280]
Nano-rods Size: 50–100 nm	MoO_x@PB/GF	CV, Amperometry	25 °C −0.2 to 0.5 V, pH: 4-5	–	No current change	0.0119 μM	[281]
3D Nano-flowers Size: 200 nm	GC/MoS_2/ISM	EDS, Potentiometry,	20 ± 2 °C Potential drift: 10.0 ± 2.7 μV/s	100 μF	Current: ± 1 nA	$10^{-5.5}$ M	[282]
3D porous nano-sphere Size: 20–40 nm	Mo_xC@C/GCE	DPV, EDX, EIS	pH: 4.5 0.2 V	–	–	0.0085 μM (Guanine) 0.008 μM (Adenine)	[271]
Uniform Size: 20–100 nm	Mo_2C@G	CV, EIS, EDX, amperometry	−0.45 V–0.35 V	–	3.45 Am^{-2}	–	[258]

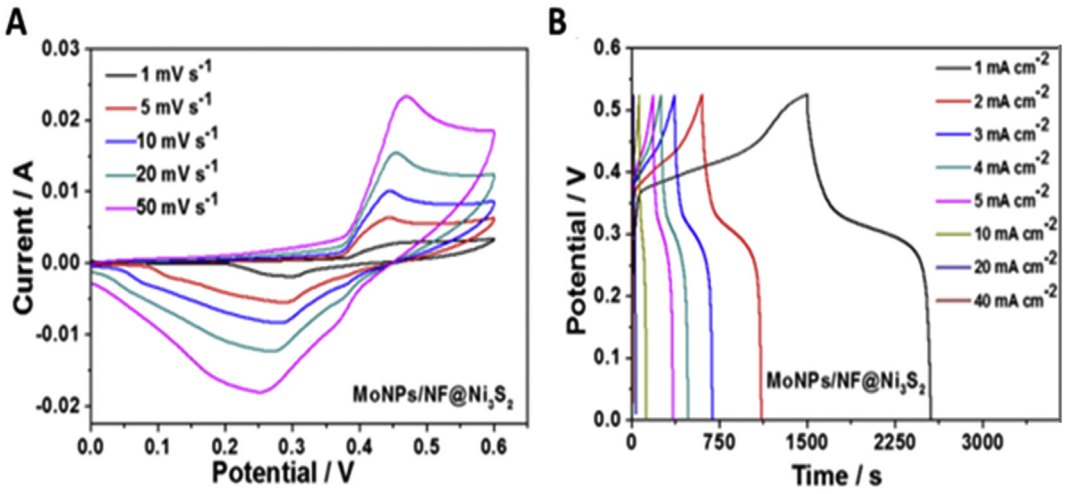

Fig. 20 – (A) CV curves of the MoNPs/NF@Ni_3S_2 electrode at different scan rates. (B) GCD curves of the MoNPs/NF@Ni_3S_2 electrode at different current densities. Reprinted with permission from Cheng et al. [223] ©2019, Elsevier.

for enhancement in catalytic activity of MoS_2 nanomaterials towards HER, water splitting and OER by coupling of iron hydroxide with MoS_2 based nanomaterials. The resultant optimized nanostructure exhibit remarkable catalytic activity at a low voltage of 1.57 V to acquire current density of 10 mA cm^{-2} [330]. The encapsulated Mo-sulfide nanostructures within Mo–N/C nanocomposite have been prepared and employed as the outstanding catalyst for discrete energy conversion process (OER, HER). The catalytic capacity and stability attributed to its large area, rapid transfer of charge and coupling stage of Mo–N bond [331]. Xu et al. investigated the preparation of MoS_2 monolayer nanostructures with low values of Tafel slope and overpotential, magnificent catalytic activity and excellent stability by a facile ultrasonic-assisted approach, along with hydrothermal process in an acidic environment for energy conversion. Highly conductive materials like carbon nanotubes and graphene have been adapted to increment the performance of MoS_2 nanosheets by supporting them. The conductivity of substrate is directly related to the transfer of charge from substrate to binding sites. The porosity of nanosheets protects them from aggregation by exposing more active sites for the binding purpose [332].

Patents of Mo-NPs

There are patents on the synthesis of Mo-NPs and their various energy-related applications. Some of the patents are described briefly here. The synthesis of platinum-free HER catalysts containing Mo for the electrolytic reduction of water was done by simultaneous reduction of a graphite oxide and a metal salt into graphene and metal oxide. The HER catalyst material included a Mo-phophide (MoP) catalyst or a MoO_2/graphene catalyst and exhibited high activity to hydrogen generation [333]. An inexpensive, stable and functional non-noble metal-based electrocatalyst such as NiMo has been developed for HER, with the aim of reducing the potential for HER overload in acidic media [334]. Thin-film solar cells high purity Mo-target preparation method has the advantage that: the Mo-target has the characteristics of high uniformity, high purity and high density, the sputtering target's utilization rate is much better, and this method is much more effective when applied to the solar cell industry [335]. The oxidation sensitivity of Mo-disulfide powder is more pronounced when the particle size is approximately five microns or less. This factor is important because the preferred powders have a degree of fineness of this magnitude [336]. Another application of Mo coatings is in the production of photovoltaic cells [337]. The Mo-NP catalyst precursors can be used in a variety of hydrocracking processes and reactors to upgrade heavy oil by being converted in situ in an active hydroprocessing catalyst [338].

Conclusion

The 'green' synthesis of metal NPs is an increasing and required field of research. Wide varieties of natural extracts (i.e., bio-ingredients such as fungi, bacteria, plant extracts, and yeast) have been used as effective resources for the fabrication or synthesis of materials. Among them, plant extracts have been shown to have high performance, such as reducing the stability of controlled material synthesis (i.e., controlled sizes, shapes, structures, and many other specific properties). This review article was designed to encompass the research studies on the green synthesis of Mo-NPs and their use in energy applications. An updated literature study on the green synthesis of Mo-NPs and detailed energy applications have been reviewed thoroughly based on the literature available. Accordingly, some possibilities remain to find new green preparation strategies based on the biogenic synthesis. The reducing, capping or stable agents participating in the green synthesis need further analysis to define the NPs structural relationship. The NPs synthesized using medicinal plant extracts should be tested for different bioactivities compared to chemically or physically synthesized, chemical compounds to understand whether the presence of observed

bioactivities can be attributed to different capping agents in the NPs. Despite the easy synthesis of NPs by the green method, achieving evenly distributed NPs is a huge challenge, as many parameters, including temperature, pH of the system, nature of capping agent, or concentration of active compounds, among others, play an important role in determining size and morphology. In light of the above discussion, it has been widely stated that green chemistry is a suitable way for the synthesis of Mo-NPs and for their implementation in energy applications, allowing improving the urgently needed sustainability of materials and processes.

Declaration of competing interest

The authors declare that they have no known competing financial interests or personal relationships that could have appeared to influence the work reported in this paper.

Acknowledgements

AES is currently on leave from CMRDI. University of Gujrat, Pakistan is accredited via the authors for the support in finishing this study. Furthermore, AES would like to thank the National Research grants from MINECO, Spain, "Juan de la Cierva" [FJCI-2018-037717]. The authors thank funding from the Basque Government Industry and Education Departments under the ELKARTEK, HAZITEK and PIBA (PIBA-2018–06) programs, respectively. MNZ acknowledges funding from Higher Education Commission of Pakistan (NRPU Project. 6515/Punjab/NRPU/R&D/HEC/2016).

REFERENCES

[1] Albrecht MA, Evans CW, Raston CL. Green chemistry and the health implications of nanoparticles. Green Chem 2006;8:417–32.
[2] Królikowska A, Kudelski A, Michota A, Bukowska J. SERS studies on the structure of thioglycolic acid monolayers on silver and gold. Surf Sci 2003;532:227–32.
[3] Thakkar KN, Mhatre SS, Parikh RY. Biological synthesis of metallic nanoparticles. Nanomed Nanotechnol Biol Med 2010;6:257–62.
[4] Agarwal H, Kumar SV, Rajeshkumar S. A review on green synthesis of zinc oxide nanoparticles–An eco-friendly approach. Resource-Efficient Technologies 2017;3:406–13.
[5] Prasad R, Bhattacharyya A, Nguyen QD. Nanotechnology in sustainable agriculture: recent developments, challenges, and perspectives. Front Microbiol 2017;8:1014.
[6] Dimkpa CO, Bindraban PS. Nanofertilizers: New products for the industry? J Agric Food Chem 2017;66:6462–73.
[7] Marek T, Karwowski W, Frankowicz M, Kantola J, Zgaga P. Human factors of a global society: A system of systems perspective. 1st ed. Boca Raton: CRC press; 2014.
[8] Panacek A, Kvitek L, Prucek R, Kolář M, Vecerova R, Pizurova N, Sharma VK, Nevecna Tj, Zboril R. Silver colloid nanoparticles: synthesis, characterization, and their antibacterial activity. J Phys Chem B 2006;110:16248–53.
[9] Shankar SS, Rai A, Ahmad A, Sastry M. Rapid synthesis of Au, Ag, and bimetallic Au core–Ag shell nanoparticles using Neem (*Azadirachta indica*) leaf broth. J Colloid Interface Sci 2004;275:496–502.
[10] Fendler JH. Nanoparticles and nanostructured films: preparation, characterization, and applications. Nanoparticles and nanostructured films: Preparation, characterization, and applications. 1st ed. Weinheim: Wiley-VCH; 1998.
[11] Arole V, Munde S. Fabrication of nanomaterials by top-down and bottom-up approaches-an overview. J Mater Sci 2014;1:89–93.
[12] Thakkar K, Mhatre S, Parikh R. Biological synthesis of metallic nanoparticles. Nanomed Nanotechnol Biol Med 2010;6:257–62.
[13] Rivas ME. Ball milling towards green synthesis: applications, projects, challenges. Johnson Matthey Tech 2016;60:148–50.
[14] Rane AV, Kanny K, Abitha V, Thomas S. Methods for synthesis of nanoparticles and fabrication of nanocomposites. In: Synthesis of inorganic nanomaterials. Amsterdam: Elsevier; 2018. p. 121–39.
[15] Shedbalkar U, Singh R, Wadhwani S, Gaidhani S, Chopade B. Microbial synthesis of gold nanoparticles: current status and future prospects. Adv Colloid Interface Sci 2014;209:40–8.
[16] Kharisov BI, Kharissova OV, Ortiz-Mendez U. CRC concise encyclopedia of nanotechnology. 1st ed. Boca Raton: CRC Press; 2016.
[17] Ahmed S, Ahmad M, Swami BL, Ikram S. A review on plants extract mediated synthesis of silver nanoparticles for antimicrobial applications: a green expertise. J Adv Res 2016;7:17–28.
[18] Gan PP, Li SFY. Potential of plant as a biological factory to synthesize gold and silver nanoparticles and their applications. Rev Environ Sci Biotechnol 2012;11:169–206.
[19] Nath D, Banerjee P. Green nanotechnology–a new hope for medical biology. Environ Toxicol Pharmacol 2013;36:997–1014.
[20] Parikh RY, Singh S, Prasad B, Patole MS, Sastry M, Shouche YS. Extracellular synthesis of crystalline silver nanoparticles and molecular evidence of silver resistance from *Morganella sp.*: towards understanding biochemical synthesis mechanism. ChemBioChem 2008;9:1415–22.
[21] Andersson M, Pedersen JS, Palmqvist AE. Silver nanoparticle formation in microemulsions acting both as template and reducing agent. Langmuir 2005;21:11387–96.
[22] Gardea-Torresdey J, Parsons J, Gomez E, Peralta-Videa J, Troiani H, Santiago P, Yacaman MJ. Formation and growth of Au nanoparticles inside live alfalfa plants. Nano Lett 2002;2:397–401.
[23] Narayanan KB, Sakthivel N. Coriander leaf mediated biosynthesis of gold nanoparticles. Mater Lett 2008;62:4588–90.
[24] Leela A, Vivekanandan M. Tapping the unexploited plant resources for the synthesis of silver nanoparticles. Afr J Biotechnol 2008;7:3162–5.
[25] Rai M, Yadav A, Gade A. CRC 675—Current trends in phytosynthesis of metal nanoparticles. Crit Rev Biotechnol 2008;28:277–84.
[26] Parashar V, Parashar R, Sharma B, Pandey AC. Parthenium leaf extract mediated synthesis of silver nanoparticles: A novel approach towards weed utilization. Dig J Nanomater Biostruct 2009;4:45–50.
[27] Song JY, Kim BS. Rapid biological synthesis of silver nanoparticles using plant leaf extracts. Bioproc Biosyst Eng 2009;32:79.

[28] Tavera-Davila L, Liu H-B, Herrera-Becerra R, Canizal G, Balcazar M, Ascencio J. Analysis of Ag nanoparticles synthesized by bioreduction. J Nanosci Nanotechnol 2009;9:1785–91.
[29] Kumar SA, Abyaneh MK, Gosavi S, Kulkarni SK, Pasricha R, Ahmad A, et al. Nitrate reductase-mediated synthesis of silver nanoparticles from $AgNO_3$. Biotechnol Lett 2007;29:439–45.
[30] Shahverdi AR, Minaeian S, Shahverdi HR, Jamalifar H, Nohi A-A. Rapid synthesis of silver nanoparticles using culture supernatants of *Enterobacteria*: a novel biological approach. Process Biochem 2007;42:919–23.
[31] Govender Y, Riddin T, Gericke M, Whiteley CG. Bioreduction of platinum salts into nanoparticles: a mechanistic perspective. Biotechnol Lett 2009;31:95–100.
[32] Gade A, Ingle A, Whiteley C, Rai M. Mycogenic metal nanoparticles: progress and applications. Biotechnol Lett 2010;32:593–600.
[33] Mohseniazar M, Barin M, Zarredar H, Alizadeh S, Shanehbandi D. Potential of microalgae and lactobacilli in biosynthesis of silver nanoparticles. Bioimpacts 2011;1:149–52.
[34] Gericke M, Pinches A. Biological synthesis of metal nanoparticles. Hydrometallurgy 2006;83:132–40.
[35] Husseiny M, El-Aziz MA, Badr Y, Mahmoud M. Biosynthesis of gold nanoparticles using *Pseudomonas aeruginosa*. Spectrochim Acta Mol Biomol Spectrosc 2007;67:1003–6.
[36] Bhattacharya R, Mukherjee P. Biological properties of "naked" metal nanoparticles. Adv Drug Deliv Rev 2008;60:1289–306.
[37] Mandal D, Bolander ME, Mukhopadhyay D, Sarkar G, Mukherjee P. The use of microorganisms for the formation of metal nanoparticles and their application. Appl Microbiol Biotechnol 2006;69:485–92.
[38] Marcato PD, Durán N. New aspects of nanopharmaceutical delivery systems. J Nanosci Nanotechnol 2008;8:2216–29.
[39] Korbekandi H, Iravani S, Abbasi S. Production of nanoparticles using organisms. Crit Rev Biotechnol 2009;29:279–306.
[40] Kumar V, Yadav SK. Synthesis of stable, polyshaped silver, and gold nanoparticles using leaf extract of *Lonicera japonica* L. Int J Green Nanotechnol 2011;3:281–91.
[41] Sharma VK, Yngard RA, Lin Y. Silver nanoparticles: green synthesis and their antimicrobial activities. Adv Colloid Interface Sci 2009;145:83–96.
[42] Tomczak MM, Slocik JM, Stone MO, Naik RR. Bio-based approaches to inorganic material synthesis. Biochem Soc Trans 2007;35:512–5.
[43] Naik RR, Stringer SJ, Agarwal G, Jones SE, Stone MO. Biomimetic synthesis and patterning of silver nanoparticles. Nat Mater 2002;1:169–72.
[44] Huang J, Li Q, Sun D, Lu Y, Su Y, Yang X, et al. Biosynthesis of silver and gold nanoparticles by novel sundried *Cinnamomum camphora* leaf. Nanotechnology 2007;18:105104.
[45] Singh J, Dutta T, Kim K-H, Rawat M, Samddar P, Kumar P. 'Green' synthesis of metals and their oxide nanoparticles: applications for environmental remediation. J Nanobiotechnol 2018;16:1–24.
[46] Zhao X, Jia W, Wu X, Lv Y, Qiu J, Guo J, et al. Ultrafine MoO_3 anchored in coal-based carbon nanofiber as anode for advanced lithium-ion batteries. Carbon 2020;156:445–52.
[47] Chen X, Wang W, Shi T, Wu G, Lu Y. One pot green synthesis and EM wave absorption performance of MoS_2@ nitrogen doped carbon hybrid decorated with ultrasmall cobalt ferrite nanoparticles. Carbon 2020;163:202–12.
[48] Nazarpour S, Hajian R, Sabzvari MH. A novel nanocomposite electrochemical sensor based on green synthesis of reduced graphene oxide/gold nanoparticles modified screen printed electrode for determination of tryptophan using response surface methodology approach. Microchem J 2020;154:104634.
[49] Guo T, Zhao R, Chen X, Du Q, Shuai X, Wang Y, et al. Mo-chelate strategy for synthesizing ultrasmall Mo2C nanoparticles embedded in carbon nanosheets for efficient hydrogen evolution. Int J Hydrogen Energy 2021;46:31598–607.
[50] Sylla NF, Sarr S, Ndiaye NM, Mutuma BK, Seck A, Ngom BD, Chaker M, Manyala N. Enhanced electrochemical behavior of peanut-shell activated carbon/molybdenum oxide/molybdenum carbide ternary composites. Nanomaterials 2021;11:1056.
[51] Cai J, Zhang X, Pan Y, Kong Y, Lin S. MoS_2||CoP heterostructure loaded on N, P-doped carbon as an efficient trifunctional catalyst for oxygen reduction, oxygen evolution, and hydrogen evolution reaction. Int J Hydrogen Energy 2021;46(69):34252–63.
[52] Wang S, Li Y, Xie J, Hao A, Cao Y. One-pot solution-free construction for hybrids of molybdenum carbide nanoparticles and porous N-doped carbon nanoplates as efficient electrocatalyst of hydrogen evolution. J Alloys Compd 2021;861:157935.
[53] Chodankar N, Nanjundan A, Losic D, Dubal D, Baek J-B. Graphene and molybdenum disulphide hybrids for energy applications: an update. Mater Today Adv 2020;6:100053.
[54] Kang Q, Li M, Wang Z, Lu Q, Gao F. Agaric-derived N-doped carbon nanorod arrays@ nanosheet networks coupled with molybdenum carbide nanoparticles as highly efficient pH-universal hydrogen evolution electrocatalysts. Nanoscale 2020;12:5159–69.
[55] Zhang Y, Ye W, Fan J, Cecen V, Shi P, Min Y, Xu Q. Cobalt-nanoparticle-decorated cobalt–molybdenum bimetal oxides embedded in flower-like N-doped carbon as a durable and efficient electrocatalyst for oxygen evolution reaction. ACS Sustain Chem Eng 2021;9:11052–61.
[56] Gupta D, Chauhan V, Kumar R. A comprehensive review on synthesis and applications of molybdenum disulfide (MoS_2) material: past and recent developments. Inorg Chem Commun 2020;121:108200.
[57] Upadhyay S, Pandey O. One-pot synthesis of pure phase molybdenum carbide (Mo_2C and MoC) nanoparticles for hydrogen evolution reaction. Int J Hydrogen Energy 2020;45:27114–28.
[58] Gong L, Mu X, Li Q, Ma L, Xiong Y, Li R. Rational design of Ni-induced NC@ Mo_2C@ MoS_2 sphere electrocatalyst for efficient hydrogen evolution reaction in acidic and alkaline media. Int J Hydrogen Energy 2021;46:5250–8.
[59] Hu M, Wang Z, Li M, Pan K, Li L. Nano-pom-pom multiphasic MoS_2 grown on carbonized wood as electrode for efficient hydrogen evolution in acidic and alkaline media. Int J Hydrogen Energy 2021;46:28087–97.
[60] Song Y, Yang P. Second diffusion of Co particles during MoS_2 incorporated in N-doped carbon nanotubes towards superior electrochemical activity. Int J Hydrogen Energy 2021;46(68):33801–8.
[61] Zhang W, Yu H, Tang D, Huang Y, Wang J, Yang L, et al. Synthesis of MoS_2 nanoparticles embedded, N, S co-doped mesoporous carbon via molten salt method as hydrogen evolution electrocatalyst under alkaline and neutral conditions. Int J Hydrogen Energy 2021;46:13936–45.
[62] Shaheen I, Ahmad KS. Chromatographic identification of "green capping agents" extracted from Nasturtium officinale (*Brassicaceae*) leaves for the synthesis of MoO_3 nanoparticles. J Separ Sci 2020;43:598–605.
[63] Qidwai A, Kumar R, Shukla S, Dikshit A. Advances in biogenic nanoparticles and the mechanisms of

antimicrobial effects. Indian J Pharmaceut Sci 2018;80:592–603.
[64] Rajendaran K, Muthuramalingam R, Ayyadurai S. Green synthesis of Ag-Mo/CuO nanoparticles using *Azadirachta indica* leaf extracts to study its solar photocatalytic and antimicrobial activities. Mater Sci Semicond Process 2019;91:230–8.
[65] Kanneganti A, Manasa C, Doddapaneni P. A sustainable approach towards synthesis of MoO_3 nanoparticles using citrus limetta pith extract. Int J Eng Adv Technol 2014;3:128–30.
[66] Sivan SK, Padinjareveetil AK, Padil VV, Pilankatta R, George B, Senan C, et al. Greener assembling of MoO_3 nanoparticles supported on gum Arabic: cytotoxic effects and catalytic efficacy towards reduction of p-nitrophenol. Clean Technol Environ Policy 2019;21:1549–61.
[67] Abbasifar A, ValizadehKaji B, Iravani MA. Effect of green synthesized molybdenum nanoparticles on nitrate accumulation and nitrate reductase activity in spinach. J Plant Nutr 2020;43:13–27.
[68] Kanneganti A, Kumar KA, Vivek V. Green synthesis of molybdenum trioxide nanoparticles using Syzygium Aromaticum flower buds extract. Int J Sci Res Dev 2014;2:116–7.
[69] Thomas E, Rathore I, Tarafdar J. Bioinspired production of molybdenum nanoparticles and its effect on chickpea (*Cicer arietinum L*). J Bionanoscience 2017;11:153–9.
[70] Gupta CP. Synthesis, characterization and application of nanoparticles of Cr, Mo and W ions using biogenic and chemical routes. J App Chem 2017;10:54–9.
[71] Zhang A, Zhu A, Chen B, Zhang S, Au C, Shi C. In-situ synthesis of nickel modified molybdenum carbide catalyst for dry reforming of methane. Catal Commun 2011;12:803–7.
[72] Serrapede M, Fontana M, Gigot A, Armandi M, Biasotto G, Tresso E, et al. A facile and green synthesis of a MoO_2-Reduced graphene oxide aerogel for energy storage devices. Materials 2020;13:594.
[73] Hulkoti NI, Taranath T. Biosynthesis of nanoparticles using microbes—a review. Colloids Surf B Biointerfaces 2014;121:474–83.
[74] Li X, Xu H, Chen Z-S, Chen G. Biosynthesis of nanoparticles by microorganisms and their applications. J Nanomater 2011;2011:270974.
[75] Yue X-Y, Li X-L, Meng J-K, Wu X-J, Zhou Y-N. Padding molybdenum net with Graphite/MoO3 composite as a multi-functional interlayer enabling high-performance lithium-sulfur batteries. J Power Sources 2018;397:150–6.
[76] Srivastava SK, Constanti M. Room temperature biogenic synthesis of multiple nanoparticles (Ag, Pd, Fe, Rh, Ni, Ru, Pt, Co, and Li) by Pseudomonas aeruginosa SM1. J Nanoparticle Res 2012;14:831.
[77] Demydov D, Pinto I, Malshe AP. Sustainable nanotechnology enabled by bio-manufacturing: 'the cell as a production plant'. Virtual Phys Prototyp 2008;3:231–6.
[78] Halmi M, Zuhainis S, Yusof M, Shaharuddin N, Helmi W, Shukor Y, et al. Hexavalent molybdenum reduction to Mo-blue by a sodium-dodecyl-sulfate-degrading Klebsiella oxytoca strain DRY14. BioMed Res Int 2013;2013:384541.
[79] Rahman M, Shukor M, Suhaili Z, Mustafa S, Shamaan N, Syed M. Reduction of Mo (VI) by the bacterium Serratia sp. strain DRY5. J Environ Biol 2009;30:65–72.
[80] Nordmeier A, Merwin A, Roeper DF, Chidambaram D. Microbial synthesis of metallic molybdenum nanoparticles. Chemosphere 2018;203:521–5.
[81] Rees JD, Gorby YA, Sawyer SM. Synthesis and characterization of molybdenum disulfide nanoparticles in Shewanella oneidensis MR-1 biofilms. Biointerphases 2020;15:041006.
[82] Marslin G, Siram K, Maqbool Q, Selvakesavan RK, Kruszka D, Kachlicki P, Franklin G. Secondary metabolites in the green synthesis of metallic nanoparticles. Materials 2018;11:940.
[83] Manimekalai G, Selvakumar S, Gopikrishnan V, Radhakrishnan M, Balagurunathan R. Antibacterial effect of medicinal plants Leucas aspera Linn and Ocimum basilicum Linn. Int. J. Adv. Pharmaceut. Res 2011;26:276–80.
[84] Cui W, Cheng N, Liu Q, Ge C, Asiri AM, Sun X. Mo_2C nanoparticles decorated graphitic carbon sheets: biopolymer-derived solid-state synthesis and application as an efficient electrocatalyst for hydrogen generation. ACS Catal 2014;4:2658–61.
[85] Wu Z-Y, Hu B-C, Wu P, Liang H-W, Yu Z-L, Lin Y, et al. Mo 2 C nanoparticles embedded within bacterial cellulose-derived 3D N-doped carbon nanofiber networks for efficient hydrogen evolution. NPG Asia Mater 2016;8:e288.
[86] Ho M, Khiew P, Chiu W. Green and facile synthesis of molybdenum oxide-graphene composite electrodes for supercapacitor application. In: Materials science forum. Trans Tech Publ; 2016. p. 90–4.
[87] Fang L, Shu Y, Wang A, Zhang T. Green synthesis and characterization of anisotropic uniform single-crystal α-MoO_3 nanostructures. J Phys Chem C 2007;111:2401–8.
[88] Li Y, Liu J, Wang Y, Wang ZL. Preparation of monodispersed Fe–Mo nanoparticles as the catalyst for CVD synthesis of carbon nanotubes. Chem Mater 2001;13:1008–14.
[89] Vollmer C, Redel E, Abu-Shandi K, Thomann R, Manyar H, Hardacre C, Janiak C. Microwave irradiation for the facile synthesis of transition-metal nanoparticles (NPs) in ionic liquids (ILs) from metal–carbonyl precursors and Ru-, Rh-, and Ir-NP/IL dispersions as biphasic liquid–liquid hydrogenation nanocatalysts for cyclohexene. Chemistry–A European Journal 2010;16:3849–58.
[90] Ho MY, Lim JHK, Khiew PS, Chiu WS. A green synthesis of grpahene based composite for energy storage application. Int J Innovative Technol Explor Eng 2019;8:393–6.
[91] Guo Y, Huang Q, Ding J, Zhong L, Li T-T, Hu Y, et al. Ultrasmall Mo_2C in N-doped carbon material from bimetallic ZnMo-MOF for efficient hydrogen evolution. Int J Hydrogen Energy 2021;46:2182–90.
[92] Tyurikov K, Alexandrov S, Speshilova A, Andreeva V, Redkov A, Kirilenko D, Lipovskii A. Molybdenum/tungsten disulfide solid solutions nanoparticles formation by aerosol-assisted CVD. Solid State Sci 2021;115:106583.
[93] Chen Q, Liang S, Li B, Chen Z, Song X, Zhuo L. Sol-gel synthesis and characterization of tungsten-molybdenum solid solution nanoparticles. Int J Refract Metals Hard Mater 2021;100:105668.
[94] Kanneganti A, Talasila M. MoO_3 nanoparticles: synthesis, characterization and its hindering effect on germination of *Vigna Unguiculata* seeds. J Eng Res Appl 2014;4:116–20.
[95] Rameshan C, Stadlmayr W, Penner S, Lorenz H, Memmel N, Hävecker M, Blume R, Teschner D, Rocha T, Zemlyanov D. Hydrogen production by methanol steam reforming on copper boosted by zinc-assisted water activation. Angew Chem Int Ed 2012;51:3002–6.
[96] Pérez-Hernández R, Gutiérrez-Martínez A, Palacios J, Vega-Hernández M, Rodríguez-Lugo V. Hydrogen production by oxidative steam reforming of methanol over Ni/CeO_2–ZrO_2 catalysts. Int J Hydrogen Energy 2011;36:6601–8.
[97] Shi C, Zhang A, Li X, Zhang S, Zhu A, Ma Y, et al. Ni-modified Mo_2C catalysts for methane dry reforming. Appl Catal Gen 2012;431:164–70.
[98] Ahn SH, Choi I, Park H-Y, Hwang SJ, Yoo SJ, Cho E, Kim H-J, Henkensmeier D, Nam SW, Kim S-K. Effect of morphology of electrodeposited Ni catalysts on the behavior of bubbles

generated during the oxygen evolution reaction in alkaline water electrolysis. Chem Commun 2013;49:9323–5.
[99] Zhang L, Pan L, Ni C, Sun T, Zhao S, Wang S, et al. CeO_2–ZrO_2-promoted CuO/ZnO catalyst for methanol steam reforming. Int J Hydrogen Energy 2013;38:4397–406.
[100] Higman C, Tam S. Advances in coal gasification, hydrogenation, and gas treating for the production of chemicals and fuels. Chem Rev 2014;114:1673–708.
[101] Yan Y, Zhang Z, Zhang L, Wang X, Liu K, Yang Z. Investigation of autothermal reforming of methane for hydrogen production in a spiral multi-cylinder micro-reactor used for mobile fuel cell. Int J Hydrogen Energy 2015;40:1886–93.
[102] Yang M, Allard LF, Flytzani-Stephanopoulos M. Atomically dispersed Au(OH)x species bound on titania catalyze the low-temperature water-gas shift reaction. J Am Chem Soc 2013;135:3768–71.
[103] Navarro R, Álvarez-Galván M, Rosa F, Fierro J. Hydrogen production by oxidative reforming of hexadecane over Ni and Pt catalysts supported on Ce/La-doped Al_2O_3. Appl Catal Gen 2006;297:60–72.
[104] Biswas P, Kunzru D. Steam reforming of ethanol for production of hydrogen over Ni/CeO_2–ZrO_2 catalyst: effect of support and metal loading. Int J Hydrogen Energy 2007;32:969–80.
[105] Dhandapani B, Clair TS, Oyama S. Simultaneous hydrodesulfurization, hydrodeoxygenation, and hydrogenation with molybdenum carbide. Appl Catal Gen 1998;168:219–28.
[106] Da Costa P, Potvin C, Manoli J-M, Genin B, Djéga-Mariadassou G. Deep hydrodesulphurization and hydrogenation of diesel fuels on alumina-supported and bulk molybdenum carbide catalysts. Fuel 2004;83:1717–26.
[107] Wang J, Cui W, Liu Q, Xing Z, Asiri AM, Sun X. Recent progress in cobalt-based heterogeneous catalysts for electrochemical water splitting. Adv Mater 2016;28:215–30.
[108] Ruqia B, Choi SI. Pt and Pt–Ni $(OH)_2$ electrodes for the hydrogen evolution reaction in alkaline electrolytes and their nanoscaled electrocatalysts. ChemSusChem 2018;11:2643–53.
[109] Zhu Y, Yuan M, Deng L, Ming R, Zhang A, Yang M, et al. High-efficiency electrochemical hydrogen evolution based on the intermetallic Pt_2Si compound prepared by magnetron-sputtering. RSC Adv 2017;7:1553–60.
[110] Ding C, Qian J, Li Z, Li Y, Peng W, Zhang G, Zhang F, Fan X. Cobalt phosphide nanoparticles anchored on molybdenum selenide nanosheets as high-performance electrocatalysts for water reduction. Int J Hydrogen Energy 2018;43:20346–53.
[111] Brungs AJ, York AP, Claridge JB, Márquez-Alvarez C, Green ML. Dry reforming of methane to synthesis gas over supported molybdenum carbide catalysts. Catal Lett 2000;70:117–22.
[112] Darujati AR, Thomson WJ. Stability of supported and promoted-molybdenum carbide catalysts in dry-methane reforming. Appl Catal Gen 2005;296:139–47.
[113] Cheng J, Huang W. Effect of cobalt (nickel) content on the catalytic performance of molybdenum carbides in dry-methane reforming. Fuel Process Technol 2010;91:185–93.
[114] Men Y, Yang M. SMSI-like behavior and Ni promotion effect on NiZnAl catalysts in steam reforming of methanol. Catal Commun 2012;22:68–73.
[115] Sá S, Silva H, Brandão L, Sousa JM, Mendes A. Catalysts for methanol steam reforming—a review. Appl Catal B Environ 2010;99:43–57.
[116] Szizybalski A, Girgsdies F, Rabis A, Wang Y, Niederberger M, Ressler T. In situ investigations of structure–activity relationships of a Cu/ZrO_2 catalyst for the steam reforming of methanol. J Catal 2005;233:297–307.
[117] Ma Y, Guan G, Shi C, Zhu A, Hao X, Wang Z, Kusakabe K, Abudula A. Low-temperature steam reforming of methanol to produce hydrogen over various metal-doped molybdenum carbide catalysts. Int J Hydrogen Energy 2014;39:258–66.
[118] Ma Y, Guan G, Phanthong P, Hao X, Huang W, Tsutsumi A, Kusakabe K, Abudula A. Catalytic activity and stability of nickel-modified molybdenum carbide catalysts for steam reforming of methanol. J Phys Chem C 2014;118:9485–96.
[119] Cai F, Ibrahim JJ, Fu Y, Kong W, Zhang J, Sun Y. Low-temperature hydrogen production from methanol steam reforming on Zn-modified Pt/MoC catalysts. Appl Catal B Environ 2020;264:118500.
[120] Thompson LT, Schaidle J, Schweitzer N. High activity carbide supported catalysts for water gas shift. In: ACS national meeting book of abstracts. American Chemical Society; 2011.
[121] Nagai M, Matsuda K. Low-temperature water–gas shift reaction over cobalt–molybdenum carbide catalyst. J Catal 2006;238:489–96.
[122] Vrubel H, Hu X. Molybdenum boride and carbide catalyze hydrogen evolution in both acidic and basic solutions. Angew Chem Int Ed 2012;51:12703–6.
[123] Chen W-F, Wang C-H, Sasaki K, Marinkovic N, Xu W, Muckerman JT, Zhu Y, Adzic R. Highly active and durable nanostructured molybdenum carbide electrocatalysts for hydrogen production. Energy Environ Sci 2013;6:943–51.
[124] Kaewpanha M, Guan G, Ma Y, Hao X, Zhang Z, Reubroychareon P, Kusakabe K, Abudula A. Hydrogen production by steam reforming of biomass tar over biomass char supported molybdenum carbide catalyst. Int J Hydrogen Energy 2015;40:7974–82.
[125] Koós Á, Solymosi F. Production of CO-free H_2 by formic acid decomposition over Mo_2C/carbon catalysts. Catal Lett 2010;138:23–7.
[126] Darshan B, Kareem A, Maiyalagan T, Geo VE. CoS_2/MoS_2 decorated with nitrogen doped reduced graphene oxide and multiwalled carbon nanotube 3D hybrid as efficient electrocatalyst for hydrogen evolution reaction. Int J Hydrogen Energy 2021;46:13952–9.
[127] Laszczyńska A, Tylus W, Szczygieł I. Electrocatalytic properties for the hydrogen evolution of the electrodeposited Ni–Mo/WC composites. Int J Hydrogen Energy 2021;46:22813–31.
[128] Ramanavičius S, Bittencourt C, Naujokaitis A, Pakštas V, Jagminas A. Interfacing perovskite strontium molybdate to molybdenum disulfide nanoplatelts for boosting HER from water. Int J Hydrogen Energy 2021;46:14359–68.
[129] Huang Y, Wang C, Song H, Bao Y, Lei X. Carbon-coated molybdenum carbide nanosheets derived from molybdenum disulfide for hydrogen evolution reaction. Int J Hydrogen Energy 2018;43:12610–7.
[130] Shi Z, Nie K, Shao Z-J, Gao B, Lin H, Zhang H, et al. Phosphorus-Mo_2C@ carbon nanowires toward efficient electrochemical hydrogen evolution: composition, structural and electronic regulation. Energy Environ Sci 2017;10:1262–71.
[131] Wan C, Leonard BM. Iron-doped molybdenum carbide catalyst with high activity and stability for the hydrogen evolution reaction. Chem Mater 2015;27:4281–8.
[132] Huang Y, Song X, Deng J, Zha C, Huang W, Wu Y, Li Y. Ultra-dispersed molybdenum phosphide and phosphosulfide nanoparticles on hierarchical carbonaceous scaffolds for hydrogen evolution electrocatalysis. Appl Catal B Environ 2019;245:656–61.

[133] Ren J-T, Chen L, Yang D-D, Yuan Z-Y. Molybdenum-based nanoparticles (Mo_2C, MoP and MoS_2) coupled heteroatoms-doped carbon nanosheets for efficient hydrogen evolution reaction. Appl Catal B Environ 2020;263:118352.
[134] Jiao Y, Zheng Y, Jaroniec M, Qiao SZ. Design of electrocatalysts for oxygen-and hydrogen-involving energy conversion reactions. Chem Soc Rev 2015;44:2060–86.
[135] Zhang W, Zhu S, Luque R, Han S, Hu L, Xu G. Recent development of carbon electrode materials and their bioanalytical and environmental applications. Chem Soc Rev 2016;45:715–52.
[136] Wang J, Xu F, Jin H, Chen Y, Wang Y. Non-noble metal-based carbon composites in hydrogen evolution reaction: fundamentals to applications. Adv Mater 2017;29:1605838.
[137] Mounfield III WP, Huang B, Cai B, Shao-Horn Y, Román-Leshkov Y. Synthesis of unsupported two-dimensional molybdenum carbide nanosheets for hydrogen evolution. Mater Lett 2020;261:126987.
[138] Xu C, Wang L, Liu Z, Chen L, Guo J, Kang N, et al. Large-area high-quality 2D ultrathin Mo_2C superconducting crystals. Nat Mater 2015;14:1135–41.
[139] Sun W, Wang X, Feng J, Li T, Huan Y, Qiao J, et al. Controlled synthesis of 2D Mo_2C/graphene heterostructure on liquid Au substrates as enhanced electrocatalytic electrodes. Nanotechnology 2019;30:385601.
[140] Cui T, Dong J, Pan X, Yu T, Fu Q, Bao X. Enhanced hydrogen evolution reaction over molybdenum carbide nanoparticles confined inside single-walled carbon nanotubes. J Energy Chem 2019;28:123–7.
[141] Chai L, Zhang L, Wang X, Ma Z, Li T-T, Li H, et al. Construction of hierarchical Mo_2C nanoparticles onto hollow N-doped carbon polyhedrons for efficient hydrogen evolution reaction. Electrochim Acta 2019;321:134680.
[142] Sun Y, Shi G. Graphene/polymer composites for energy applications. J Polym Sci B Polym Phys 2013;51:231–53.
[143] Gopi CVM, Ravi S, Rao SS, Reddy AE, Kim H-J. Carbon nanotube/metal-sulfide composite flexible electrodes for high-performance quantum dot-sensitized solar cells and supercapacitors. Sci Rep 2017;7:46519.
[144] Mondal A, Jana NR. Graphene-nanoparticle composites and their applications in energy, environmental and biomedical science. Reviews in Nanoscience and Nanotechnology 2014;3:177–92.
[145] Zhu C, Liu D, Chen Z, Li L, You T. Superior catalytic activity of Pt/carbon nanohorns nanocomposites toward methanol and formic acid oxidation reactions. J Colloid Interface Sci 2018;511:77–83.
[146] Laursen AB, Kegnæs S, Dahl S, Chorkendorff I. Molybdenum sulfides—efficient and viable materials for electro-and photoelectrocatalytic hydrogen evolution. Energy Environ Sci 2012;5:5577–91.
[147] Huang H, Huang W, Yang Z, Huang J, Lin J, Liu W, et al. Strongly coupled MoS_2 nanoflake–carbon nanotube nanocomposite as an excellent electrocatalyst for hydrogen evolution reaction. J Mater Chem 2017;5:1558–66.
[148] Mahesh KN, Balaji R, Dhathathreyan K. Palladium nanoparticles as hydrogen evolution reaction (HER) electrocatalyst in electrochemical methanol reformer. Int J Hydrogen Energy 2016;41:46–51.
[149] Devadas B, Chang CC, Imae T. Hydrogen evolution reaction efficiency of carbon nanohorn incorporating molybdenum sulfide and polydopamine/palladium nanoparticles. Journal of the Taiwan Institute of Chemical Engineers 2019;102:378–86.
[150] Xing J, Lin F, Huang L, Si Y, Wang Y, Jiao L. Coupled cobalt-doped molybdenum carbide@ N-doped carbon nanosheets/nanotubes supported on nickel foam as a binder-free electrode for overall water splitting. Chin J Catal 2019;40:1352–9.
[151] Rozenfeld S, Teller H, Schechter M, Farber R, Krichevski O, Schechter A, et al. Exfoliated molybdenum di-sulfide (MoS_2) electrode for hydrogen production in microbial electrolysis cell. Bioelectrochemistry 2018;123:201–10.
[152] Chi J-Q, Gao W-K, Lin J-H, Dong B, Yan K-L, Qin J-F, Liu Z-Z, Chai Y-M, Liu C-G. Nitrogen, phosphorus dual-doped molybdenum-carbide/molybdenum-phosphide-@-carbon nanospheres for efficient hydrogen evolution over the whole pH range. J Colloid Interface Sci 2018;513:151–60.
[153] Tuomi S, Guil-Lopez R, Kallio T. Molybdenum carbide nanoparticles as a catalyst for the hydrogen evolution reaction and the effect of pH. J Catal 2016;334:102–9.
[154] Xiao P, Ge X, Wang H, Liu Z, Fisher A, Wang X. Novel molybdenum carbide–tungsten carbide composite nanowires and their electrochemical activation for efficient and stable hydrogen evolution. Adv Funct Mater 2015;25:1520–6.
[155] Miao M, Pan J, He T, Yan Y, Xia BY, Wang X. Molybdenum carbide-based electrocatalysts for hydrogen evolution reaction. Chemistry–A European Journal 2017;23:10947–61.
[156] Jiang J, Liu Q, Zeng C, Ai L. Cobalt/molybdenum carbide@ N-doped carbon as a bifunctional electrocatalyst for hydrogen and oxygen evolution reactions. J Mater Chem 2017;5:16929–35.
[157] Kim M, Kim S, Song D, Oh S, Chang KJ, Cho E. Promotion of electrochemical oxygen evolution reaction by chemical coupling of cobalt to molybdenum carbide. Appl Catal B Environ 2018;227:340–8.
[158] Tariq M, Zaman WQ, Sun W, Zhou Z, Wu Y, Cao L-m, et al. Unraveling the beneficial electrochemistry of IrO_2/MoO_3 hybrid as a highly stable and efficient oxygen evolution reaction catalyst. ACS Sustain Chem Eng 2018;6:4854–62.
[159] Dymerska A, Kukułka W, Wenelska K, Mijowska E. Two-dimensional molybdenum diselenide tuned by bimetal Co/Ni nanoparticles for oxygen evolution reaction. ACS Omega 2020;5:28730–7.
[160] Ji S, Chen W, Zhao Z, Yu X, Park HS. Molybdenum oxynitride nanoparticles on nitrogen-doped CNT architectures for the oxygen evolution reaction. Nanoscale Advances 2020;2(12):5659–65.
[161] Anjum MAR, Lee MH, Lee JS. Boron-and nitrogen-codoped molybdenum carbide nanoparticles imbedded in a BCN network as a bifunctional electrocatalyst for hydrogen and oxygen evolution reactions. ACS Catal 2018;8:8296–305.
[162] Wang X, Zhou L, Yang T, Gao J, He P, Jia L, Dong F, Jia B, Zhang H. Facile one-step synthesis of tunable nanochain-like Fe–Mo–B: a highly efficient and stable catalyst for oxygen evolution reaction. J Alloys Compd 2020;822:153517.
[163] Chiu K-L, Lin L-Y. Applied potential-dependent performance of the nickel cobalt oxysulfide nanotube/nickel molybdenum oxide nanosheet core–shell structure in energy storage and oxygen evolution. J Mater Chem 2019;7:4626–39.
[164] Chen S, Dai J, Ren F, Xu H, Du Y. 3D hollow nanoflowers assembled by ultrathin molybdenum-nickel phosphide nanosheets as robust electrocatalysts for oxygen evolution reaction. J Colloid Interface Sci 2019;536:71–9.
[165] Jeong S, Hu K, Ohto T, Nagata Y, Masuda H, Fujita J-i, Ito Y. Effect of graphene encapsulation of NiMo alloys on oxygen evolution reaction. ACS Catal 2019;10:792–9.
[166] Xiao J, Zhang Y, Zhang Z, Lv Q, Jing F, Chi K, Wang S. Self-supported biocarbon-fiber electrode decorated with molybdenum carbide nanoparticles for highly active hydrogen-evolution reaction. ACS Appl Mater Interfaces 2017;9:22604–11.

[167] Xun S, Xu Y, He J, Jiang D, Yang R, Li D, et al. MOF-derived cobalt oxides nanoparticles anchored on $CoMoO_4$ as a highly active electrocatalyst for oxygen evolution reaction. J Alloys Compd 2019;806:1097–104.
[168] Sun H, Xu X, Yan Z, Chen X, Cheng F, Weiss PS, et al. Porous multishelled Ni_2P hollow microspheres as an active electrocatalyst for hydrogen and oxygen evolution. Chem Mater 2017;29:8539–47.
[169] Dong H, Liu C, Ye H, Hu L, Fugetsu B, Dai W, Cao Y, Qi X, Lu H, Zhang X. Three-dimensional nitrogen-doped graphene supported molybdenum disulfide nanoparticles as an advanced catalyst for hydrogen evolution reaction. Sci Rep 2015;5:17542.
[170] Ai L, Su J, Wang M, Jiang J. Bamboo-structured nitrogen-doped carbon nanotube coencapsulating cobalt and molybdenum carbide nanoparticles: an efficient bifunctional electrocatalyst for overall water splitting. ACS Sustain Chem Eng 2018;6:9912–20.
[171] Lu K, Gu T, Zhang L, Wu Z, Wang R, Li X. POM-assisted coating of MOF-derived Mo-doped Co3O4 nanoparticles on carbon nanotubes for upgrading oxygen evolution reaction. Chem Eng J 2021;408:127352.
[172] Rani BJ, Keerthana S, Yuvakkumar R, Ravi G, Velauthapillai D, Shivatharsiny Y, Babu ES, Almoallim HS, Alharbi SA. La–Mo binary metal oxides for oxygen evolution reaction. Int J Hydrogen Energy 2021;46:6197–205.
[173] Bauer D, Roberts AJ, Matsumi N, Darr JA. Nano-sized Mo- and Nb-doped TiO_2 as anode materials for high energy and high power hybrid Li-ion capacitors. Nanotechnology 2017;28:195403.
[174] Bağcı C, Akyıldız Ö. Synthesis, characterization and electrochemical performance of Nb doped LiFePO4/C cathodes by mechanochemical activation. Hittite J Sci Eng 2018;5:49–55.
[175] Genovese M, Lian K. Metal oxides in supercapacitors. Toronto, ON, Canada: University of Toronto; 2017. p. 133.
[176] Visakh P, Della Pina C, Falletta E. Polyaniline blends, composites, and nanocomposites. 1st ed. Amsterdam: Elsevier; 2017.
[177] Bauer D, Ashton TE, Brett DJ, Shearing PR, Matsumi N, Darr JA. Mixed molybdenum and vanadium oxide nanoparticles with excellent high-power performance as Li-ion battery negative electrodes. Electrochim Acta 2019;322:134695.
[178] Ren J, Ren R-P, Lv Y-K. A flexible 3D graphene@CNT@MoS_2 hybrid foam anode for high-performance lithium-ion battery. Chem Eng J 2018;353:419–24.
[179] Oh YJ, Kim JH, Lee JY, Park S-K, Kang YC. Design of house centipede-like MoC–Mo_2C nanorods grafted with N-doped carbon nanotubes as bifunctional catalysts for high-performance Li–O_2 batteries. Chem Eng J 2020;384:123344.
[180] Oh YJ, Kim JH, Park S-K, Park J-S, Lee J-K, Kang YC. Highly efficient hierarchical multiroom-structured molybdenum carbide/carbon composite microspheres grafted with nickel-nanoparticle-embedded nitrogen-doped carbon nanotubes as air electrode for lithium-oxygen batteries. Chem Eng J 2018;351:886–96.
[181] Bulusheva L, Koroteev V, Stolyarova S, Chuvilin A, Plyusnin P, Shubin YV, et al. Effect of in-plane size of MoS_2 nanoparticles grown over multilayer graphene on the electrochemical performance of anodes in Li-ion batteries. Electrochim Acta 2018;283:45–53.
[182] Cao L, Li Y, Wu J, Li W, Huang J, Feng Y, et al. Facile synthesis of carbon coated MoO_3 nanorods decorated with WO_2 nanoparticles as stable anodes for lithium-ion batteries. J Alloys Compd 2018;744:672–8.
[183] Hu A, Shu C, Xu C, Li J, Liang R, Zheng R, et al. Interface-engineered metallic 1T-MoS_2 nanosheet array induced via palladium doping enabling catalysis enhancement for lithium–oxygen battery. Chem Eng J 2020;382:122854.
[184] Huo J, Xue Y, Liu Y, Ren Y, Yue G. Polyvinyl alcohol-assisted synthesis of porous MoO_2/C microrods as anodes for lithium-ion batteries. J Electroanal Chem 2020;857:113751.
[185] Kim H, Nguyen QH, Kim IT, Hur J. Scalable synthesis of high-performance molybdenum diselenide-graphite nanocomposite anodes for lithium-ion batteries. Appl Surf Sci 2019;481:1196–205.
[186] Li Z, Wang C, Chen X, Wang X, Li X, Yamauchi Y, Xu X, Wang J, Lin C, Luo D. MoOx nanoparticles anchored on N-doped porous carbon as Li-ion battery electrode. Chem Eng J 2020;381:122588.
[187] Liu H, Wang Y, Zheng H, Zou H, Feng X, Chen C, et al. MoO_2 nanoparticle-modified $Li_4Ti_5O_{12}$ as high rate anode material for lithium ion batteries. Ceram Int 2017;43:15339–44.
[188] Lou Y, He D, Wang Z, Hu Y, Shen Y, Ming J, et al. Nanocomposite of ultrasmall Co_3O_4 nanoparticles deposited on ultrathin MoS_2 surfaces for excellent performance anode materials in lithium ion batteries. Chem Eng J 2017;313:1269–77.
[189] Naresh N, Jena P, Satyanarayana N. Facile synthesis of MoO_3/rGO nanocomposite as anode materials for high performance lithium-ion battery applications. J Alloys Compd 2019;810:151920.
[190] Lee DY, Seo SD, Song HJ, Kim DW. Free-standing molybdenum disulfides on porous carbon cloth for lithium-ion battery anodes. Int J Energy Res 2021;45(7):11329–37.
[191] Duan L, Li X. Lithiated Mo_4O_{11} to improve excellent cycle stability of MoO_2 nanoparticles for lithium-ion battery. Synth Met 2021;272:116672.
[192] Ke G, Chen H, He J, Wu X, Gao Y, Li Y, et al. Ultrathin MoS_2 anchored on 3D carbon skeleton containing SnS quantum dots as a high-performance anode for advanced lithium ion batteries. Chem Eng J 2021;403:126251.
[193] Zhao G, Cheng Y, Sun P, Ma W, Hao S, Wang X, et al. Biocarbon based template synthesis of uniform lamellar MoS_2 nanoflowers with excellent energy storage performance in lithium-ion battery and supercapacitors. Electrochim Acta 2020;331:135262.
[194] Chen G, Li Y, Zhong W, Zheng F, Hu J, Ji X, et al. MOFs-derived porous Mo_2C–C nano-octahedrons enable high-performance lithium–sulfur batteries. Energy Storage Materials 2020;25:547–54.
[195] Hu A, Shu C, Xu C, Li J, Liang R, Zheng R, et al. Interface-engineered metallic 1T-MoS_2 nanosheet array induced via palladium doping enabling catalysis enhancement for lithium–oxygen battery. Chem Eng J 2019;382:122854.
[196] Wang H, Jiang H, Hu Y, Deng Z, Li C. Interface engineering of few-layered MoS_2 nanosheets with ultrafine TiO_2 nanoparticles for ultrastable Li-ion batteries. Chem Eng J 2018;345:320–6.
[197] Lee H-J, Shim H-W, Kim J-C, Kim D-W. Mo-MoO_3-graphene nanocomposites as anode materials for lithium-ion batteries: scalable, facile preparation and characterization. Electrochim Acta 2017;251:81–90.
[198] Ma F, Wang X, Wang J, Tian Y, Liang J, Fan Y, et al. Phase-transformed Mo_4P_3 nanoparticles as efficient catalysts towards lithium polysulfide conversion for lithium–sulfur battery. Electrochim Acta 2020;330:135310.
[199] Pan Q-c, Huang Y-g, Wang H-q, Yang G-h, Wang L-c, Chen J, et al. MoS_2/C nanosheets Encapsulated Sn@SnOx nanoparticles as high-performance Lithium-iom battery anode material. Electrochim Acta 2016;197:50–7.
[200] Pan Q, Zheng F, Ou X, Yang C, Xiong X, Liu M. MoS_2 encapsulated SnO_2-SnS/C nanosheets as a high performance anode material for lithium ion batteries. Chem Eng J 2017;316:393–400.

[201] Qi D, Li S, Chen Y, Huang J. A hierarchical carbon@ TiO_2@ MoS_2 nanofibrous composite derived from cellulose substance as an anodic material for lithium-ion batteries. J Alloys Compd 2017;728:506–17.
[202] Qing M, Meng Y, Wang Y, Li X, Zhou C, Liang Y, et al. Building nanoparticle-stacking MoO_2-CDs via in-situ carbon dots reduction as high-performance anode material for lithium ion and sodium ion batteries. Electrochim Acta 2019;319:740–52.
[203] Wang X, Fei S, Huang S, Wu C, Zhao J, Chen Z, et al. MoS_2 nanosheets inlaid in 3D fibrous N-doped carbon spheres for lithium-ion batteries and electrocatalytic hydrogen evolution reaction. Carbon 2019;150:363–70.
[204] Xiong F, Cai Z, Qu L, Zhang P, Yuan Z, Asare OK, et al. Three-dimensional crumpled reduced graphene oxide/MoS_2 nanoflowers: a stable anode for lithium-ion batteries. ACS Appl Mater Interfaces 2015;7:12625–30.
[205] Xiu Z, Kim D, Alfaruqi MH, Song J, Kim S, Duong PT, Mathew V, Baboo JP, Kim J. Ultrafine molybdenum oxycarbide nanoparticles embedded in N-doped carbon as a superior anode material for lithium-ion batteries. J Alloys Compd 2017;696:143–9.
[206] Zhang W, Wang B, Luo H, Jin F, Ruan T, Wang D. MoO_2 nanobelts modified with an MOF-derived carbon layer for high performance lithium-ion battery anodes. J Alloys Compd 2019;803:664–70.
[207] Zhou E, Wang C, Shao M, Deng X, Xu X. MoO_2 nanoparticles grown on carbon fibers as anode materials for lithium-ion batteries. Ceram Int 2017;43:760–5.
[208] Fang X, Guo X, Mao Y, Hua C, Shen L, Hu Y, et al. Mechanism of lithium storage in MoS_2 and the feasibility of using Li_2S/Mo nanocomposites as cathode materials for lithium–sulfur batteries. Chemistry–An Asian Journal 2012;7:1013–7.
[209] Zhuang R, Yao S, Jing M, Shen X, Xiang J, Li T, Xiao K, Qin S. Synthesis and characterization of electrospun molybdenum dioxide–carbon nanofibers as sulfur matrix additives for rechargeable lithium–sulfur battery applications. Beilstein J Nanotechnol 2018;9:262–70.
[210] Imtiaz S, Ali Zafar Z, Razaq R, Sun D, Xin Y, Li Q, Zhang Z, Zheng L, Huang Y, Anderson JA. Electrocatalysis on separator modified by molybdenum trioxide nanobelts for lithium–sulfur batteries. Advanced Materials Interfaces 2018;5:1800243.
[211] Shang C, Cao L, Yang M, Wang Z, Li M, Zhou G, et al. Freestanding Mo_2C-decorating N-doped carbon nanofibers as 3D current collector for ultra-stable Li-S batteries. Energy Storage Materials 2019;18:375–81.
[212] Han P, Chung S-H, Manthiram A. Thin-layered molybdenum disulfide nanoparticles as an effective polysulfide mediator in lithium–sulfur batteries. ACS Appl Mater Interfaces 2018;10:23122–30.
[213] Mosavati N, Salley SO, Ng KS. Characterization and electrochemical activities of nanostructured transition metal nitrides as cathode materials for lithium sulfur batteries. J Power Sources 2017;340:210–6.
[214] He M, Li X, Li W, Zheng M, Wang J, Ma S, Ma Y, Yin G, Zuo P, Sun X. Immobilization and kinetic promotion of polysulfides by molybdenum carbide in lithium-sulfur batteries. Chem Eng J 2021;411:128563.
[215] Jiang N, Jiang G, Niu D, Mao J, Chen M, Li K, et al. Decorating ketjen black with ultra-small Mo_2C nanoparticles to enhance polysulfides chemisorption and redox kinetics for lithium-sulfur batteries. J Energy Chem 2020;51:207–15.
[216] Walle MD, Zeng K, Zhang M, Li Y, Liu Y-N. Flower-like molybdenum disulfide/carbon nanotubes composites for high sulfur utilization and high-performance lithium–sulfur battery cathodes. Appl Surf Sci 2019;473:540–7.
[217] Nam MS, Patil U, Park B, Sim HB, Jun SC. A binder free synthesis of 1D PANI and 2D MoS_2 nanostructured hybrid composite electrodes by the electrophoretic deposition (EPD) method for supercapacitor application. RSC Adv 2016;6:101592–601.
[218] Wang Y-Z, Shan X-Y, Wang D-W, Sun Z-H, Cheng H-M, Li F. A rechargeable Quasi-symmetrical MoS_2 battery. Joule 2018;2:1278–86.
[219] Dirlam PT, Park J, Simmonds AG, Domanik K, Arrington CB, Schaefer JL, Oleshko VP, Kleine TS, Char K, Glass RS. Elemental sulfur and molybdenum disulfide composites for Li–S batteries with long cycle life and high-rate capability. ACS Appl Mater Interfaces 2016;8:13437–48.
[220] Zhang D-A, Wang Q, Wang Q, Sun J, Xing L-L, Xue X-Y. High capacity and cyclability of hierarchical MoS_2/SnO_2 nanocomposites as the cathode of lithium-sulfur battery. Electrochim Acta 2015;173:476–82.
[221] Byun S, Sim DM, Yu J, Yoo JJ. High-power supercapacitive properties of graphene oxide hybrid films with highly conductive molybdenum disulfide nanosheets. ChemElectroChem 2015;2:1938–46.
[222] Cao X, Zheng B, Shi W, Yang J, Fan Z, Luo Z, et al. Reduced graphene oxide-wrapped MoO_3 composites prepared by using metal–organic frameworks as precursor for all-solid-state flexible supercapacitors. Adv Mater 2015;27:4695–701.
[223] Cheng Y, Zhai M, Guo M, Yu Y, Hu J. A novel electrode for supercapacitors: spicules-like Ni_3S_2 shell grown on molybdenum nanoparticles doped nickel foam. Appl Surf Sci 2019;467:1113–21.
[224] Fang L, Qiu Y, Zhai T, Wang F, Lan M, Huang K, et al. Flower-like nanoarchitecture assembled from Bi_2S_3 nanorod/MoS_2 nanosheet heterostructures for high-performance supercapacitor electrodes. Colloid Surface Physicochem Eng Aspect 2017;535:41–8.
[225] Giardi R, Porro S, Topuria T, Thompson L, Pirri CF, Kim H-C. One-pot synthesis of graphene-molybdenum oxide hybrids and their application to supercapacitor electrodes. Applied Materials Today 2015;1:27–32.
[226] Huang K-J, Wang L, Zhang J-Z, Xing K. Synthesis of molybdenum disulfide/carbon aerogel composites for supercapacitors electrode material application. J Electroanal Chem 2015;752:33–40.
[227] Krishnamoorthy K, Veerasubramani GK, Pazhamalai P, Kim SJ. Designing two dimensional nanoarchitectured MoS_2 sheets grown on Mo foil as a binder free electrode for supercapacitors. Electrochim Acta 2016;190:305–12.
[228] Li X-L, Yan X, Hua W, Wang H-L, Wang W-D, Chen X-Y. Synthesis and characterization of uniform nanoparticles of γ-Mo_2N for supercapacitors. Trans Nonferrous Metals Soc China 2009;19:620–5.
[229] Tao T, Chen Q, Hu H, Chen Y. MoO_3 nanoparticles distributed uniformly in carbon matrix for supercapacitor applications. Mater Lett 2012;66:102–5.
[230] Li S, Chen T, Wen J, Gui P, Fang G. In situ grown Ni_9S_8 nanorod/O-MoS_2 nanosheet nanocomposite on carbon cloth as a free binder supercapacitor electrode and hydrogen evolution catalyst. Nanotechnology 2017;28:445407.
[231] Zhang W, Xing L, Chen J, Zhou H, Liang S, Huang W, et al. Improving the cyclic stability of MoO_2 anode for sodium ion batteries via film-forming electrolyte additive. J Alloys Compd 2020;822:153530.
[232] Cai Y, Yang H, Zhou J, Luo Z, Fang G, Liu S, et al. Nitrogen doped hollow MoS_2/C nanospheres as anode for long-life sodium-ion batteries. Chem Eng J 2017;327:522–9.
[233] Bang GS, Nam KW, Kim JY, Shin J, Choi JW, Choi S-Y. Effective liquid-phase exfoliation and sodium ion battery

application of MoS_2 nanosheets. ACS Appl Mater Interfaces 2014;6:7084–9.
[234] Oksel C, Subramanian V, Semenzin E, Ma CY, Hristozov D, Wang XZ, Hunt N, Costa A, Fransman W, Marcomini A. Evaluation of existing control measures in reducing health and safety risks of engineered nanomaterials. Environ Sci: Nano 2016;3:869–82.
[235] Vadahanambi S, Park H. Carbon sheathed molybdenum nitride nanoparticles anchored on reduced graphene oxide as high-capacity sodium-ion battery anodes and supercapacitors. New J Chem 2018;42:5668–73.
[236] Pan Q, Zhang Q, Zheng F, Liu Y, Li Y, Ou X, et al. Construction of MoS_2/C hierarchical tubular heterostructures for high-performance sodium ion batteries. ACS Nano 2018;12:12578–86.
[237] Teng Y, Zhao H, Zhang Z, Zhao L, Zhang Y, Li Z, et al. MoS_2 nanosheets vertically grown on reduced graphene oxide via oxygen bonds with carbon coating as ultrafast sodium ion batteries anodes. Carbon 2017;119:91–100.
[238] Pan Q, Zheng F, Ou X, Yang C, Xiong X, Tang Z, et al. MoS_2 decorated $Fe_3O_4/Fe_{1-x}S$@C nanosheets as high-performance anode materials for lithium ion and sodium ion batteries. ACS Sustainable Chem Eng 2017;5:4739–45.
[239] Lv X, Song J, Lai Y, Fang J, Li J, Zhang Z. Ultrafine nanoparticles assembled Mo_2C nanoplates as promising anode materials for sodium ion batteries with excellent performance. Journal of Energy Storage 2016;8:205–11.
[240] Liu S-L, Huang J, Liu J, Lei M, Min J, Li S, et al. Porous Mo_2N nanobelts as a new anode material for sodium-ion batteries. Mater Lett 2016;172:56–9.
[241] Lim H, Kim H, Kim S-O, Choi W. Self-assembled N-doped MoS_2/carbon spheres by naturally occurring acid-catalyzed reaction for improved sodium-ion batteries. Chem Eng J 2020;387:124144.
[242] Zhao X, Zhao Y, Huang B, Yang Z, Cai W, Sui J, Cao G, Wang H-E. Dual interface coupled molybdenum diselenide for high-performance sodium ion batteries and capacitors. J Power Sources 2020;446:227298.
[243] Choi SH, Kang YC. Fullerene-like MoSe 2 nanoparticles-embedded CNT balls with excellent structural stability for highly reversible sodium-ion storage. Nanoscale 2016;8:4209–16.
[244] Jiang Y, Guo Y, Lu W, Feng Z, Xi B, Kai S, et al. Rationally incorporated MoS_2/SnS_2 nanoparticles on graphene sheets for lithium-ion and sodium-ion batteries. ACS Appl Mater Interfaces 2017;9:27697–706.
[245] Li Q, Yao Z, Wu J, Mitra S, Hao S, Sahu TS, et al. Intermediate phases in sodium intercalation into MoS_2 nanosheets and their implications for sodium-ion batteries. Nanomater Energy 2017;38:342–9.
[246] Li M, Yu S, Chen Z, Wang Z, Lv F, Nan B, Zhu Y, Shi Y, Wang W, Wu S. MoC ultrafine nanoparticles confined in porous graphitic carbon as extremely stable anode materials for lithium-and sodium-ion batteries. Inorganic Chemistry Frontiers 2017;4:289–95.
[247] Lu B, Liu J, Hu R, Wang H, Liu J, Zhu M. C@MoS_2@PPy sandwich-like nanotube arrays as an ultrastable and high-rate flexible anode for Li/Na-ion batteries. Energy Storage Materials 2018;14:118–28.
[248] Lovley DR. Bug juice: harvesting electricity with microorganisms. Nat Rev Microbiol 2006;4:497–508.
[249] Logan BE, Rossi R, Saikaly PE. Electroactive microorganisms in bioelectrochemical systems. Nat Rev Microbiol 2019;17:307–19.
[250] Zhang L, Zhou S, Zhuang L, Li W, Zhang J, Lu N, Deng L. Microbial fuel cell based on Klebsiella pneumoniae biofilm. Electrochem Commun 2008;10:1641–3.
[251] Chen X, Wang X, Liao K, Zeng L, Xing L, Zhou X, Zheng X, Li W. Improved power output by incorporating polyvinyl alcohol into the anode of a microbial fuel cell. J Mater Chem 2015;3:19402–9.
[252] Wang Y-Q, Huang H-X, Li B, Li W-S. Novelly developed three-dimensional carbon scaffold anodes from polyacrylonitrile for microbial fuel cells. J Mater Chem 2015;3:5110–8.
[253] Xie X, Criddle C, Cui Y. Design and fabrication of bioelectrodes for microbial bioelectrochemical systems. Energy Environ Sci 2015;8:3418–41.
[254] Rosenbaum M, Zhao F, Schröder U, Scholz F. Interfacing electrocatalysis and biocatalysis with tungsten carbide: a high-performance, noble-metal-free microbial fuel cell. Angew Chem Int Ed 2006;45:6658–61.
[255] Zou L, Lu Z, Huang Y, Long Z-e, Qiao Y. Nanoporous Mo_2C functionalized 3D carbon architecture anode for boosting flavins mediated interfacial bioelectrocatalysis in microbial fuel cells. J Power Sources 2017;359:549–55.
[256] Zou L, Qiao Y, Wu X-S, Ma C-X, Li X, Li CM. Synergistic effect of titanium dioxide nanocrystal/reduced graphene oxide hybrid on enhancement of microbial electrocatalysis. J Power Sources 2015;276:208–14.
[257] ElMekawy A, Hegab HM, Losic D, Saint CP, Pant D. Applications of graphene in microbial fuel cells: the gap between promise and reality. Renew Sustain Energy Rev 2017;72:1389–403.
[258] Zou L, Huang Y, Wu X, Long Z-er. Synergistically promoting microbial biofilm growth and interfacial bioelectrocatalysis by molybdenum carbide nanoparticles functionalized graphene anode for bioelectricity production. J Power Sources 2019;413:174–81.
[259] Li X, Hu M, Zeng L, Xiong J, Tang B, Hu Z, et al. Co-modified MoO_2 nanoparticles highly dispersed on N-doped carbon nanorods as anode electrocatalyst of microbial fuel cells. Biosens Bioelectron 2019;145:111727.
[260] Rani R, Kumar S. High-capacity polyaniline-coated molybdenum oxide composite as an effective catalyst for enhancing the electrochemical performance of the microbial fuel cell. Int J Hydrogen Energy 2019;44:16933–43.
[261] Wen H, Cao G-X, Chen M-H, Qiu Y-P, Gan L-Y, Wang P. Surface phosphorization of hierarchically nanostructured nickel molybdenum oxide derived electrocatalyst for direct hydrazine fuel cell. Appl Catal B: Environ 2020;268:118388.
[262] Kou Z, Zang W, Ma Y, Pan Z, Mu S, Gao X, Tang B, Xiong M, Zhao X, Cheetham AK. Cage-confinement pyrolysis route to size-controlled molybdenum-based oxygen electrode catalysts: from isolated atoms to clusters and nanoparticles. Nanomater Energy 2020;67:104288.
[263] Bouazizi N, Khelil M, Ajala F, Boudharaa T, Benghnia A, Lachheb H, Slama RB, Chaouachi B, M'nif A, Azzouz A. Molybdenum-loaded 1, 5-diaminonaphthalene/ZnO materials with improved electrical properties and affinity towards hydrogen at ambient conditions. Int J Hydrogen Energy 2016;41:11232–41.
[264] Geng D, Bo X, Guo L. Ni-doped molybdenum disulfide nanoparticles anchored on reduced graphene oxide as novel electroactive material for a non-enzymatic glucose sensor. Sensor Actuator B Chem 2017;244:131–41.
[265] Kolozof P-A, Florou AB, Spyrou K, Hrbac J, Prodromidis MI. In-situ tailoring of the electrocatalytic properties of screen-printed graphite electrodes with sparked generated molybdenum nanoparticles for the simultaneous voltammetric determination of sunset yellow and tartrazine. Sensor Actuator B Chem 2020;304:127268.
[266] Ardakani MM, Taleat Z, Beitollahi H, Salavati-Niasari M, Mirjalili B, Taghavinia N. Electrocatalytic oxidation and

nanomolar determination of guanine at the surface of a molybdenum (VI) complex–TiO_2 nanoparticle modified carbon paste electrode. J Electroanal Chem 2008;624:73–8.
[267] Mu Y, Zhang Y, Fang L, Liu L, Zhang H, Wang Y. Controllable synthesis of molybdenum carbide nanoparticles embedded in porous graphitized carbon matrixes as efficient electrocatalyst for hydrogen evolution reaction. Electrochim Acta 2016;215:357–65.
[268] Yang X, Feng X, Tan H, Zang H, Wang X, Wang Y, Wang E, Li Y. N-Doped graphene-coated molybdenum carbide nanoparticles as highly efficient electrocatalysts for the hydrogen evolution reaction. J Mater Chem 2016;4:3947–54.
[269] Mohamed SN, Thomas N, Tamilmani J, Boobalan T, Matheswaran M, Kalaichelvi P, Alagarsamy A, Pugazhendhi A. Bioelectricity generation using iron (II) molybdate nanocatalyst coated anode during treatment of sugar wastewater in microbial fuel cell. Fuel 2020;277:118119.
[270] Karthick S, Haribabu K. Bioelectricity generation in a microbial fuel cell using polypyrrole-molybdenum oxide composite as an effective cathode catalyst. Fuel 2020;275:117994.
[271] Zhang L, Zhang J. Multiporous molybdenum carbide nanosphere as a new charming electrode material for highly sensitive simultaneous detection of guanine and adenine. Biosens Bioelectron 2018;110:218–24.
[272] Çakar İ, Özdokur KV, Demir B, Yavuz E, Demirkol DO, Koçak S, Timur S, Ertaş FN. Molybdenum oxide/platinum modified glassy carbon electrode: a novel electrocatalytic platform for the monitoring of electrochemical reduction of oxygen and its biosensing applications. Sensor Actuator B Chem 2013;185:331–6.
[273] Devi R, Gogoi S, Barua S, Dutta HS, Bordoloi M, Khan R. Electrochemical detection of monosodium glutamate in foodstuffs based on Au@MoS_2/chitosan modified glassy carbon electrode. Food Chem 2019;276:350–7.
[274] Duan Y, Li S, Lei S, Qiao J, Zou L, Ye B. Highly sensitive determination of bisphenol A based on MoCuSe nanoparticles decorated reduced graphene oxide modified electrode. J Electroanal Chem 2018;827:137–44.
[275] Gan Y-p, Huang H, Zhang W-K. Electrocatalytic oxidation of methanol on carbon-nanotubes/graphite electrode modified with platinum and molybdenum oxide nanoparticles. Trans Nonferrous Metals Soc China 2007;17:214–9.
[276] Ozdokur KV, Demir B, Atman E, Tatli AY, Yilmaz B, Demirkol DO, Kocak S, Timur S, Ertas FN. A novel ethanol biosensor on pulsed deposited MnOx-MoOx electrode decorated with Pt nanoparticles. Sensor Actuator B Chem 2016;237:291–7.
[277] Sarmah D, Kumar A. Ion beam modified molybdenum disulfide-reduced graphene oxide/polypyrrole nanotubes ternary nanocomposite for hybrid supercapacitor electrode. Electrochim Acta 2019;312:392–410.
[278] Senthilkumar R, Balu M, Ramakrishnan S, Ramamurthy PC, Batabyal SK, Kumaresan D, Kothurkar NK. Molybdenum disulfide/reduced graphene oxide hybrids with enhanced electrocatalytic activity: an efficient counter electrode for dye-sensitized solar cells. J Electroanal Chem 2019;847:113236.
[279] Sun H, Wang H, Bai W, Bao L, Lin J, Li Y. Sensitive electrogenerated chemiluminescence biosensing method for the determination of DNA hydroxymethylation based on Ru $(bpy)_3^{2+}$-doped silica nanoparticles labeling and MoS_2-poly (acrylic acid) nanosheets modified electrode. Talanta 2019;191:350–6.
[280] Xu X, Du Z, Wang Y, Mao X, Jiang L, Yang J, et al. Electrochemical properties of a 2D-molybdenum disulfide–modified electrode and its application in SO_2 detection. J Electroanal Chem 2018;815:220–4.
[281] Yu L, Zhao J, Tricard S, Wang Q, Fang J. Efficient detection of ascorbic acid utilizing molybdenum oxide@Prussian Blue/graphite felt composite electrodes. Electrochim Acta 2019;322:134712.
[282] Zeng X, Yu S, Yuan Q, Qin W. Solid-contact K^+-selective electrode based on three-dimensional molybdenum sulfide nanoflowers as ion-to-electron transducer. Sensor Actuator B Chem 2016;234:80–3.
[283] Peng H, Wei C, Wang K, Meng T, Ma G, Lei Z, et al. $Ni_{0.85}Se$@$MoSe_2$ nanosheet arrays as the electrode for high-performance supercapacitors. ACS Appl Mater Interfaces 2017;9:17067–75.
[284] Wang X, Shi B, Fang Y, Rong F, Huang F, Que R, et al. High capacitance and rate capability of a Ni_3S_2@CdS core–shell nanostructure supercapacitor. J Mater Chem 2017;5:7165–72.
[285] Xu L, Shi R, Li H, Han C, Wu M, Wong C-P, Kang F, Li B. Pseudocapacitive anthraquinone modified with reduced graphene oxide for flexible symmetric all-solid-state supercapacitors. Carbon 2018;127:459–68.
[286] Hu T, Liu Y, Zhang Y, Chen M, Zheng J, Tang J, et al. 3D hierarchical porous $V_3O_7{\cdot}H_2O$ nanobelts/CNT/reduced graphene oxide integrated composite with synergistic effect for supercapacitors with high capacitance and long cycling life. J Colloid Interface Sci 2018;531:382–93.
[287] Chen X, Chen D, Guo X, Wang R, Zhang H. Facile growth of caterpillar-like $NiCo_2S_4$ nanocrystal arrays on nickle foam for high-performance supercapacitors. ACS Appl Mater Interfaces 2017;9:18774–81.
[288] Khani H, Wipf DO. Iron oxide nanosheets and pulse-electrodeposited Ni–Co–S nanoflake arrays for high-performance charge storage. ACS Appl Mater Interfaces 2017;9:6967–78.
[289] Lin J, Liu Y, Wang Y, Jia H, Chen S, Qi J, Qu C, Cao J, Fei W, Feng J. Rational construction of nickel cobalt sulfide nanoflakes on CoO nanosheets with the help of carbon layer as the battery-like electrode for supercapacitors. J Power Sources 2017;362:64–72.
[290] Jiao Y, Pei J, Chen D, Yan C, Hu Y, Zhang Q, Chen G. Mixed-metallic MOF based electrode materials for high performance hybrid supercapacitors. J Mater Chem 2017;5:1094–102.
[291] Yang M, Zhong Y, Bao J, Zhou X, Wei J, Zhou Z. Achieving battery-level energy density by constructing aqueous carbonaceous supercapacitors with hierarchical porous N-rich carbon materials. J Mater Chem 2015;3:11387–94.
[292] Zhang X, Jiang J, Chen Y, Cheng K, Yang F, Yan J, Zhu K, Ye K, Wang G, Zhou L. A flexible and high voltage symmetric supercapacitor based on hybrid configuration of cobalt hexacyanoferrate/reduced graphene oxide hydrogels. Chem Eng J 2018;335:321–9.
[293] Wang G, Zhang L, Zhang J. A review of electrode materials for electrochemical supercapacitors. Chem Soc Rev 2012;41:797–828.
[294] Shi Y, Peng L, Ding Y, Zhao Y, Yu G. Nanostructured conductive polymers for advanced energy storage. Chem Soc Rev 2015;44:6684–96.
[295] Zhang P, Guan BY, Yu L, Lou XW. formation of double-shelled zinc–cobalt sulfide dodecahedral cages from bimetallic zeolitic imidazolate frameworks for hybrid supercapacitors. Angew Chem Int Ed 2017;56:7141–5.
[296] Wang R, Lang J, Zhang P, Lin Z, Yan X. Fast and large lithium storage in 3D porous VN nanowires–Graphene composite as a superior anode toward high-performance hybrid Supercapacitors. Adv Funct Mater 2015;25:2270–8.
[297] Ghidiu M, Lukatskaya MR, Zhao M-Q, Gogotsi Y, Barsoum MW. Conductive two-dimensional titanium

carbide 'clay'with high volumetric capacitance. Nature 2014;516:78–81.
[298] Liu T, Jiang C, Cheng B, You W, Yu J. Hierarchical NiS/N-doped carbon composite hollow spheres with excellent supercapacitor performance. J Mater Chem 2017;5:21257–65.
[299] Niu S, Zheng J. Mo_2S_3@Ni_3S_2 nanowries on nickel foam as a highly-stable supercapacitor material. J Alloys Compd 2018;737:809–14.
[300] Qi J, Chang Y, Sui Y, He Y, Meng Q, Wei F, et al. Facile synthesis of Ag-decorated Ni_3S_2 nanosheets with 3D bush structure grown on rGO and its application as positive electrode material in asymmetric supercapacitor. Advanced Materials Interfaces 2018;5:1700985.
[301] Qi J, Chang Y, Sui Y, He Y, Meng Q, Wei F, et al. Facile construction of 3D reduced graphene oxide wrapped Ni_3S_2 nanoparticles on Ni foam for high-performance asymmetric supercapacitor electrodes. Part Part Syst Char 2017;34:1700196.
[302] Hussain S, Rabani I, Vikraman D, Feroze A, Karuppasamy K, Haq Zu, et al. Hybrid design using carbon nanotubes decorated with Mo_2C and W_2C nanoparticles for supercapacitors and hydrogen evolution reactions. ACS Sustain Chem Eng 2020;8:12248–59.
[303] Mao X, Zou Y, Liang J, Xiang C, Chu H, Yan E, Zhang H, Xu F, Hu X, Sun L. Facile synthesis of hierarchical Co–Mo–O–S porous microspheres for high-performance supercapacitors. Ceram Int 2020;46:1448–56.
[304] Zhu L, Sun L, Zhang H, Yu D, Aslan H, Zhao J, et al. Dual-phase molybdenum nitride nanorambutans for solar steam generation under one sun illumination. Nano Energy 2019;57:842–50.
[305] Faber MS, Jin S. Earth-abundant inorganic electrocatalysts and their nanostructures for energy conversion applications. Energy Environ Sci 2014;7:3519–42.
[306] Bartley J, Dummer N, Hutchings G. In: Metal oxide catalysis. Weinheim: Wiley-VCH Verlag; 2009.
[307] Artero V, Chavarot-Kerlidou M, Fontecave M. Splitting water with cobalt. Angew Chem Int Ed 2011;50:7238–66.
[308] Thoi VS, Sun Y, Long JR, Chang CJ. Complexes of earth-abundant metals for catalytic electrochemical hydrogen generation under aqueous conditions. Chem Soc Rev 2013;42:2388–400.
[309] Jaramillo TF, Bonde J, Zhang J, Ooi B-L, Andersson K, Ulstrup J, et al. Hydrogen evolution on supported incomplete cubane-type $[Mo_3S_4]^{4+}$ electrocatalysts. J Phys Chem C 2008;112:17492–8.
[310] Pi M, Wu T, Guo W, Wang X, Zhang D, Wang S, Chen S. Phase-controlled synthesis of polymorphic tungsten diphosphide with hybridization of monoclinic and orthorhombic phases as a novel electrocatalyst for efficient hydrogen evolution. J Power Sources 2017;349:138–43.
[311] Navarro-Flores E, Chong Z, Omanovic S. Characterization of Ni, NiMo, NiW and NiFe electroactive coatings as electrocatalysts for hydrogen evolution in an acidic medium. J Mol Catal Chem 2005;226:179–97.
[312] Hinnemann B, Moses PG, Bonde J, Jørgensen KP, Nielsen JH, Horch S, et al. Biomimetic hydrogen evolution: MoS_2 nanoparticles as catalyst for hydrogen evolution. J Am Chem Soc 2005;127:5308–9.
[313] Jaramillo TF, Jørgensen KP, Bonde J, Nielsen JH, Horch S, Chorkendorff I. Identification of active edge sites for electrochemical H_2 evolution from MoS_2 nanocatalysts. Science 2007;317:100–2.
[314] Merki D, Fierro S, Vrubel H, Hu X. Amorphous molybdenum sulfide films as catalysts for electrochemical hydrogen production in water. Chem Sci 2011;2:1262–7.
[315] Chen JG. Carbide and nitride overlayers on early transition metal surfaces: preparation, characterization, and reactivities. Chem Rev 1996;96:1477–98.
[316] Jaksic MM. Hypo–hyper-d-electronic interactive nature of interionic synergism in catalysis and electrocatalysis for hydrogen reactions. Int J Hydrogen Energy 2001;26:559–78.
[317] Wu M, Lin X, Hagfeldt A, Ma T. Low-cost molybdenum carbide and tungsten carbide counter electrodes for dye-sensitized solar cells. Angew Chem 2011;123:3582–6.
[318] Jin W, Maduraiveeran G. Recent advances of porous transition metal-based nanomaterials for electrochemical energy conversion and storage applications. Materials Today Energy 2019;13:64–84.
[319] Lu Z, Zhang H, Zhu W, Yu X, Kuang Y, Chang Z, et al. In situ fabrication of porous MoS_2 thin-films as high-performance catalysts for electrochemical hydrogen evolution. Chem Commun 2013;49:7516–8.
[320] Huo J, Ge R, Liu Y, Guo J, Lu L, Chen W, Liu C, Gao H, Liu H. Recent advances of two–dimensional molybdenum disulfide based materials: synthesis, modification and applications in energy conversion and storage. Sustainable Materials and Technologies 2020;24:e00161.
[321] Liu Q, Li X, He Q, Khalil A, Liu D, Xiang T, et al. Gram-scale aqueous synthesis of stable few-layered 1T-MoS_2: applications for visible-light-driven photocatalytic hydrogen evolution. Small 2015;11:5556–64.
[322] Stern C, Grinvald S, Kirshner M, Sinai O, Oksman M, Alon H, et al. Growth mechanisms and electronic properties of vertically aligned MoS_2. Sci Rep 2018;8:1–7.
[323] Peng J, Liu Y, Luo X, Wu J, Lin Y, Guo Y, et al. High phase purity of large-sized 1t′-MoS_2 monolayers with 2D superconductivity. Adv Mater 2019;31:1900568.
[324] Ma F, Lu J, Pu L, Wang W, Dai Y. Construction of hierarchical cobalt-molybdenum selenide hollow nanospheres architectures for high performance battery-supercapacitor hybrid devices. J Colloid Interface Sci 2020;563:435–46.
[325] Ruan Y, Lv L, Li Z, Wang C, Jiang J. Ni nanoparticles@Ni–Mo nitride nanorod arrays: a novel 3D-network hierarchical structure for high areal capacitance hybrid supercapacitors. Nanoscale 2017;9:18032–41.
[326] Li H, McRae L, Elezzabi AY. Solution-processed interfacial PEDOT: PSS assembly into porous tungsten molybdenum oxide nanocomposite films for electrochromic applications. ACS Appl Mater Interfaces 2018;10:10520–7.
[327] Yoonessi M, Borenstein A, El-Kady MF, Turner CL, Wang H, Stieg AZ, Pilon L. Hybrid transparent PEDOT: PSS molybdenum oxide battery-like supercapacitors. ACS Appl Energy Mater 2019;2:4629–39.
[328] Anjum MAR, Jeong HY, Lee MH, Shin HS, Lee JS. Efficient hydrogen evolution reaction catalysis in alkaline media by all-in-one MoS_2 with multifunctional active sites. Adv Mater 2018;30:1707105.
[329] Fu C, Tan L, Ren X, Wu Q, Shao H, Ren J, et al. Interlayer expansion of 2D MoS_2 nanosheets for highly improved photothermal therapy of tumors in vitro and in vivo. Chem Commun 2018;54:13989–92.
[330] Zheng M, Guo K, Jiang W-J, Tang T, Wang X, Zhou P, et al. When MoS_2 meets FeOOH: a "one-stone-two-birds"heterostructure as a bifunctional electrocatalyst for efficient alkaline water splitting. Appl Catal B Environ 2019;244:1004–12.
[331] Amiinu IS, Pu Z, Liu X, Owusu KA, Monestel HGR, Boakye FO, et al. Multifunctional Mo–N/C@MoS_2 electrocatalysts for HER, OER, ORR, and Zn–air batteries. Adv Funct Mater 2017;27:1702300.
[332] Xu Y, Wang L, Liu X, Zhang S, Liu C, Yan D, et al. Monolayer MoS_2 with S vacancies from interlayer spacing expanded

counterparts for highly efficient electrochemical hydrogen production. J Mater Chem 2016;4:16524–30.
[333] Vaden TD, Ramanujachary KV, Mugweru A, Aravind J. Synthesis of molybdenum catalyst formulations for hydrogen generation. US Patent, US20150167181A1; 2015.
[334] Sasaki K, Chen W-F, Muckerman JT, Adzic RR. Molybdenum and tungsten nanostructures and methods for making and using same. WIPO (PCT) Patent, WO2013159115A3; 2014.
[335] Han W, Wang Y, Yong M, Han Y. Method for preparing high-purity molybdenum target for thin film solar cell. China Patent, CN102127741A; 2011.
[336] Wheeler ES. Method of preparing pulverized molybdenum disulfide. US Patent, US3082065A; 1963.
[337] Honecker D, Michaluk C, Cox C, Cole J. Sodium/molybdenum powder compacts and methods for producing the same. US Patent, US20090188789A1; 2009.
[338] Qiu H, Zhou B. Highly stable hydrocarbon-soluble molybdenum catalyst precursors and methods for making same. US Patent, US9403153B2; 2016.